Department of Physics and Astronomy

University of Heidelberg

Germany

Bachelor thesis

in Physics

submitted by

Dominik Dold

born in Titisee - Neustadt, Germany

2014

Energy Conservation
In
Fano Spectral Line Shape Control

This Bachelor thesis has been carried out by

Dominik Dold

at the

Max-Planck-Institut für Kernphysik

under the supervision of

PD Dr. Jörg Evers

Abstract

This thesis addresses the question if and how energy is conserved in optical systems with Fano spectral line shape control. The focus is mainly set on the dynamics of two - and three level atoms. To investigate the time dependent energy distribution in these systems, a semiclassical version of the well known Poynting vector from Classical Electrodynamics has been derived. Furthermore, a transition from one irradiated atom to many atoms has been implemented to simplify the expression for the scattered electromagnetic field, enabling us to perform energy calculations for laser pulses as well. Thus, Fano control can be realised in a three-level system via a probe - and control pulse. Doing so, it is possible to show that energy is indeed conserved in systems with Fano control. In fact, the energy in the spectral line is just being redistributed. Additionally, it has been observed that an overlap between probe - and control pulse leads to a manipulation of the scattering behaviour of the atom, without breaking energy conservation.

Ziel dieser Bachelorarbeit ist es, Energieerhaltung in Systemen mit Fano Kontrolle der Spektrallinien zu untersuchen. Die Analyse wird dabei hauptsächlich anhand von Zwei - und Drei Level Atomen durchgeführt. Um die zeitliche Energieverteilung in solchen Systemen untersuchen zu können, wurde zunächst eine semiklassische Version des aus der klassischen Elektrodynamik bekannten Poynting Vektors hergeleitet. Zudem wurde der Fall von nur einem angestrahlten Atom auf viele Atome verallgemeinert, wodurch sich das gestreute elektromagnetische Feld stark vereinfachen lässt. Dies ermöglicht, auch Analysen für gepulste Laser durchzuführen. Letztendlich kann dadurch ein realistisches Modell, bestehend aus einem Drei-Level Atom sowie einem Probe - und Kontrollpuls, zur Implementierung von Fano Kontrolle in optischen Systemen aufgestellt werden. Ausführliche Untersuchungen zeigen, dass in solchen Systemen in der Tat Energieerhaltung gilt und die Manipulation der Absorptionslinie durch eine Umverteilung der Gesamtenergie im Absorptionsspektrum bedingt ist. Darüberhinaus wird das Streuverhalten des Atoms maßgeblich beeinflusst, wenn sich Probe - und Kontrollpuls überlappen. Dieser Effekt führt jedoch nicht zu einem Verstoß der Energieerhaltung.

Contents

1 Introduction

La nature paraît s'être proposé de faire beaucoup avec peu : c'est un principe que le perfectionnement des sciences physiques appuie sans cesse de preuves nouvelles. [1]

In spectroscopy, the most well known line shape is the Lorentzian, originating from the fact that excited atomic states have a finite lifetime. Even though other physical effects like Doppler broadening can alter the spectral line shape, the underlying form describing the atomic resonance is still Lorentzian, which can almost always be recovered by adjusting the experimental setup accordingly, e.g. using saturation spectroscopy to get rid of Doppler broadening. Furthermore, the resonance curve of a driven harmonic oscillator in classical mechanics is also a Lorentzian. Consequently, for a long time, the Lorentz profile was assumed to be the fundamental line shape concerning resonance phenomena.

However, already back in 1902, Wood observed asymmetric line shapes in an optical experiment, calling them "anomalies" [2]. The most prominent example for asymmetric resonance lines is probably the absorption spectrum of the autoionizing states of Helium. The mechanism behind these has first been explained in a paper by Ugo Fano in 1961 [3]. Briefly speaking, the line shape results from an interference between a) a continuum of excited states and b) a discrete excited state with the same energy level [2].

The formula found by Fano for the shape of the resonance profile is [4]:

$$\sigma_{Fano}(\omega) = \sigma_0 \frac{(q+\epsilon)^2}{1+\epsilon^2} \tag{1}$$

With $\epsilon = \frac{\omega-\omega_0}{\gamma/2}$, ω_0 the resonance frequency, γ the width of the resonance and σ_0 the cross section far away from the resonance. q is the so called Fano parameter and measures the ratio of the transition probabilities to the continuum of states and the discrete state. For instance, for $q \to \infty$, the transition to the discrete state dominates and we observe a Lorentz profile. For $q = 1$, both contributions are on par and we get an asymmetric line shape.

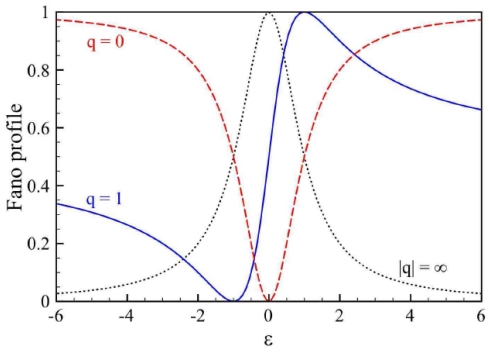

Figure 1: Line shape dependent on the Fano parameter q. [2]

A more detailed analysis reveals, that this interference between two excitation channels leads to a phase kick between the atomic dipole response function and the Lorentzian response. Thus, it is possible to map this phase kick into the q-parameter, as has been demonstrated in a recent experiment [4]. As a consequence, it is possible to manipulate the absorption line of an atomic excitation by giving its dipole response a phase kick. This process is generally denoted as "Fano control" in this work.

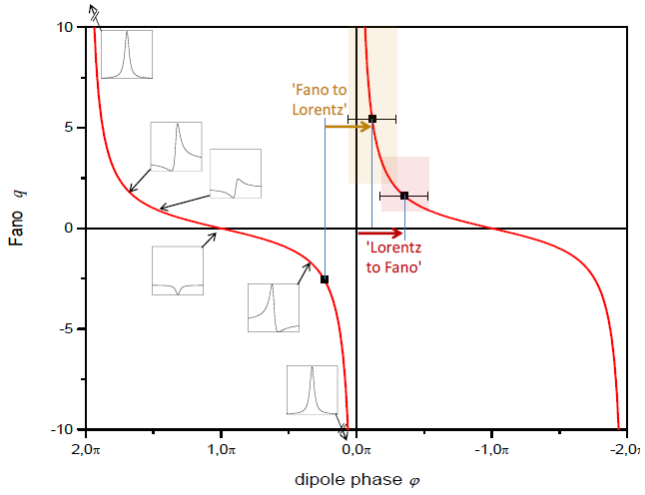

Figure 2: Bijective mapping between phase kick and q-parameter. [4]

The goal of this thesis is to derive a theoretical framework, in which the energy conservation of optical systems with such a Fano control can be understood. First, all the necessary basics and formulas for the coming calculations will be derived or motivated. Furthermore, we will start by analysing simple systems, like a single two-level atom that interacts with a plane laser wave, and gradually increase the complexity of this system, e.g. by adding more atoms or switching to laser pulses. This will allow us to construct a realistic theoretical model for Fano control, in which energy conservation can be extensively examined.

2 Theoretical Basics

In this chapter, we will repeat the most important basics for understanding the scattering of light by two level atoms. First of all, a short recap of classical electromagnetic waves will be given, followed by a more indepth analysis of the quantum mechanical description for coherent interactions between light and atoms. Afterwards, the inclusion of spontaneous emission as a loss channel will be discussed. Even though the first chapters focus more on energy conservation in scattering processes, the main goal of this work is to derive a framework in which the energy distribution in systems with Fano control as seen in [5] and [4] can be better understood. Hence, a subchapter about absorption lines and Fano profiles has been included as well.

2.1 Classical Electrodynamics

Initially, a short revision of Classical Electrodynamics will be given. All formulas are shown in their non-covariant form, since none of the coming calculations are relativistic. Throughout the whole document, vectors will be denoted by bold and scalars by standard font. Furthermore, unit vectors will be marked with a hat.

2.1.1 Maxwell Equations

The foundations of Electrodynamics, one of the most successful theories in physics predating our modern Quantum Theory and Einstein's Special and General Theory of Relativity, are the Maxwell Equations. These are the equations of motion for the electric and magnetic field, from which every electrodynamic phenomena that has no quantum nature can be described. They have the following form (in SI units) [6]:

$$\boldsymbol{\nabla} \cdot \boldsymbol{E} = \frac{\rho}{\epsilon_0} \qquad \boldsymbol{\nabla} \times \boldsymbol{E} = -\dot{\boldsymbol{B}} \tag{2a}$$

$$\boldsymbol{\nabla} \cdot \boldsymbol{B} = 0 \qquad \boldsymbol{\nabla} \times \boldsymbol{B} = \mu_0 \boldsymbol{j} + \mu_0 \epsilon_0 \dot{\boldsymbol{E}} \tag{2b}$$

Eqs. 2a roughly state that either a charge or a changing magnetic flux can create an electric field. In the same manner, eqs. 2b tell us that magnetic fields have no source in the form of a magnetic charge. Thus, magnetic fields can only be created by a current density or a changing electric flux.

2.1.2 Electromagnetic Waves

Electromagnetic waves are a special solution of the Maxwell Equations (Eqs. 2). Since electromagnetic waves propagate through space-time independently of their initial source, we can eliminate all matter sources of the electromagnetic field. Thus, we get

$$\boldsymbol{\nabla} \cdot \boldsymbol{E} = 0 \qquad \boldsymbol{\nabla} \times \boldsymbol{E} = -\dot{\boldsymbol{B}} \tag{3a}$$

$$\boldsymbol{\nabla} \cdot \boldsymbol{B} = 0 \qquad \boldsymbol{\nabla} \times \boldsymbol{B} = \frac{1}{c^2}\dot{\boldsymbol{E}} \tag{3b}$$

whereby we replaced $\mu_0\epsilon_0 = \frac{1}{c^2}$ and set $\rho = 0$, $\boldsymbol{j} = 0$.
The equation of motion for the electric part of the electromagnetic field can now be derived as follows: First, we evaluate the expression $\boldsymbol{\nabla} \times (\boldsymbol{\nabla} \times \boldsymbol{E})$

$$\boldsymbol{\nabla} \times (\boldsymbol{\nabla} \times \boldsymbol{E}) = \boldsymbol{\nabla} \underbrace{(\boldsymbol{\nabla} \cdot \boldsymbol{E})}_{=0} - \boldsymbol{\Delta}\boldsymbol{E} \tag{4a}$$

$$= -\boldsymbol{\Delta}\boldsymbol{E} \tag{4b}$$

Next, we evaluate $\boldsymbol{\nabla} \times \dot{\boldsymbol{B}}$

$$\boldsymbol{\nabla} \times \dot{\boldsymbol{B}} = \frac{d}{dt}(\boldsymbol{\nabla} \times \boldsymbol{B}) \tag{5a}$$

$$= \frac{1}{c^2}\ddot{\boldsymbol{E}} \tag{5b}$$

Consequently, using eqs. 3a our final result is [6]

$$\boldsymbol{\Delta}\boldsymbol{E} - \frac{1}{c^2}\ddot{\boldsymbol{E}} = 0 \tag{6}$$

This partial differential equation is commonly known as the wave-equation, since its solution space is spanned by waves with wave vector $\boldsymbol{k}$ and frequency ω. Note that the magnetic field has to obey the same differential equation as the electric part.

$$\boldsymbol{\Delta}\boldsymbol{B} - \frac{1}{c^2}\ddot{\boldsymbol{B}} = 0 \tag{7}$$

Now, an example for a solution would be plane waves:

$$\boldsymbol{E} = \boldsymbol{E_0}\ e^{i(\boldsymbol{k}\boldsymbol{r} - \omega t)} \tag{8a}$$

$$\boldsymbol{B} = \boldsymbol{B_0}\ e^{i(\boldsymbol{k'}\boldsymbol{r} - \omega' t)} \tag{8b}$$

Beside the wave equation, these solutions still have to obey the Maxwell Equations. Therefore, we get an additional set of restrictions. For instance, we can insert our solutions into eqs. 3a:

$$\nabla \times \boldsymbol{E} = -\dot{\boldsymbol{B}}$$
$$\Rightarrow \; i(\boldsymbol{k} \times \boldsymbol{E_0}) e^{i(\boldsymbol{kr}-\omega t)} = i\boldsymbol{B_0}\omega' e^{i(\boldsymbol{k'r}-\omega' t)} \tag{9}$$

This gives us the following restrictions:

$$\boldsymbol{k} = \boldsymbol{k'} \tag{10a}$$
$$\boldsymbol{\omega} = \boldsymbol{\omega'} \tag{10b}$$
$$\boldsymbol{k} \times \boldsymbol{E_0} = \omega \boldsymbol{B_0} \tag{10c}$$

If one does this for all Maxwell Equations, the main result is that $\boldsymbol{E} \perp \boldsymbol{B} \perp \boldsymbol{k}$ (see [6]).
Additionally, we can insert the plane wave 8a into the wave equation 6. From this we get

$$\omega = k \cdot c \tag{11}$$

which is the dispersion relation for light in vacuum. It describes how spatial and time evolution of the electromagnetic wave are connected to each other. Note that c is the propagation velocity of the wave.

By taking into account that electromagnetic waves are real and not complex quantities, we can write a general plane wave which solves the Maxwell Equations for vacuum in the following way:

$$\boldsymbol{E} = \boldsymbol{E}^{(+)} + \boldsymbol{E}^{(-)} \tag{12a}$$
$$\text{with } \boldsymbol{E}^{(+)} = E_0 \, \hat{\boldsymbol{\epsilon}} \, e^{i(\boldsymbol{kr}-\omega t)} \text{ and } \boldsymbol{E}^{(-)} = \boldsymbol{E}^{(+)\dagger} \tag{12b}$$
$$\boldsymbol{B} = \boldsymbol{B}^{(+)} + \boldsymbol{B}^{(-)} \tag{12c}$$
$$\text{with } \boldsymbol{B}^{(+)} = \frac{E_0}{c} \, (\hat{\boldsymbol{k}} \times \hat{\boldsymbol{\epsilon}}) \, e^{i(\boldsymbol{kr}-\omega t)} \text{ and } \boldsymbol{B}^{(-)} = \boldsymbol{B}^{(+)\dagger} \tag{12d}$$

Here, $\hat{\boldsymbol{\epsilon}}$ is the unit poliarization vector, which has to be in the plane orthogonal to the propagation direction $\hat{\boldsymbol{k}}$. We will use this notation of the electromagnetic field throughout the whole thesis.

2.1.3 Electromagnetic Field of an Oscillating Dipole

In the previous chapter, we calculated the form of the electromagnetic field which propagates through space-time independently of its initial source. Now, we will take a closer look at what happens when we introduce a source, e.g. an oscillating dipole. In this case, one normally first derives the potentials $\Phi(\boldsymbol{r}, t)$ and $\boldsymbol{A}(\boldsymbol{r}, t)$. The electric and magnetic field is then calculated via (in SI units):

$$\boldsymbol{E} = -\partial_t \boldsymbol{A}(\boldsymbol{r}, t) - \boldsymbol{\nabla}\Phi(\boldsymbol{r}, t) \tag{13a}$$

$$\boldsymbol{B} = \boldsymbol{\nabla} \times \boldsymbol{A}(\boldsymbol{r}, t) \tag{13b}$$

Hereby, $\Phi(\boldsymbol{r}, t)$ is the standard scalar potential known from classical electrostatics and $\boldsymbol{A}(\boldsymbol{r}, t)$ is the vector potential, which is normally introduced in magnetostatics.

In this notation, the wave equation can be rewritten for the potentials. Thus, we get [7]

$$(-\frac{1}{c^2}\partial_t^2 + \boldsymbol{\nabla}^2)\Phi = -\frac{\rho}{\epsilon_0} \tag{14a}$$

$$(-\frac{1}{c^2}\partial_t^2 + \boldsymbol{\nabla}^2)\boldsymbol{A} = -\mu_0 \boldsymbol{j} \tag{14b}$$

where ρ is the charge density. For the case of vacuum, the righthand sides would all be 0 and we'd get the same results as in chapter 2.1.2. So due to the introduction of sources, we have to solve an inhomogeneous partial differential equation now.

The standard technique is to introduce a function $G(\boldsymbol{r}, t; \boldsymbol{r'}, t')$ called Green's Function which suffices the equation

$$(-\frac{1}{c^2}\partial_t^2 + \boldsymbol{\nabla}^2)\ G(\boldsymbol{r}, t; \boldsymbol{r'}, t') = -\ \delta(\boldsymbol{r} - \boldsymbol{r'})\ \delta(t - t') \tag{15}$$

As soon as we have found the expression for $G(\boldsymbol{r}, t; \boldsymbol{r'}, t')$, we can calculate the potentials via

$$\Phi(\boldsymbol{r}, t) = \frac{1}{\epsilon_0} \int G(\boldsymbol{r}, t; \boldsymbol{r'}, t')\ \rho(\boldsymbol{r'}, t')\ \mathrm{d}^3 r'\ dt' \tag{16a}$$

$$\boldsymbol{A}(\boldsymbol{r}, t) = \mu_0 \int G(\boldsymbol{r}, t; \boldsymbol{r'}, t')\ \boldsymbol{j}(\boldsymbol{r'}, t')\ \mathrm{d}^3 r'\ dt' \tag{16b}$$

Here, the meaning of the Green's Function becomes instantly clear. When we, for instance, change the configuration of our charge distribution, this won't instantly affect the electric field someone far away sees as the information of our change travels with a finite velocity through space. Roughly speaking, the Green's Function somewhat correctly "couples" the charge configuration at $(\boldsymbol{r'}, t')$ to the space-time point $(\boldsymbol{r}, t)$.

This can be seen even better if one solves these equations (for the calculation, see [7]):

$$\Phi(\boldsymbol{r}, t) = \frac{1}{4\pi\epsilon_0} \int \frac{\rho(\boldsymbol{r'}, t - \frac{|\boldsymbol{r}-\boldsymbol{r'}|}{c})}{|\boldsymbol{r} - \boldsymbol{r'}|}\ \mathrm{d}^3 r' \tag{17a}$$

$$\boldsymbol{A}(\boldsymbol{r}, t) = \frac{\mu_0}{4\pi} \int \frac{\boldsymbol{j}(\boldsymbol{r'}, t - \frac{|\boldsymbol{r}-\boldsymbol{r'}|}{c})}{|\boldsymbol{r} - \boldsymbol{r'}|}\ \mathrm{d}^3 r' \tag{17b}$$

As we can see, the end results resemble the normal expressions for the electromagnetic potentials, with the exception that the finiteness of information transport has been included.

With eqs. 13 and 17, one can now calculate the electromagnetic field of an oscillating dipole $\boldsymbol{d}(t)$. Again, we skip the calculation and only give the results in SI units (for the calculation, see again [7]).

$$\boldsymbol{E}(\boldsymbol{r},t) = -\frac{\ddot{\boldsymbol{d}}(t')}{4\pi\epsilon_0 r c^2} - \frac{1}{4\pi\epsilon_0}\left(\frac{\dot{\boldsymbol{d}}(t')}{r^2 c} - \frac{\boldsymbol{d}(t')}{r^3} + \frac{(\ddot{\boldsymbol{d}}(t')\cdot\boldsymbol{r})\boldsymbol{r}}{r^3 c^2} + \frac{3(\dot{\boldsymbol{d}}(t')\cdot\boldsymbol{r})\boldsymbol{r}}{r^4 c} + \frac{3(\boldsymbol{d}(t')\cdot\boldsymbol{r})\boldsymbol{r}}{r^5}\right) \tag{18a}$$

$$\boldsymbol{B}(\boldsymbol{r},t) = \frac{1}{4\pi\epsilon_0 c^2}\left(\frac{\dot{\boldsymbol{d}}(t')\times\boldsymbol{r}}{r^3 c} + \frac{\ddot{\boldsymbol{d}}(t')\times\boldsymbol{r}}{r^2 c^2}\right) \tag{18b}$$

Here, t' is given by $t' = (t - \frac{r}{c})$. For the field far away from the source ($r \to \infty$) and $\boldsymbol{d} \sim e^{i\omega t'} + e^{-i\omega t'}$, we therefore get (in SI units) [7]:

$$\boldsymbol{E}(\boldsymbol{r},t) = \frac{k^2}{4\pi\epsilon_0 r}(e^{i(kr-\omega t)} + c.c.)\ (\hat{\boldsymbol{r}}\times\hat{\boldsymbol{d}})\times\hat{\boldsymbol{r}} \tag{19a}$$

$$\boldsymbol{B}(\boldsymbol{r},t) = \frac{1}{c}(\hat{\boldsymbol{r}}\times\boldsymbol{E}) \tag{19b}$$

Note that here, $\boldsymbol{d}$ has no time dependence anymore. Furthermore, as one would expect, the field of an oscillating dipole with frequency ω is a spherical wave with exactly this frequency. In chapter 2.2.2, we will derive a similar expression for the emitted field of a two-level atom that is being excited by a laser.

2.2 Coherent Atom-Light Interaction for a Two-Level System

Next, we will give a short recap of the most fundamental parts of light-matter interaction. Operators will also be denoted with a hat, but it should always be clear by context whether a given symbol represents an operator or a unit vector. Furthermore, operators won't be in bold face.

2.2.1 Jaynes Cummings Hamiltonian

Whenever we analyse a quantum mechanical system, one almost always starts with writing down the Hamiltonian for the system. The reason for this is quite simple: When we succeed in diagonalizing the Hamiltonian, we have a complete set of states that are invariant under time translation. All further allowed states of the system are therefore superpositions of the Hamiltonian's Eigenstates and their time dependence can be constructed trivially by using the Schrödinger Equation.

Without an electromagnetic field present, the Schrödinger Equation has the following form [8]:

$$i\hbar\partial_t\psi = \left(-\frac{\hbar^2}{2m}\boldsymbol{\nabla}^2 + V(\boldsymbol{r})\right)\psi \tag{20}$$

For instance, in the case of the Hydrogen Atom, $V(\boldsymbol{r})$ would be the Coulomb Potential and m the reduced mass of the electron-proton system. We can now introduce an electromagnetic field by the principle of minimal coupling (for a subtle motivation of this step, see [8] or [9]). Thus, we get

$$i\hbar\partial_t\psi = \left(-\frac{\hbar^2}{2m}\left(\boldsymbol{\nabla} - \frac{ie}{\hbar}\boldsymbol{A}(\boldsymbol{r},t)\right)^2 + V(\boldsymbol{r})\right)\psi \tag{21}$$

whereby $\boldsymbol{A}(\boldsymbol{r},t)$ is the vector potential of the electromagnetic field, already introduced in chapter 2.1.3. By assuming that the light's wavelength is much larger than the atomsize, we can make the approximation $\boldsymbol{A}(\boldsymbol{r},t) \simeq \boldsymbol{A}(\boldsymbol{r_0},t)$, with $\boldsymbol{r_0}$ the atom position (dipole approximation [8]). By using the unitary transformation $U = e^{-\frac{ie}{\hbar}\boldsymbol{A}(\boldsymbol{r_0},t)\boldsymbol{r}}$, we can write $\psi = U^\dagger U\psi = U^\dagger\psi_{int}$ and therefore:

$$i\hbar\partial_t\psi_{int} = \left(-\frac{\hbar^2}{2m}\boldsymbol{\nabla}^2 + V(\boldsymbol{r}) - e\boldsymbol{E}(\boldsymbol{r_0},t)\boldsymbol{r}\right)\psi_{int} \tag{22}$$

$\boldsymbol{E}(\boldsymbol{r_0}, \mathrm{t})$ is the electric field of the light. So by using minimal coupling and doing one transformation, we were able to bring the Hamiltonian into a form which resembles the Hamiltonian without any electromagnetic field, but modified with an interaction term $H_{int} = -e\boldsymbol{E}(\boldsymbol{r_0},t)\boldsymbol{r}$. From here on, one normally chooses an appropriate Interaction Picture to get rid of the time dependence of the electric field. This leads to the following Hamiltonian (see [10]):

$$\hat{H} = -\hbar\Delta\hat{S}_{ee} + \hbar\left(\Omega\ \hat{S}_{eg} + \Omega^*\ \hat{S}_{ge}\right) \tag{23}$$

with $\hat{S}_{xy} = |x\rangle\langle y|$,

$\Delta \rightarrow$ detuning,

$\Omega = -\frac{E_0\hat{\boldsymbol{\epsilon}}\boldsymbol{d}}{\hbar} \rightarrow$ Rabi Frequency,

$|g\rangle \rightarrow$ ground state, $|e\rangle \rightarrow$ excited state

Furthermore, one would have to quantize the electromagnetic field, such that we have a fully quantum mechanical theory. As our Hamiltonian is right now, only the matter part is quantized and the fields are classical. Quantizing the electromagnetic field will lead to the Jaynes Cummings Hamiltonian (for an in-depth derivation, see [8] or [10]). Thus, the J.C. Hamiltonian for a two-level atom (with rotating wave approximation) takes the form:

$$\hat{H}_{J.C.} = \underbrace{\hbar\omega_e\hat{S}_{ee} + \hbar\omega_g\hat{S}_{gg}}_{\text{atomic electron structure}} + \underbrace{\hbar\omega_0\left(\hat{a}^\dagger\hat{a} + \frac{1}{2}\right)}_{\text{quantized field}} + \underbrace{\hbar\left(g\hat{S}_{eg}\hat{a} + g^*\hat{S}_{ge}\hat{a}^\dagger\right)}_{\text{interaction between atom and field}} \tag{24}$$

Note that in this form, we haven't chosen a specific Interaction Picture yet. Moreover, g is the Rabi Frequency $g = -\frac{E_0\hat{\boldsymbol{\epsilon}}\boldsymbol{d}}{\hbar}$ and a, $a^\dagger$ are the annihilation and creation operator for the quantized electromagnetic field. In most textbooks, E_0 is chosen as $E_0 = \sqrt{\frac{\hbar\omega_0}{2\epsilon_0 V}}$ with V the quantization volume (see [11], [12]). We will make use of this definition for some theoretical calculations, but for more experimental orientated calculations, we will only use E_0 as a variable.

Additionally, the Jaynes Cummings Hamiltonian can be written in the following form:

$$\hat{H}_{J.C.} = \hbar\omega_e \hat{S}_{ee} + \hbar\omega_g \hat{S}_{gg} + \hbar\omega_0 \left(\hat{a}^\dagger \hat{a} + \frac{1}{2}\right) + i\hbar \left(g\hat{S}_{eg}\hat{a} - g^* \hat{S}_{ge}\hat{a}^\dagger\right) \tag{25}$$

This version is equivalent to eq. 24, but for some calculations, it's more practical. Note that this Hamiltonian still fulfills the condition $\hat{H}^\dagger_{J.C.} = \hat{H}_{J.C.}$, which is necessary for the Hamiltonian to be an operator.

2.2.2 Quantum Mechanical Derivation of the Scattered Field

We will now derive the scattered field of a two level-atom. The calculation is mostly taken from [11] and [12]. First, we start with the positive frequency part of the electric field operator in its quantized form:

$$\hat{\boldsymbol{E}}^{(+)}(\boldsymbol{r}, t_r) = i \sum_{\boldsymbol{k},\lambda} \sqrt{\frac{\hbar\omega_{\boldsymbol{k}\lambda}}{2\epsilon_0 V}} \hat{\boldsymbol{\epsilon}}_{\boldsymbol{k},\lambda} \hat{a}_{\boldsymbol{k},\lambda}(t_r) e^{i\boldsymbol{k}\boldsymbol{r}} \tag{26}$$

Note that we a) assume a general polarisation and b) sum over all possible momenta. Moreover, we assume that the atom sits at the origin. The time dependence lies in the annihilation operator $\hat{a}_{\boldsymbol{k},\lambda}(t_r)$ with $t_r = t + \frac{r}{c}$. In our case, t_r is the time when we detect the field at the detector's position $\boldsymbol{r}$. This signal depends on the evolution of the source field emitted at the earlier time t [11]. The reaction of the atom due to the field is best calculated in the Heisenberg picture. Thus, we get $\hat{a}_{\boldsymbol{k},\lambda}(t_r)$ via the Heisenberg Equation:

$$i\hbar\dot{\hat{a}}(t) = [\hat{a}, \hat{H}_{J.C.}] \tag{27}$$

$\hat{H}_{J.C.}$ is the Jaynes Cummings Hamiltonian defined in eq. 25. Hence, we obtain:

$$\dot{\hat{a}}(t) = -i\omega\hat{a}(t) - g^*(t)\hat{S}_{ge}(t) \tag{28a}$$

$$\Rightarrow \quad e^{i\omega t}\dot{\hat{a}}(t) + e^{i\omega t} i\omega \hat{a}(t) = -g^*(t)\hat{S}_{ge}(t)e^{i\omega t} \tag{28b}$$

$$\Rightarrow \quad \frac{d}{dt}\left(e^{i\omega t}\hat{a}(t)\right) = -g^*(t)\hat{S}_{ge}(t)e^{i\omega t} \tag{28c}$$

Integrating this equation, we get:

$$\hat{a}(t_r) = \hat{a}(0)e^{-i\omega t_r} - \int_0^{t_r} g^*(t')\hat{S}_{ge}(t')e^{i\omega(t'-t_r)}dt' \tag{29}$$

We can insert this now into eq. 26:

$$\begin{aligned}\boldsymbol{E}^{(+)}(\boldsymbol{r},t_r) = i\sum_{\boldsymbol{k},\lambda}\sqrt{\frac{\hbar\omega_{\boldsymbol{k}\lambda}}{2\epsilon_0 V}}\hat{\boldsymbol{\epsilon}}_{\boldsymbol{k},\lambda}\hat{a}_{\boldsymbol{k},\lambda}(0)e^{i(\boldsymbol{kr}-\omega_{\boldsymbol{k}\lambda}t_r)} \\ - i\sum_{\boldsymbol{k},\lambda}\sqrt{\frac{\hbar\omega_{\boldsymbol{k}\lambda}}{2\epsilon_0 V}}\hat{\boldsymbol{\epsilon}}_{\boldsymbol{k},\lambda}e^{i\boldsymbol{kr}}\int_0^{t_r} g^*(t')\hat{S}_{ge}(t')e^{i\omega_{\boldsymbol{k}\lambda}(t'-t_r)}dt' \end{aligned} \tag{30}$$

The first part represents the solution for the electromagnetic field as if no atom was present, i.e. it's similar to the incident field. Therefore, it looks identical to the solution of the homogeneous Maxwell Equations in chapter 2.1.2. The second part is the reply of the atom to the incident laser beam, i.e. the field scattered by the atom. In the following, we will take a closer look at the expression for the scattered field.

First, we can use the lowest order approximation of $\hat{S}_{ge}$ to simplify the time integral. This can be obtained by evaluating the Heisenberg Equation just for the free Hamiltonian without any laser. Thus, we can say [12]:

$$\hat{S}_{ge}(t') \simeq \hat{S}_{ge}(t_r)e^{-i\omega_0(t'-t_r)} \tag{31a}$$

$$\Rightarrow \quad \int_0^{t_r} g^*(t')\hat{S}_{ge}(t')e^{i\omega_{\boldsymbol{k}\lambda}(t'-t_r)}dt' \simeq \hat{S}_{ge}(t_r)\int_0^{t_r} g^*(t')e^{i(\omega_{\boldsymbol{k}\lambda}-\omega_0)(t'-t_r)}dt' \tag{31b}$$

In our case, $g^*(t')$ is independent of time and we can pull it out of the integrand. To simplify our notation, we will define $J_-(t_r) = \int_0^{t_r} e^{i(\omega_{\boldsymbol{k}\lambda}-\omega_0)(t'-t_r)}dt'$ to get

$$\boldsymbol{E}^{(+)}_{scat}(\boldsymbol{r},t_r) = -i\sum_{\boldsymbol{k},\lambda}\sqrt{\frac{\hbar\omega_{\boldsymbol{k}\lambda}}{2\epsilon_0 V}}\hat{\boldsymbol{\epsilon}}_{\boldsymbol{k},\lambda}e^{i\boldsymbol{kr}}\hat{S}_{ge}(t_r)g^*J_-(t_r) \tag{32a}$$

$$= i\sum_{\boldsymbol{k},\lambda}\frac{\omega_{\boldsymbol{k}\lambda}}{2\epsilon_0 V}(\boldsymbol{d}\cdot\hat{\boldsymbol{\epsilon}}_{\boldsymbol{k},\lambda})\hat{\boldsymbol{\epsilon}}_{\boldsymbol{k},\lambda}e^{i\boldsymbol{kr}}\hat{S}_{ge}(t_r)J_-(t_r) \tag{32b}$$

$$= i\sum_{\boldsymbol{k}}\frac{\omega_{\boldsymbol{k}\lambda}}{2\epsilon_0 V}\left(\boldsymbol{d}-(\boldsymbol{d}\cdot\hat{\boldsymbol{k}})\hat{\boldsymbol{k}}\right)e^{i\boldsymbol{kr}}\hat{S}_{ge}(t_r)J_-(t_r) \tag{32c}$$

where we replaced g^* and evaluated the polarization-sum $\sum_\lambda(\boldsymbol{d}\cdot\hat{\boldsymbol{\epsilon}}_{\boldsymbol{k},\lambda})\hat{\boldsymbol{\epsilon}}_{\boldsymbol{k},\lambda} = \boldsymbol{d}-(\boldsymbol{d}\cdot\hat{\boldsymbol{k}})\hat{\boldsymbol{k}}$ (see Appendix A.1). Next, we can replace the summation over the wave vectors with an integral containing the appropriate density of modes $\sum_{\boldsymbol{k}} \to \frac{V}{(2\pi)^3c^3}\int_0^\infty\int_0^{2\pi}\int_0^\pi \omega^2\sin\theta\,\mathrm{d}\omega\mathrm{d}\phi\mathrm{d}\theta$.

$$\boldsymbol{E}^{(+)}_{scat}(\boldsymbol{r},t_r) = i\frac{V}{(2\pi)^3c^3 2\epsilon_0 V}\hat{S}_{ge}(t_r)J_-(t_r)\int_0^\infty\int_0^{2\pi}\int_0^\pi \omega^3\sin\theta\left(\boldsymbol{d}-(\boldsymbol{d}\cdot\hat{\boldsymbol{k}})\hat{\boldsymbol{k}}\right)e^{i\boldsymbol{kr}}\,\mathrm{d}\omega\mathrm{d}\phi\mathrm{d}\theta \tag{33}$$

The surface integral can be solved by using the stationary phase argument: Only those directions contribute to the integral for which the phase $i\boldsymbol{kr}$ is stationary. Thus, the wavevector has to obey $\hat{\boldsymbol{k}} = \pm\hat{\boldsymbol{r}}$

[11]. Therefore, we can simplify the integral by approximating $\boldsymbol{d} - (\boldsymbol{d} \cdot \hat{\boldsymbol{k}})\hat{\boldsymbol{k}} \to \boldsymbol{d} - (\boldsymbol{d} \cdot \hat{\boldsymbol{r}})\hat{\boldsymbol{r}}$. A short explanation of the stationary phase argument is given in Appendix A.2. Further, it's important to remark that this approximation is only valid for the case of large r, i.e. $r \to \infty$. This is equivalent to the far-field transition in eq. 19 for the classical dipole field. Using the Grassmann-identity $\boldsymbol{d} - (\boldsymbol{d} \cdot \hat{\boldsymbol{r}})\hat{\boldsymbol{r}} = (\hat{\boldsymbol{r}} \times \boldsymbol{d}) \times \hat{\boldsymbol{r}}$, we now have

$$\boldsymbol{E}^{(+)}_{scat}(\boldsymbol{r}, t_r) = i\frac{1}{16\pi^3 c^3 \epsilon_0} \hat{S}_{ge}(t_r) J_-(t_r) \int_0^\infty \int_0^{2\pi} \int_0^\pi \omega^3 \sin\theta e^{i\boldsymbol{kr}} \, \mathrm{d}\omega \mathrm{d}\phi \mathrm{d}\theta \; (\hat{\boldsymbol{r}} \times \boldsymbol{d}) \times \hat{\boldsymbol{r}} \tag{34}$$

and choosing $\boldsymbol{r}$ along the z-direction, we get $i\boldsymbol{kr} = ikr\cos\theta$ such that the surface integral can be easily evaluated to $\int_0^{2\pi} \int_0^\pi \sin\theta e^{ikr\cos\theta} \, \mathrm{d}\phi \mathrm{d}\theta = -i\frac{2\pi c}{\omega r}\left(e^{i\frac{\omega r}{c}} - e^{-i\frac{\omega r}{c}}\right)$.

$$\boldsymbol{E}^{(+)}_{scat}(\boldsymbol{r}, t_r) = \frac{1}{8\pi^2 c^2 \epsilon_0 r} \hat{S}_{ge}(t_r) J_-(t_r) \int_0^\infty \omega^2 \left(e^{i\frac{\omega r}{c}} - e^{-i\frac{\omega r}{c}}\right) \, \mathrm{d}\omega \; (\hat{\boldsymbol{r}} \times \boldsymbol{d}) \times \hat{\boldsymbol{r}} \tag{35}$$

Using again $\hat{S}_{ge}(t_r) \simeq \hat{S}_{ge}(t) e^{-i\omega_0(t_r - t)} = \hat{S}_{ge}(t) e^{-i\omega_0(t + \frac{r}{c} - t)} = \hat{S}_{ge}(t) e^{-i\frac{\omega_0 r}{c}}$ we have a term $\sim e^{-i\frac{\omega - \omega_0}{c} r}$ and $\sim e^{-i\frac{\omega + \omega_0}{c} r}$. The second term is strongly oscillating and thus won't contribute to the field. Therefore, we get:

$$\boldsymbol{E}^{(+)}_{scat}(\boldsymbol{r}, t_r) = \frac{1}{8\pi^2 c^2 \epsilon_0 r} \hat{S}_{ge}(t) J_-(t_r) \int_0^\infty \omega^2 e^{i\frac{\omega - \omega_0}{c} r} \, \mathrm{d}\omega \; (\hat{\boldsymbol{r}} \times \boldsymbol{d}) \times \hat{\boldsymbol{r}} \tag{36}$$

We can now approximate $J_-(t_r) = \int_0^{t_r} e^{i(\omega - \omega_0)(t' - t_r)} \mathrm{d}t' \simeq 2\pi\delta(\omega - \omega_0)$ [11] to get:

$$\boldsymbol{E}^{(+)}_{scat}(\boldsymbol{r}, t_r) = \frac{k_0^2}{4\pi\epsilon_0 r} \hat{S}_{ge}(t) \; (\hat{\boldsymbol{r}} \times \boldsymbol{d}) \times \hat{\boldsymbol{r}} \tag{37}$$

Defining $\hat{S}_{ge}(t) = \hat{S}_-(t) e^{-i\omega_0 t}$ [13], our final result becomes:

$$\boldsymbol{E}^{(+)}_{scat}(\boldsymbol{r}, t_r) = \frac{k_0^2}{4\pi\epsilon_0 r} \hat{S}_-(t) e^{i(k_0 r - \omega_0 t_r)} \; (\hat{\boldsymbol{r}} \times \boldsymbol{d}) \times \hat{\boldsymbol{r}} \tag{38}$$

As expected, the scattered field of a two-level atom is almost equivalent to the field of a classical oscillating dipole (eq. 19). The only exception is the atom-operator, which allows new quantum effects to occur. We will take this form of the scattered field for all coming calculations.

2.3 Modelling Spontaneous Emission

In this chapter, we will motivate spontaneous emission and solve the density matrices for a two-level atom.

2.3.1 Introducing Density Matrices

Normally, analysing the interaction between a monochromatic laser and a two-level atom consists of finding the eigenbasis of the Jaynes-Cummings Hamiltonian (eq. 24). However, Hamiltonian dynamics only includes coherent (reversible) processes, i.e. absorption and stimulated emission. Thus, we are missing incoherent (irreversible) processes like spontaneous emission, which arise from the fact that our system is also coupled to the vacuum (so called "bath"). This means that an excited atom can also emit a photon by exciting a mode of the vacuum electromagnetic field.

This is considered as a loss channel, since the vacuum is "so large" that the photon will never come back to the atom to be reabsorbed. Furthermore, superposition states will be destroyed by spontaneous emission and instead, we get a statistical mixture. Such mixed states can't be described with a wave function, therefore we have to introduce a new quantity: The Density Matrix.

The Density Matrix of a system is defined as:

$$\hat{\rho} = \sum_i p_i \left|\psi_i\right\rangle \left\langle\psi_i\right| \tag{39}$$

$|\psi_i\rangle$ are all the possible states our physical system can be in and p_i are the probabilities to find it in state $|\psi_i\rangle$. Note that a statistical mixture is no superposition of states, thus we won't observe any interference effects. The system is in either of these states, not in "all of them" at once. The expectation value of an observable $\hat{O}$ can be calculated via:

$$\langle\hat{O}\rangle = \mathrm{Tr}\{\hat{O}\hat{\rho}\} \tag{40}$$

Therefore, we get in the case of a two-level atom:

$$\langle\hat{S}_-\rangle = \hat{\rho}_{eg} \tag{41a}$$

$$\langle\hat{S}_+\rangle = \hat{\rho}_{ge} \tag{41b}$$

$$\langle\hat{S}_+\hat{S}_-\rangle = \hat{\rho}_{ee} \tag{41c}$$

Additionally, the Schrödinger Equation is replaced by the Liouville Equation:

$$i\hbar\partial_t\hat{\rho} = [\hat{H}, \hat{\rho}] \tag{42}$$

A more detailed introduction with examples can be found in [8] or [10]. With these definitions, we are now able to describe spontaneous emission.

2.3.2 Master Equation

The main idea now is to separate our system into two coupled parts: The atom and the environment or "bath" (vacuum). Explicitely speaking, our density matrix $\hat{\rho}$ describes both parts, thus when we are only interested in the dynamics of the atom, we have to trace out the vacuum and vice versa. This is the same as integrating out all degrees of freedom we don't care about in statistical physics, i.e. in our case, we are not interested in the state the vacuum is in. This is very nicely explained in [8] with respect to the EPR-Paradox. Hence, formally we can write

$$\hat{\rho}_A = Tr_V\{\hat{\rho}\} \tag{43}$$

whereby A stands for atom and V for vacuum. This ansatz can now be used to derive the Master Equation. However, since this calculation is very long, only the result will be stated here [10].

$$\partial_t \hat{\rho}_A(t) = -\frac{\gamma}{2}\left(\hat{S}_{eg}\hat{S}_{ge}\hat{\rho}_A(t) + \hat{\rho}_A(t)\hat{S}_{eg}\hat{S}_{ge} - 2\hat{S}_{ge}\hat{\rho}_A(t)\hat{S}_{eg}\right) \tag{44a}$$

$$\text{with} \quad \gamma = \frac{d^2\omega_0^3}{3\pi\epsilon_0\hbar c^3} \tag{44b}$$

This is the so called Lindblad form of the Master Equation [10] with γ the decay rate and d the induced dipole moment of the atom.

Thus, our total equation of motion including coherent and incoherent processes now is:

$$\partial_t \hat{\rho}_A(t) = \frac{1}{i\hbar}[\hat{H}, \hat{\rho}_A(t)] - \frac{\gamma}{2}\left(\hat{S}_{eg}\hat{S}_{ge}\hat{\rho}_A(t) + \hat{\rho}_A(t)\hat{S}_{eg}\hat{S}_{ge} - 2\hat{S}_{ge}\hat{\rho}_A(t)\hat{S}_{eg}\right) \tag{45}$$

2.3.3 Density Matrix Elements for a Two-Level System

Taking eq. 23 for the Hamiltonian, we get the following differential equations for the density matrix elements ([8], [10]):

$$\partial_t \hat{\rho}_{ee} = -\gamma\hat{\rho}_{ee} + i\Omega(\hat{\rho}_{eg} - \hat{\rho}_{ge}) \tag{46a}$$

$$\partial_t \hat{\rho}_{eg} = -(\frac{\gamma}{2} - i\Delta)\hat{\rho}_{eg} + i\Omega(\hat{\rho}_{ee} - \hat{\rho}_{gg}) \tag{46b}$$

The simplest way to solve these is to only look at the stationary solutions, i.e. the solutions for $\partial_t\hat{\rho}_{ee} = 0$ and $\partial_t\hat{\rho}_{eg} = 0$. This can be calculated quite easily by hand or with Mathematica (see Appendix B.1).

The solutions are:

$$\hat{\rho}_{ee} = \frac{4\Omega^2}{\gamma^2 + 4\Delta^2 + 8\Omega^2} \tag{47a}$$

$$\hat{\rho}_{eg} = \frac{\Omega(4\Delta - 2i\gamma)}{\gamma^2 + 4\Delta^2 + 8\Omega^2} \tag{47b}$$

$$\hat{\rho}_{ge} = \frac{\Omega(4\Delta + 2i\gamma)}{\gamma^2 + 4\Delta^2 + 8\Omega^2} \tag{47c}$$

From this, we can easily deduce that for the stationary case we have:

$$\mathrm{Im}(\hat{\rho}_{eg}) = -\frac{\gamma}{2\Omega}\hat{\rho}_{ee} \tag{48}$$

The equations of motion can also be solved for the non-stationary case. Hereby, only the special cases with either $\Delta = 0$ or $\gamma = 0$ can be solved analytically. The general case with both values $\neq 0$ has to be solved numerically. For a documentation of how to do this in Mathematica, see Appendix B.1 and B.2.

In the following, some examples for the possible solutions are shown:

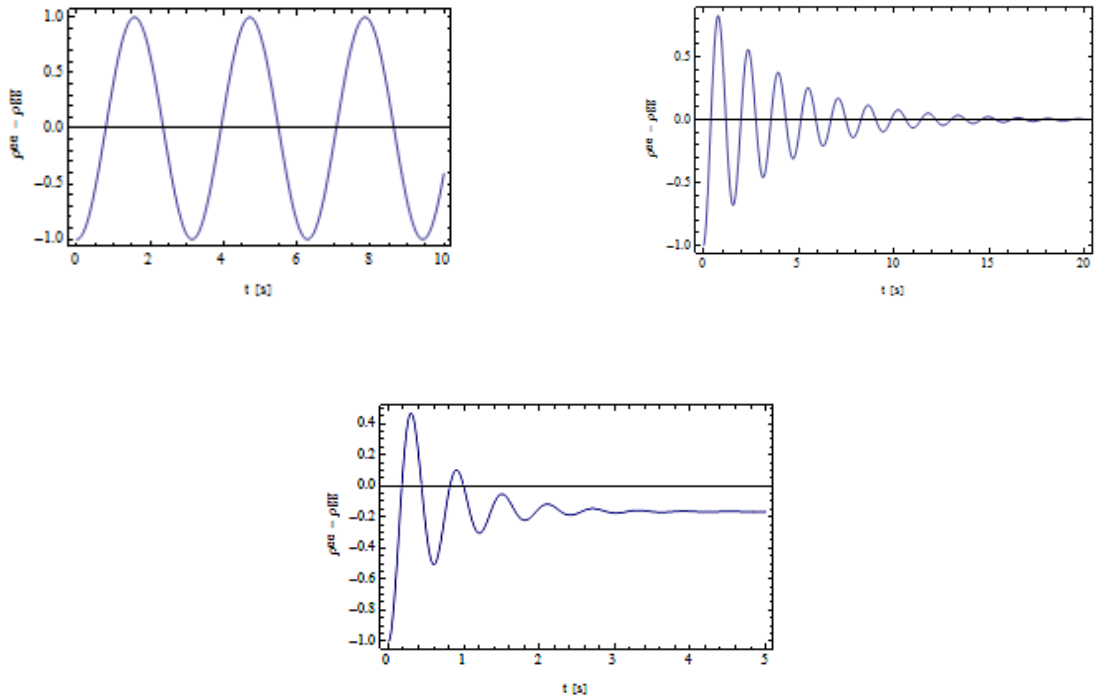

Figure 3: Population difference as a function of time for different values of Δ, γ and Ω. (top left) For $\gamma = 0, \Delta = 0$ we get normal Rabi oscillations which go on as long as the laser is active. (top right) For $\gamma \neq 0, \Delta = 0$, damping is introduced which stops the oscillations and leads to a steady state. (bottom) The most general case with $\gamma \neq 0$, $\Delta \neq 0$ which leads to reduced and damped Rabi oscillations.

2.4 Detector Signal

The detection of light normally includes the excitation of an electronic configuration. A brief introduction, which neglects the details of the experimental realization, will be given in this chapter. Moreover, the expected detection signal for the scattering of light at a two-level atom will be discussed.

2.4.1 Correlation Function

We will now study the detection of light by considering an ideal photon-counter. This counter shall work via photon absorption, i.e. a photon is absorbed by freeing an electron from a metal's surface (Photoeffect). This electron can then be detected with a Photomultiplier. The following derivation has been taken from [14]:

First, the probability for the detection of a photon is given by

$$P_{fi} \sim |\langle f| \boldsymbol{E}^{(+)}(\boldsymbol{r},t) |i\rangle|^2 \tag{49}$$

with $|i\rangle$ the initial state of the electromagnetic field and $|f\rangle$ the final state after the detector absorbed one photon. To get the total detection probability, we have to take into account all possible final states. Note that we can just sum over all states, since those that can't be reached from $|i\rangle$ by absorbing only one photon will give no contribution (they are orthogonal to $\boldsymbol{E}^{(+)}(\boldsymbol{r},t)|i\rangle$, i.e. $\langle f_\perp| \boldsymbol{E}^{(+)}(\boldsymbol{r},t)|i\rangle = 0$). Thus, the total counting rate is given by

$$\begin{aligned} I(\boldsymbol{r},t) &\sim \sum_f |\langle f| \boldsymbol{E}^{(+)}(\boldsymbol{r},t)|i\rangle|^2 && \text{(50a)}\\ &= \sum_f \Big(\langle i| \boldsymbol{E}^{(-)}(\boldsymbol{r},t)|f\rangle \langle f| \boldsymbol{E}^{(+)}(\boldsymbol{r},t)|i\rangle\Big) && \text{(50b)}\\ &= \langle i| \boldsymbol{E}^{(-)}(\boldsymbol{r},t)\boldsymbol{E}^{(+)}(\boldsymbol{r},t)|i\rangle && \text{(50c)} \end{aligned}$$

where we used $\sum_f |f\rangle\langle f| = \mathbb{1}$. Here, we assumed that the field is initially in a pure state $|i\rangle$. We can further generalize this for statistical mixtures with probability p_i for the state $|i\rangle$.

$$\begin{aligned} I(\boldsymbol{r},t) &\sim \sum_i p_i \langle i| \boldsymbol{E}^{(-)}(\boldsymbol{r},t)\boldsymbol{E}^{(+)}(\boldsymbol{r},t)|i\rangle && \text{(51a)}\\ &= \mathrm{Tr}\{\hat{\rho}\boldsymbol{E}^{(-)}(\boldsymbol{r},t)\boldsymbol{E}^{(+)}(\boldsymbol{r},t)\} && \text{(51b)} \end{aligned}$$

We can also write the result in a more neutral fashion:

$$I(\boldsymbol{r},t) \sim \langle \boldsymbol{E}^{(-)}(\boldsymbol{r},t)\boldsymbol{E}^{(+)}(\boldsymbol{r},t)\rangle \tag{52}$$

Furthermore, in the case that the electromagnetic field is a superposition of two fields $\boldsymbol{E} = \boldsymbol{E}_1 + \boldsymbol{E}_2$, we get

$$I(\boldsymbol{r}, t) \sim \langle \boldsymbol{E}^{(-)} \boldsymbol{E}^{(+)} \rangle \tag{53a}$$

$$= \underbrace{\langle \boldsymbol{E}_1^{(-)} \boldsymbol{E}_1^{(+)} \rangle}_{field\ 1\ alone} + \underbrace{\langle \boldsymbol{E}_2^{(-)} \boldsymbol{E}_2^{(+)} \rangle}_{field\ 2\ alone} + \underbrace{\langle \boldsymbol{E}_1^{(-)} \boldsymbol{E}_2^{(+)} \rangle + \langle \boldsymbol{E}_2^{(-)} \boldsymbol{E}_1^{(+)} \rangle}_{interference\ between\ field\ 1\ and\ 2} \tag{53b}$$

Later on, when we talk about the detected intensity from scattering experiments, we will get similar expressions like this one (see chapter 3.1).

2.4.2 Lorentzian Lines

Whenever we perform a standard spectroscopy experiment on a gas like ^{87}Rb or ^{133}Cs, we ordinarily irradiate a sample of the substance with a laser and detect the laser beam's intensity with a photo diode after it has passed the gas. Scanning the laser-frequency over a small range around the resonance-frequency of a certain electronic transition of the atoms, we obtain (neglecting additional broadening mechanisms like Doppler-broadening) Lorentzian line shapes. More thorough, the detected signal of the scattered light will have the form of a positive Lorentzian in dependence of the detuning Δ, and the light that passed the atomic gas will show a negative Lorentzian ([15], [16]).

This line form originates from the fact that an excited atom has a finite lifetime, i.e. it won't reemit the light spontaneously but statistically after a certain finite time γ^{-1} with γ the decay rate. We can model this by using the equation of motions for the density matrix elements from chapter 2.3.3. We will assume our atom to be in the excited state and our laser to be off. Therefore, choosing $\hat{\rho}_{ee}(0) = 1$, $\hat{\rho}_{eg}(0) = \hat{\rho}_{ge}(0) = \hat{\rho}_{gg}(0) = 0$ and $\Omega = 0$, we obtain:

$$\partial_t \hat{\rho}_{ee}(t) = -\gamma \hat{\rho}_{ee}(t) \tag{54a}$$

$$\Rightarrow \hat{\rho}_{ee}(t) = e^{-\gamma t} \tag{54b}$$

Consequently, the probability of the atom to be in the excited state decays exponentially, i.e. for early times it is very likely to observe a decay and for larger values of t it becomes more and more unlikely. The decay time of the atom is therefore exponentially distributed with expectation value γ^{-1}, which is normally denoted as the lifetime.

The emitted light is proportional to $e^{i\omega_0 t} + c.c.$ with ω_0 the frequency of the emitted light. Combining the statistical decay and the emitted plane wave, we get for the signal of a statistical ensemble of atoms [17]:

$$E(t) \sim e^{-\gamma t} e^{i\omega_0 t} + c.c. \tag{55}$$

The frequency spectrum $c(\omega)$ of this signal can be obtained by calculating the Fourier-Transform [17]:

$$c(\omega) = \int_0^\infty E(t)e^{-i\omega t}\mathrm{d}t \tag{56a}$$

$$\Rightarrow |c(\omega)|^2 \sim \frac{1}{(\omega-\omega_0)^2+\gamma^2} \tag{56b}$$

where $|c(\omega)|^2$ gives us the frequency-dependence of the emitted light's intensity. As already stated, this has the form of a Lorentzian which results from the finite decay rate γ. This is also known as the natural lineshape of a spectral line.

2.4.3 Fano Lines

In spectroscopy, Fano profiles occur due to an interference between "a spectrally broad continuum (...) with a spectrally narrow bound state" [5]. A straight forward example for this is the photoionization of an atom, which can happen two ways. For simplicity, we assume the atom to have only two electrons in its innermost shell, as it's the case for e.g. Helium.

The first way to remove one of the electrons is to excite one of them with enough energy to pass the ionization threshold. Thus, we directly excite the electron into a continuum of states. However, the electron can also be removed by exciting the atom into a quasi-discrete level, from which it can spontaneously eject one of the electrons [2]. This process is called Autoionization. For instance, one autoionizing state can be reached by exciting both electrons with only one photon, whereby the total transferred energy is larger than the ionization threshold. This way, one of the electrons can again decay to a lower level by further exciting the second electron, and therefore ionizing it (Auger effect).

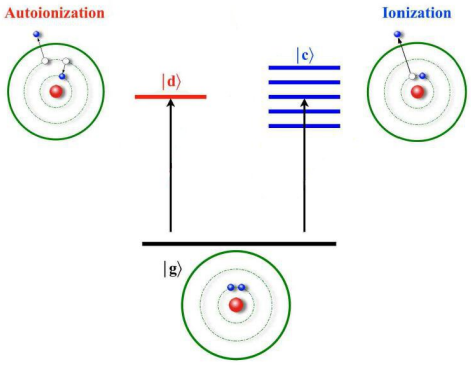

Figure 4: Ionization of Helium. There are two ways to free one of the electrons from the atom: First, via a quasi-discrete state $|d\rangle$ (Autoionization) or a continuum of states $|c\rangle$ (direct excitation). [2]

Therefore, we have two states which are coupled by two different paths, the states being a) the atom in its ground state and b) the atom with one electron ejected. As we can't be certain which ionization mechanism was used, interference occurs which leads to the observation of Fano profiles.

This effect has also been recently observed in the X-ray light reflected by thin-film cavities with Mössbauer nuclei, where the light can either a) be reflected without interacting with the nuclei (continuum channel) or b) interact with the nuclei before leaving the cavity again (discrete channel). The superposition of these two reflection channels leads again to Fano profiles [5].

Moreover, it has recently been demonstrated that this coupling between two ionization/reflection - channels can be understood in terms of a phase kick between the exciting light and the scattered field of the atom [4]. Therefore, giving the atomic dipole response an artificial phase kick enables us to manipulate the detected absorption line.

Also note that the asymmetric Fano profile can be recovered from the calculation in chapter 2.4.2:

$$c(\omega) = \int_0^\infty e^{-\gamma t} e^{-i(\omega-\omega_0)t} \mathrm{d}t \tag{57a}$$

$$= \frac{\gamma}{\gamma^2 + (\omega-\omega_0)^2} + i\frac{\omega-\omega_0}{\gamma^2 + (\omega-\omega_0)^2} \tag{57b}$$

Thus, the asymmetric Fano profile is the imaginary part of the exponential decay's spectrum. Since the absorption is proportional to $-\mathrm{Re}\big(c(\omega)\big)$ (see chapter 3.1.3 and 6.1.4), giving the decay a phase kick will mix the real - and imaginary part, such that the Fano profile is revealed.

Exactly this mechanism will be investigated thoroughly in the following chapters.

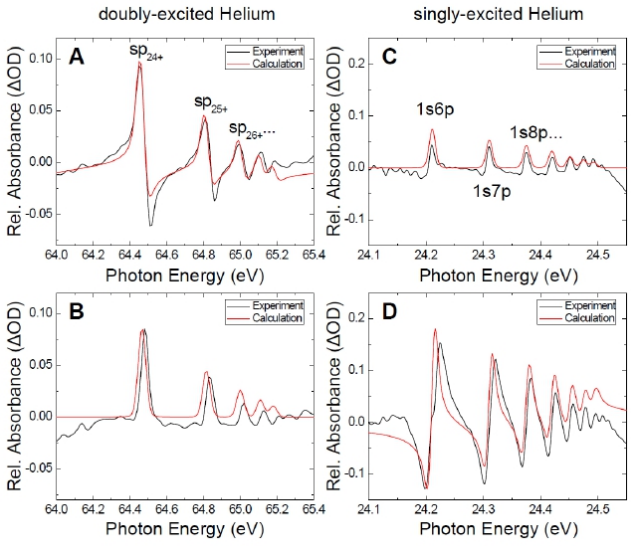

Figure 5: Experimental data showing the manipulation of the detected absorption profile. (A) Fano lines are observed in the spectrum of the transmitted broadband attosecond pulse, which originate from the interference between a discrete and a continuous ionization channel. (B) Giving the atomic response an additional phase kick transforms the absorption profile into Lorentzians. (C) Lorentz profiles which originate from the excitation of a single electron below the ionization threshold. (D) Introducing a phase kick allows us to transform the absorption profiles into Fano lines. For a more detailed explanation of the experiment and its results, see [4].

3 Scattering of Light with one Two-Level Atom

The first system we will analyse is the simple case of one atom with two-level structure which is excited by a monochromatic plane wave. By two-level structure it is meant that the laser can only drive the transition between two levels and even a larger detuning won't drive a transition to a new third level. For investigating the energy conservation in this system, appropriate "semiclassical" versions of the Poynting vectors known from Electrodynamics will be derived. These are of utter importance for all coming investigations, as they provide a nice formalism for checking energy conservation in systems where Fano control can be implemented. At the end of this chapter, we will also investigate the signal of a pointlike detector, which will reveal a Fano profile.

As has been shown in chapter 2.2.2, when a two-level atom is irradiated by a laser with the correct frequency to drive the transition $|g\rangle \leftrightarrow |e\rangle$, the resulting electromagnetic field is composed of two parts: An unscattered field $\boldsymbol{E}_{in}$ which behaves as no atom was present and a scattered field $\boldsymbol{E}_{scat}$ which is the response of the atom to the incoming field. The positive frequency part of the resulting field therefore is:

$$\boldsymbol{E}^{(+)} = \boldsymbol{E}_{in}^{(+)} + \boldsymbol{E}_{scat}^{(+)} \tag{58a}$$

$$\text{with} \quad \boldsymbol{E}_{in}^{(+)} = E_{in}\ \hat{\boldsymbol{\epsilon}}\ e^{i(\boldsymbol{k}_{in}\boldsymbol{r}-\omega_{in}t)} \tag{58b}$$

$$\text{and} \quad \boldsymbol{E}_{scat}^{(+)} = \frac{k_{in}^2}{4\pi\epsilon_0 r} e^{i(k_{in}r-\omega_{in}t)}\ \hat{S}_-\ (\hat{\boldsymbol{r}} \times \boldsymbol{d}) \times \hat{\boldsymbol{r}} \tag{58c}$$

The same decomposition can be done with the magnetic field:

$$\boldsymbol{B}^{(+)} = \boldsymbol{B}_{in}^{(+)} + \boldsymbol{B}_{scat}^{(+)} \tag{59a}$$

$$\text{with} \quad \boldsymbol{B}_{in}^{(+)} = \frac{1}{c}\left(\hat{\boldsymbol{k}}_{in} \times \boldsymbol{E}_{in}^{(+)}\right) \tag{59b}$$

$$\text{and} \quad \boldsymbol{B}_{scat}^{(+)} = \frac{1}{c}\left(\hat{\boldsymbol{r}} \times \boldsymbol{E}_{scat}^{(+)}\right) \tag{59c}$$

Of course the analogous formulas hold for the negative frequency parts of the electromagnetic field.

3.1 Energy Distribution

When we try to detect the unscattered electromagnetic field as well as the atomic response, we can't directly measure the electric and magnetic field components. The only quantity accessible for us is the intensity of the light, i.e. the energy per area and time that is transferred into our detector from the light source (here: laser and atom). In Classical Electrodynamics, the Poynting vector represents the energy current density of an electromagnetic field. Thus, it is a quantity which verifies in what directions and how much energy is transported with the electromagnetic wave. We will now motivate a semiclassical version of the Poynting vector, which is almost identical to its classical counterpart.

3.1.1 Classical Treatment: Poynting Vector

The Poynting vector is defined as [6]:

$$\boldsymbol{P} = \frac{1}{\mu_0} (\boldsymbol{E} \times \boldsymbol{B}) \tag{60}$$

Inserting the incident and scattered field components yields:

$$\begin{aligned} \boldsymbol{P} &= \frac{1}{\mu_0} ((\boldsymbol{E}_{in} + \boldsymbol{E}_{scat}) \times (\boldsymbol{B}_{in} + \boldsymbol{B}_{scat})) && \text{(61a)} \\ &= \frac{1}{\mu_0} (\boldsymbol{E}_{in} \times \boldsymbol{B}_{in} + \boldsymbol{E}_{scat} \times \boldsymbol{B}_{scat} + \boldsymbol{E}_{in} \times \boldsymbol{B}_{scat} + \boldsymbol{E}_{scat} \times \boldsymbol{B}_{in}) && \text{(61b)} \end{aligned}$$

This can be further simplified when we split up the fields in their complex parts as in eqs. 12 and take the time average over one characteristic period $T = \frac{2\pi}{\omega_{in}}$. Since the only time dependence is $e^{i\omega_{in}t}$ or $e^{-i\omega_{in}t}$, the time-averaged version of the Poynting vector can be written in a very easy form. We will demonstrate this for the first term in eq. 61b.

$$\begin{aligned} &\frac{1}{T\mu_0} \int_0^T \boldsymbol{E}_{in} \times \boldsymbol{B}_{in} \, \mathrm{d}t && \text{(62a)} \\ =&\frac{1}{T\mu_0} \int_0^T \left(\boldsymbol{E}_{in}^{(+)} + \boldsymbol{E}_{in}^{(-)}\right) \times \left(\boldsymbol{B}_{in}^{(+)} + \boldsymbol{B}_{in}^{(-)}\right) \, \mathrm{d}t && \text{(62b)} \\ =&\frac{1}{T\mu_0} \int_0^T \left(\underbrace{\boldsymbol{E}_{in}^{(-)} \times \boldsymbol{B}_{in}^{(-)}}_{\sim e^{-2i\omega t}} + \underbrace{\boldsymbol{E}_{in}^{(+)} \times \boldsymbol{B}_{in}^{(+)}}_{\sim e^{2i\omega t}} + \underbrace{\boldsymbol{E}_{in}^{(-)} \times \boldsymbol{B}_{in}^{(+)}}_{\text{no time dependence}} + \underbrace{\boldsymbol{E}_{in}^{(+)} \times \boldsymbol{B}_{in}^{(-)}}_{\text{no time dependence}} \right) \mathrm{d}t && \text{(62c)} \end{aligned}$$

The first two parts will give 0 integrated over one period. The other two parts will just give an additional factor of T which cancels the normalization factor $\frac{1}{T}$. With $\frac{1}{\epsilon_0 \mu_0} = c^2$, we can write

$$\frac{1}{T\mu_0} \int_0^T \boldsymbol{E}_{in} \times \boldsymbol{B}_{in} \, \mathrm{d}t = 2\epsilon_0 c^2 \, \mathrm{Re}(\boldsymbol{E}_{in}^{(-)} \times \boldsymbol{B}_{in}^{(+)}) \tag{63}$$

since $(\boldsymbol{E}_{in}^{(+)} \times \boldsymbol{B}_{in}^{(-)})^* = \boldsymbol{E}_{in}^{(-)} \times \boldsymbol{B}_{in}^{(+)}$. Thus, we get for the time-averaged Poynting vector:

$$\begin{aligned} \bar{\boldsymbol{P}} = &2\epsilon_0 c^2 \, \mathrm{Re}(\boldsymbol{E}_{in}^{(-)} \times \boldsymbol{B}_{in}^{(+)}) + 2\epsilon_0 c^2 \, \mathrm{Re}(\boldsymbol{E}_{scat}^{(-)} \times \boldsymbol{B}_{scat}^{(+)}) \\ &+ 2\epsilon_0 c^2 \, \mathrm{Re}(\boldsymbol{E}_{in}^{(-)} \times \boldsymbol{B}_{scat}^{(+)}) + 2\epsilon_0 c^2 \, \mathrm{Re}(\boldsymbol{E}_{scat}^{(-)} \times \boldsymbol{B}_{in}^{(+)}) \end{aligned} \tag{64}$$

Note that this resembles very much eq. 53: We have one energy part for the unscattered and scattered fields alone as well as two parts for the interference of these.

3.1.2 Quantum Mechanical Treatment

At least for the purely scattered energy part, we can't simply take eq. 64, as the scattered field contains non-commuting operators. Therefore, we will make a quantum mechanical derivation for the scattered power, inspired by [12]. In this derivation, we assume again that the laser is not purely monochromatic but has a finite spectral width $\Delta\omega$.

First, the expectation value for the energy of a single mode of the electromagnetic field is given by $\hbar\omega \langle \hat{a}^\dagger(t)\hat{a}(t)\rangle$. Therefore, the power delivered by the unscattered and scattered field can be calculated via

$$P(t) = \frac{d}{dt}\sum_{\boldsymbol{k},\lambda} \hbar\omega_{\boldsymbol{k},\lambda} \langle \hat{a}^\dagger(t)\hat{a}(t)\rangle \tag{65}$$

where we sum over all possible wave vectors $\boldsymbol{k}$ and the two contributions from the polarizations λ. $\hat{a}(t)$ has already been calculated in chapter 2.2.2. Thus, we get:

$$\begin{aligned} P(t) = \frac{d}{dt}\sum_{\boldsymbol{k},\lambda} \hbar\omega_{\boldsymbol{k},\lambda} \Big(& \underbrace{\langle \hat{a}^\dagger(0)\hat{a}(0)\rangle}_{incident\ energy} - \underbrace{\int_0^t g \langle \hat{S}_{eg}(t')\hat{a}(0)\rangle e^{-i\omega t'}\,\mathrm{d}t' - \int_0^t g^* \langle \hat{a}^\dagger(0)\hat{S}_{ge}(t')\rangle e^{i\omega t'}\,\mathrm{d}t'}_{interference\ energy} \\ & + \underbrace{\int_0^t\int_0^t |g|^2 \langle \hat{S}_{eg}(t'')\hat{S}_{ge}(t')\rangle e^{i\omega(t'-t)} e^{i\omega(t-t'')}\mathrm{d}t'\mathrm{d}t''}_{scattered\ energy} \Big) \end{aligned} \tag{66}$$

Note that again, we have contributions from the scattered and unscattered fields as well as an interference part. However, since we are only looking at the change in energy of the electromagnetic field that is being induced by the interaction with the atom, the unscattered part vanishes when we calculate the power. Also, it's important to keep in mind that a rotating wave approximation has already been done here, getting rid of the terms that were averaged out in the classical case (see eq. 62c). In the following, we will further analyse the scattered part. To reduce the notation, we will neglect some of the prefactors and add them again later:

$$\begin{aligned} & \frac{d}{dt}\left(\int_0^t\int_0^t |g|^2 \langle \hat{S}_{eg}(t'')\hat{S}_{ge}(t')\rangle e^{i\omega(t'-t)} e^{i\omega(t-t'')}\mathrm{d}t'\mathrm{d}t''\right) \\ =& |g|^2 \int_0^t \frac{d}{dt}\left(\int_0^t \langle \hat{S}_{eg}(t'')\hat{S}_{ge}(t')\rangle e^{i\omega(t'-t)}\mathrm{d}t'\right) e^{i\omega(t-t'')}\mathrm{d}t'' \\ +& |g|^2 \int_0^t \frac{d}{dt}\left(\int_0^t \langle \hat{S}_{eg}(t'')\hat{S}_{ge}(t')\rangle e^{i\omega(t-t'')}\mathrm{d}t''\right) e^{i\omega(t'-t)}\mathrm{d}t' \end{aligned} \tag{67}$$

This can be evaluated by using the following identity: Let $g(t)$ be an integrable function g: $\mathbb{R}_0^+ \to \mathbb{C}$.

Furthermore let $G(t)$ be the general antiderivative of $g(t)$. Then we have:

$$\frac{d}{dt}\left(\int_0^t g(t')\mathrm{d}t'\right) \tag{68a}$$

$$=\frac{d}{dt}\left(G(t)-G(0)\right) \tag{68b}$$

$$=g(t) \tag{68c}$$

We can use this to evaluate eq. 67. Note that in the e-functions, there is also a factor t which has to be considered when taking the derivative. However, the resulting terms due to these derivatives cancel each other and we get:

$$P_{scat}(t) = |g|^2 \int_0^t \langle \hat{S}_{eg}(t'')\hat{S}_{ge}(t)\rangle \, e^{i\omega(t-t'')}\mathrm{d}t'' + |g|^2 \int_0^t \langle \hat{S}_{eg}(t)\hat{S}_{ge}(t')\rangle \, e^{i\omega(t'-t)}\mathrm{d}t' \tag{69}$$

Substituting $t' \to t''$, this can be further simplified:

$$P_{scat}(t) = 2\mathrm{Re}(\int_0^t |g|^2 \, \langle \hat{S}_{eg}(t'')\hat{S}_{ge}(t)\rangle \, e^{i\omega(t-t'')}\mathrm{d}t'') \tag{70}$$

We will now reintroduce the prefactors and replace $g = -\sqrt{\frac{\omega_{\boldsymbol{k},\lambda}}{2\hbar\epsilon_0 V}}\ \boldsymbol{d}\cdot\hat{\boldsymbol{\epsilon}}_{\boldsymbol{k},\lambda} = -\sqrt{\frac{\omega_{\boldsymbol{k},\lambda}}{2\hbar\epsilon_0 V}}\ d\cos\left(\frac{\pi}{2}-\theta\right) = -\sqrt{\frac{\omega_{\boldsymbol{k},\lambda}}{2\hbar\epsilon_0 V}}\ d\sin\theta$. It is important to remember that θ is the angle between the z-axis and the wave-vector $\boldsymbol{k}$. Furthermore, the polarization-vectors $\hat{\boldsymbol{\epsilon}}_{\boldsymbol{k},\lambda}$ is always orthogonal to the wave-vector. Therefore, when we define $\boldsymbol{d}$ to be along the z-direction, we can choose $\hat{\boldsymbol{\epsilon}}_{\boldsymbol{k},1}$ such that the angle between $\boldsymbol{d}$ and $\hat{\boldsymbol{\epsilon}}_{\boldsymbol{k},1}$ is $\frac{\pi}{2}-\theta$. This way, $\boldsymbol{d}\cdot\hat{\boldsymbol{\epsilon}}_{\boldsymbol{k},2} = 0$ for all θ and we can neglect the polarization sum.

$$P_{scat}(t) = \sum_{\boldsymbol{k}} \frac{\omega_{\boldsymbol{k},\lambda}^2 d^2 \sin^2\theta}{\epsilon_0 V}\mathrm{Re}(\int_0^t \langle \hat{S}_{eg}(t'')\hat{S}_{ge}(t)\rangle \, e^{i\omega(t-t'')}\mathrm{d}t'') \tag{71}$$

Next, we can replace the sum by an integral with the appropriate density of modes $\sum_{\boldsymbol{k}} \to \frac{V}{(2\pi)^3 c^3}\int_0^\infty\int_0^{2\pi}\int_0^\pi \omega^2\sin\theta\ \mathrm{d}\omega\mathrm{d}\phi\mathrm{d}\theta$.

$$P_{scat}(t) = \frac{V}{(2\pi)^3 c^3}\int_0^\infty\int_0^{2\pi}\int_0^\pi \mathrm{d}\omega\mathrm{d}\phi\mathrm{d}\theta\frac{\omega^4 d^2\sin^3\theta}{\epsilon_0 V}\mathrm{Re}(\int_0^t \langle \hat{S}_{eg}(t'')\hat{S}_{ge}(t)\rangle \, e^{i\omega(t-t'')}\mathrm{d}t'') \tag{72a}$$

$$= \int_0^\infty \mathrm{d}\omega\ \frac{\omega^4 d^2}{3\pi^2 c^3\epsilon_0}\mathrm{Re}(\int_0^t \langle \hat{S}_{eg}(t'')\hat{S}_{ge}(t)\rangle \, e^{i\omega(t-t'')}\mathrm{d}t'') \tag{72b}$$

For this step, we also used $\int_0^{2\pi}\int_0^\pi \sin^3\theta\ \mathrm{d}\phi\mathrm{d}\theta = \frac{8\pi}{3}$. We will now use the same approximation as in

chapter 2.2.2 to solve the integral $\int_0^t \langle \hat{S}_{eg}(t'')\hat{S}_{ge}(t)\rangle\, e^{i\omega(t-t'')}\mathrm{d}t''$. Hence, we get:

$$P_{scat}(t) \simeq \int_0^\infty \mathrm{d}\omega\ \frac{\omega^4 d^2}{3\pi^2 c^3 \epsilon_0} \mathrm{Re}\Big(\int_0^t \langle \hat{S}_{eg}(t)\hat{S}_{ge}(t)\rangle\, e^{i(\omega-\omega_0)(t-t'')}\mathrm{d}t''\Big) \tag{73a}$$

$$\simeq \int_0^\infty \mathrm{d}\omega\ \frac{\omega^4 d^2}{3\pi^2 c^3 \epsilon_0} \mathrm{Re}\,\langle \hat{S}_{eg}(t)\hat{S}_{ge}(t)\rangle\, \delta(\omega-\omega_0) \tag{73b}$$

$$= \frac{\omega_0^4 d^2}{3\pi^2 c^3 \epsilon_0} \mathrm{Re}\,\langle \hat{S}_{eg}(t)\hat{S}_{ge}(t)\rangle \tag{73c}$$

Here, we used $\int_0^t e^{i(\omega-\omega_0)(t-t'')}\mathrm{d}t'' \simeq 2\pi\delta(\omega-\omega_0)$ [11]. It's now possible to insert the scattered fields for the operators (eqs. 58).

$$\langle \boldsymbol{E}^{(-)}\boldsymbol{E}^{(+)}\rangle = \frac{k_0^4}{(4\pi\epsilon_0 r)^2}\langle \hat{S}_{eg}\hat{S}_{ge}\rangle \int_0^{2\pi}\int_0^{\pi} |(\hat{\boldsymbol{r}}\times\boldsymbol{d})\times\hat{\boldsymbol{r}}|^2 r^2 \sin\theta\ \mathrm{d}\phi\mathrm{d}\theta \tag{74a}$$

$$= \frac{8\pi k_0^4 d^2}{3(4\pi\epsilon_0)^2}\langle \hat{S}_{eg}\hat{S}_{ge}\rangle \tag{74b}$$

An integration over a spherical surface has been performed, since the Poynting vector has the dimension of an energy current density, not a power. Thus, we have to transform eq. 73c into an intensity. This is the same as reversing the surface integral in eq. 72. The integral in eq. 74a can be solved as follows:

$$|(\hat{\boldsymbol{r}}\times\boldsymbol{d})\times\hat{\boldsymbol{r}}|^2 \tag{75a}$$

$$= |\boldsymbol{d} - \hat{\boldsymbol{r}}(\hat{\boldsymbol{r}}\cdot\boldsymbol{d})|^2 \tag{75b}$$

$$= d^2 - 2(\hat{\boldsymbol{r}}\cdot\boldsymbol{d})^2 + (\hat{\boldsymbol{r}}\cdot\boldsymbol{d})^2 \tag{75c}$$

$$= d^2(1-\cos^2\theta) \tag{75d}$$

$$= d^2\sin^2\theta \tag{75e}$$

$$\Rightarrow \int_0^{2\pi}\int_0^{\pi} \sin^3\theta\ \mathrm{d}\phi\mathrm{d}\theta = \frac{8\pi}{3} \tag{75f}$$

where the angle between $\hat{\boldsymbol{r}}$ and $\boldsymbol{d}$ is again defined as θ and we used the Grassmann-Identity to simplify the vector-products. Inserting this into eq. 73c yields:

$$I_{scat} = \frac{3(4\pi\epsilon_0)^2\hbar\omega_0^4 d^2}{24\pi^2\epsilon_0\hbar c^3 k_0^4 d^2}\ \mathrm{Re}\,\langle \boldsymbol{E}^{(-)}\boldsymbol{E}^{(+)}\rangle \tag{76a}$$

$$= 2\epsilon_0 c\ \mathrm{Re}\,\langle \boldsymbol{E}^{(-)}\boldsymbol{E}^{(+)}\rangle \tag{76b}$$

The direction of the energy current density can be obtained by remembering that the Poynting vector is

proportional to $\boldsymbol{E} \times \boldsymbol{B}$ and $\hat{\boldsymbol{B}} = \hat{\boldsymbol{r}} \times \hat{\boldsymbol{E}}$:

$$\hat{\boldsymbol{P}}_{scat} \sim \hat{\boldsymbol{E}} \times \hat{\boldsymbol{B}} \tag{77a}$$

$$= \hat{\boldsymbol{E}} \times (\hat{\boldsymbol{r}} \times \hat{\boldsymbol{E}}) \tag{77b}$$

$$= \hat{\boldsymbol{r}} \underbrace{(\hat{\boldsymbol{E}} \cdot \hat{\boldsymbol{E}})}_{=1} - \hat{\boldsymbol{E}} \underbrace{(\hat{\boldsymbol{r}} \cdot \hat{\boldsymbol{E}})}_{=0} \tag{77c}$$

$$= \hat{\boldsymbol{r}} \tag{77d}$$

Thus, our final result for the Poynting vector is:

$$P_{scat} = 2\epsilon_0 c \, \mathrm{Re} \, \langle \boldsymbol{E}^{(-)} \boldsymbol{E}^{(+)} \rangle \, \hat{\boldsymbol{r}} \tag{78}$$

In the next chapter, we will see that this strongly resembles the classical version of the Poynting vector.

3.1.3 "Semiclassical" - Version of the Poynting Vector

Our goal now is to find a general expression for the Poynting vector of the atom-light system. First, we will rewrite eq. 63 to show that it can be brought into a similar form as eq. 78.

$$\boldsymbol{P}_{in} = 2\epsilon_0 c^2 \, \mathrm{Re}(\boldsymbol{E}_{in}^{(-)} \times \boldsymbol{B}_{in}^{(+)}) \tag{79a}$$

$$= 2\epsilon_0 c^2 \, \mathrm{Re}(\boldsymbol{E}_{in}^{(-)} \times (\frac{1}{c} \hat{\boldsymbol{k}} \times \boldsymbol{E}_{in}^{(+)})) \tag{79b}$$

$$= 2\epsilon_0 c \, \mathrm{Re}(\boldsymbol{E}_{in}^{(-)} \times (\hat{\boldsymbol{k}} \times \boldsymbol{E}_{in}^{(+)})) \tag{79c}$$

$$= 2\epsilon_0 c \, \mathrm{Re}(\hat{\boldsymbol{k}} (\boldsymbol{E}_{in}^{(-)} \boldsymbol{E}_{in}^{(+)}) - \boldsymbol{E}_{in}^{(+)} \underbrace{(\boldsymbol{E}_{in}^{(-)} \hat{\boldsymbol{k}})}_{=0}) \tag{79d}$$

$$= 2\epsilon_0 c \, \mathrm{Re}(\boldsymbol{E}_{in}^{(-)} \boldsymbol{E}_{in}^{(+)}) \, \hat{\boldsymbol{k}} \tag{79e}$$

Analogous, we get for the classical Poynting vector of the scattered field:

$$\boldsymbol{P}_{scat} = 2\epsilon_0 c \, \mathrm{Re}(\boldsymbol{E}_{scat}^{(-)} \boldsymbol{E}_{scat}^{(+)}) \, \hat{\boldsymbol{r}} \tag{80}$$

This is the same as the quantum mechanical version (eq. 78), except that in the classical case, no expectation value is taken. Thus, to transition from the classical case to the quantum case, we only have to take the expectation value of the fields, as they have been promoted to operators.

Now, only the interference parts are missing:

$$2\epsilon_0 c^2 \ \mathrm{Re}(\boldsymbol{E}_{in}^{(-)} \times \boldsymbol{B}_{scat}^{(+)}) = 2\epsilon_0 c^2 \ \mathrm{Re}(\boldsymbol{E}_{in}^{(-)} \times (\frac{1}{c}\hat{\boldsymbol{r}} \times \boldsymbol{E}_{scat}^{(+)})) \tag{81a}$$

$$= 2\epsilon_0 c \ \mathrm{Re}(\hat{\boldsymbol{r}}(\boldsymbol{E}_{in}^{(-)}\boldsymbol{E}_{scat}^{(+)}) - \boldsymbol{E}_{scat}^{(+)}(\boldsymbol{E}_{in}^{(-)}\hat{\boldsymbol{r}})) \tag{81b}$$

The same way, we get:

$$2\epsilon_0 c^2 \ \mathrm{Re}(\boldsymbol{E}_{scat}^{(-)} \times \boldsymbol{B}_{in}^{(+)}) = 2\epsilon_0 c \ \mathrm{Re}(\hat{\boldsymbol{k}}(\boldsymbol{E}_{scat}^{(-)}\boldsymbol{E}_{in}^{(+)}) - \boldsymbol{E}_{in}^{(+)}(\boldsymbol{E}_{scat}^{(-)}\hat{\boldsymbol{k}})) \tag{82}$$

For $r \to \infty$, the second part in both expressions vanishes, as can be shown by performing brute-force calculations. Consequently, the interference part can be written as:

$$\boldsymbol{P}_{inter} = 2\epsilon_0 c \ \mathrm{Re}(\boldsymbol{E}_{in}^{(-)}\boldsymbol{E}_{scat}^{(+)}) \ \hat{\boldsymbol{r}} + 2\epsilon_0 c \ \mathrm{Re}(\boldsymbol{E}_{scat}^{(-)}\boldsymbol{E}_{in}^{(+)}) \ \hat{\boldsymbol{k}} \tag{83}$$

Finally, when we include taking expectation values as has been shown in the previous chapter, we get as our final result:

$$\begin{aligned}\boldsymbol{P} = &\underbrace{2\epsilon_0 c \ \mathrm{Re}\,\langle \boldsymbol{E}_{in}^{(-)}\boldsymbol{E}_{in}^{(+)}\rangle \,\hat{\boldsymbol{k}}}_{=\boldsymbol{P}_{in}} + \underbrace{2\epsilon_0 c \ \mathrm{Re}\,\langle \boldsymbol{E}_{scat}^{(-)}\boldsymbol{E}_{scat}^{(+)}\rangle \,\hat{\boldsymbol{r}}}_{=\boldsymbol{P}_{scat}} \\ &+ \underbrace{2\epsilon_0 c \ \mathrm{Re}\,\langle \boldsymbol{E}_{in}^{(-)}\boldsymbol{E}_{scat}^{(+)}\rangle \ \hat{\boldsymbol{r}} + 2\epsilon_0 c \ \mathrm{Re}\,\langle \boldsymbol{E}_{scat}^{(-)}\boldsymbol{E}_{in}^{(+)}\rangle \ \hat{\boldsymbol{k}}}_{=\boldsymbol{P}_{inter}}\end{aligned} \tag{84}$$

Note that this is the same result as for the correlation function in chapter 2.4.1. We added only the prefactor $2\epsilon_0 c$, through which the Poynting vector also gets the correct units of an energy current density:

$$[\epsilon_0 c E^2] = \frac{\mathrm{As}}{\mathrm{Vm}}\frac{\mathrm{m}}{\mathrm{s}}\frac{\mathrm{V}^2}{\mathrm{m}^2} = \frac{\mathrm{J}}{\mathrm{s\ m}^2} \tag{85}$$

Further on, the directions in which the energy current density flows has been included as unit vectors. These have been taken from the classical Poynting vectors of the unscattered and scattered electromagnetic fields. This Poynting vector will be our starting point for every energy analysis we perform in this thesis.

3.2 Analysis without Phase Kick

Now that we have taken a look at the correct Poynting vectors, we can investigate the energy conservation in a system consisting of one atom which is being excited by a plane laser beam. However, we will neglect

loss channels like momentum transfer to the atom by assuming these to give no contribution in a time average. Furthermore, we will analyse the detector signal in forward direction and investigate what happens when an additional phase kick is introduced to the scattered field.

3.2.1 Energy Conservation

We start by examining if energy conservation holds. The main idea is to put the whole system into a sphere, such that it is totally isolated from any outside influences. Then, the power flowing into the sphere has to equal the one leaving the sphere for energy conservation to hold. If both contributions didn't cancel out to zero, there had to be an energy source inside the sphere which we didn't take into account. Otherwise, energy would have been created from nothing.

The Poynting vector for the scattering of light by a two level atom has already been derived in the previous chapter. Consequently, we get for the incident field

$$\boldsymbol{P}_{in} = 2\epsilon_0 c \ \mathrm{Re}\,\langle \boldsymbol{E}_{in}^{(-)} \boldsymbol{E}_{in}^{(+)} \rangle \ \hat{\boldsymbol{k}} \tag{86a}$$

$$= 2\epsilon_0 c E_{in}^2 \ \hat{\boldsymbol{k}} \tag{86b}$$

where we used eqs. 58. The flux out of an imaginary sphere with radius r and the atom's position as the center can now be calculated as follows:

$$W_{in} = \oint \boldsymbol{P}_{in} \cdot \mathrm{d}\boldsymbol{A} \tag{87a}$$

$$= 2\epsilon_0 c E_{in}^2 \int_0^{2\pi} \int_0^{\pi} \hat{\boldsymbol{k}} \cdot \hat{\boldsymbol{r}} \ r^2 \sin\theta \ \mathrm{d}\phi \mathrm{d}\theta \tag{87b}$$

$$= 2\epsilon_0 c E_{in}^2 k r^2 \int_0^{2\pi} \int_0^{\pi} \cos\phi \sin^2\theta \ \mathrm{d}\phi \mathrm{d}\theta \tag{87c}$$

$$= 0 \tag{87d}$$

Here, we defined $\boldsymbol{k} = (k, 0, 0)$ and used $\hat{\boldsymbol{r}} = (\cos\phi \sin\theta, \sin\phi \sin\theta, \cos\theta)$. The result is of course expected, since for a plane wave that goes through a sphere, what comes in has to come out again. For the scattered part, we get (with eq. 75 and eq. 41c):

$$\boldsymbol{P}_{scat} = 2\epsilon_0 c \ \mathrm{Re}\,\langle \boldsymbol{E}_{scat}^{(-)} \boldsymbol{E}_{scat}^{(+)} \rangle \ \hat{\boldsymbol{r}} \tag{88a}$$

$$= 2\epsilon_0 c \frac{k_0^4}{16\pi^2 \epsilon_0^2 r^2} \langle \hat{S}_+ \hat{S}_- \rangle \left| \boldsymbol{d} - \hat{\boldsymbol{r}}(\hat{\boldsymbol{r}} \cdot \boldsymbol{d}) \right|^2 \hat{\boldsymbol{r}} \tag{88b}$$

$$= \frac{\omega_0 k_0^3 d^2}{8\pi^2 \epsilon_0 r^2} \hat{\rho}_{ee} \sin^2\theta \ \hat{\boldsymbol{r}} \tag{88c}$$

$$= \frac{3}{8\pi r^2} \hbar \omega_0 \gamma \hat{\rho}_{ee} \sin^2\theta \ \hat{\boldsymbol{r}} \tag{88d}$$

Thus, the flux is:

$$W_{scat} = \oint \boldsymbol{P}_{scat} \cdot \mathrm{d}\boldsymbol{A} \tag{89a}$$

$$= \frac{3}{8\pi r^2}\hbar\omega_0\gamma\hat{\rho}_{ee}\int_0^{2\pi}\int_0^{\pi} r^2 \sin^3\theta \; \hat{\boldsymbol{r}} \cdot \hat{\boldsymbol{r}} \; \mathrm{d}\phi\mathrm{d}\theta \tag{89b}$$

$$= \hbar\omega_0\gamma\hat{\rho}_{ee} \tag{89c}$$

This is the well known energy scattering rate of a two level atom. Moreover, the contribution is positive, since the atom is a source of electromagnetic waves which start at the atom's position and leave the sphere. Now, the energy taken out of the incident field is represented by the interference part. For the Poynting vector, we get:

$$\boldsymbol{P}_{inter} = 2\epsilon_0 c \; \mathrm{Re}\,\langle \boldsymbol{E}_{in}^{(-)} \boldsymbol{E}_{scat}^{(+)} \rangle \;\; \hat{\boldsymbol{r}} + 2\epsilon_0 c \; \mathrm{Re}\,\langle \boldsymbol{E}_{scat}^{(-)} \boldsymbol{E}_{in}^{(+)} \rangle \;\; \hat{\boldsymbol{k}} \tag{90a}$$

$$= 2\epsilon_0 c \frac{E_0 k_0^2}{4\pi\epsilon_0 r}\hat{\boldsymbol{\epsilon}} \cdot ((\hat{\boldsymbol{r}} \times \boldsymbol{d}) \times \hat{\boldsymbol{r}})\,\mathrm{Re}\big(e^{i(k_0 r - \boldsymbol{k_0 r})} \langle \hat{S}_- \rangle \;\; \hat{\boldsymbol{r}}\big)$$

$$+ 2\epsilon_0 c \frac{E_0 k_0^2}{4\pi\epsilon_0 r}\hat{\boldsymbol{\epsilon}} \cdot ((\hat{\boldsymbol{r}} \times \boldsymbol{d}) \times \hat{\boldsymbol{r}})\,\mathrm{Re}\big(e^{-i(k_0 r - \boldsymbol{k_0 r})} \langle \hat{S}_+ \rangle \;\; \hat{\boldsymbol{k}}\big) \tag{90b}$$

$$= \frac{E_0 k_0 \omega_0}{\pi r}\hat{\boldsymbol{\epsilon}} \cdot ((\hat{\boldsymbol{r}} \times \boldsymbol{d}) \times \hat{\boldsymbol{r}})\,\mathrm{Re}\left(e^{i(k_0 r - \boldsymbol{k_0 r})}\hat{\rho}_{eg} \;\; \hat{\boldsymbol{r}} + e^{-i(k_0 r - \boldsymbol{k_0 r})}\hat{\rho}_{ge} \;\; \hat{\boldsymbol{k}}\right) \tag{90c}$$

Calculating the flux of this expression is quite difficult, but we can do this numerically in Mathematica. For $r \to \infty$, our result then is:

$$W_{inter} = \lim_{r\to\infty} \oint \boldsymbol{P}_{inter} \cdot \mathrm{d}\boldsymbol{A} \tag{91a}$$

$$= 2\hbar\omega_0\Omega\mathrm{Im}(\hat{\rho}_{eg}) \tag{91b}$$

$$= 2\hbar\omega_0\Omega(-\frac{\gamma}{2\Omega})\hat{\rho}_{ee} \tag{91c}$$

$$= -\hbar\omega_0\gamma\hat{\rho}_{ee} \tag{91d}$$

And thus, we get for the total flux entering and leaving the closed sphere with radius r:

$$W = \oint \boldsymbol{P} \cdot \mathrm{d}\boldsymbol{A} \tag{92a}$$

$$= \oint (\boldsymbol{P}_{in} + \boldsymbol{P}_{scat} + \boldsymbol{P}_{inter}) \cdot \mathrm{d}\boldsymbol{A} \tag{92b}$$

$$= 0 + \hbar\omega_0\gamma\hat{\rho}_{ee} - \hbar\omega_0\gamma\hat{\rho}_{ee} \tag{92c}$$

$$= 0 \tag{92d}$$

As we see, the energy is conserved. Therefore, the energy used to create the scattered field has been taken directly from the incident field. The atom scatters some of the ingoing wave into radial direction, as we already expected.

3.2.2 Detected Signal

Up next we have a look at the detected signal of the total field. As can be easily obtained, the scattered part $\boldsymbol{P}_{scat}$ (eq. 88d) has the form of a positive Lorentzian in dependence of the detuning Δ. This is a result of the finite emission time or, better said, of the fact that the decay time is finite and distributed exponentially, leading to a Lorentzian spectrum. Furthermore, the energy distribution only depends on the angle θ, what originates from the fact that a) a dipole doesn't radiate energy along its oscillation axis and b) emits most energy into the plane orthogonal to its oscillation.

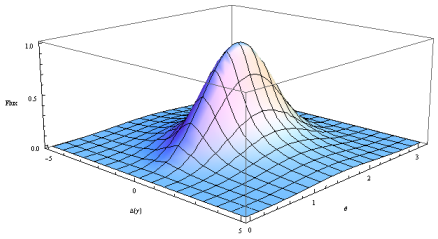

Figure 6: Norm of $\boldsymbol{P}_{scat}$ in different directions and with different detunings Δ. While changing Δ, we get a Lorentz profile. Changing θ only results into altering the amplitude of the signal due to the factor $\sin^3\theta$.

The interference part $\boldsymbol{P}_{inter}$ is much more complicated. For instance, for $\theta = \frac{\pi}{2}$, we get for the differential flux $\boldsymbol{P}_{inter} \cdot \hat{\boldsymbol{r}}$ with $\hat{\boldsymbol{r}}$ the unit vector in radial direction of the sphere:

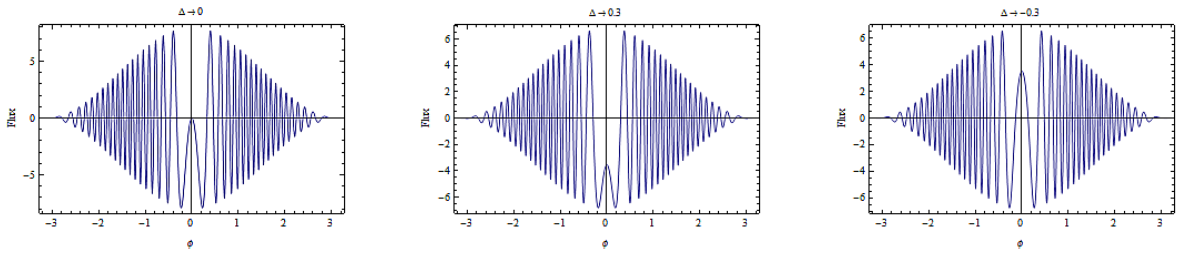

Figure 7: Detected signal of the interference part for $\theta = \frac{\pi}{2}$ and different values of Δ in dependence of ϕ. For large values of ϕ, we get rapid oscillations. Varying Δ only changes the signal around $\phi = 0$.

Thus, for $\phi \simeq 0$, we have a well defined behaviour which evolves to strong oscillations for larger values of ϕ. This can be explained quite intuitively in our picture, since $\phi = 0$ is the propagation direction of the incident wave. Therefore, small changes in ϕ will only result in small changes in the phase difference between incident and scattered wave. But for larger values of ϕ, these phase differences will become big for small deviations of ϕ, hence the signal starts oscillating very rapidly. Also, Δ changes the flux in forward direction. Because of this, we will investigate the signal detected by a pointlike detector in

forward direction more closely:

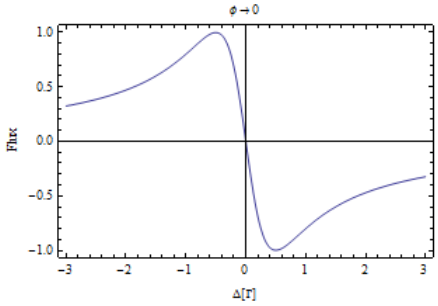

Figure 8: Detected signal of the interference part in forward direction for a pointlike detector. Rather unexpected, we get a Fano profile and not an Lorentzian absorption profile as in standard spectroscopy experiments.

Despite expectation, this is not a negative Lorentz profile. Instead, we have a Fano profile what can be seen even easier by rearranging eq. 90c for the case $\phi = 0$ and $\theta = \frac{\pi}{2}$.

$$P_{scat}\Big|_{(\phi=0,\ \theta=\frac{\pi}{2})} = -\frac{k_0}{\pi r}\hbar\omega_0\Omega\mathrm{Re}(\hat{\rho}_{eg}) \tag{93a}$$

$$= -\frac{4\hbar\omega_0 k_0}{\pi r}\frac{\Omega^2\Delta}{\gamma^2 + 4\Delta^2 + 8\Omega^2} \tag{93b}$$

Further, the contribution in forward direction depends on the real-part of $\hat{\rho}_{eg}$, which is responsible for the refraction of light in optical physics. As a reminder, the imaginary part of $\hat{\rho}_{eg}$ leads to absorption of light by a given medium [10]. Therefore, we are scanning the refractive index of the atom by comparing the scattered light in forward direction with an unscattered wave. The phase difference between the two leads to the observed profile. However, a real detector has a finite detection size and thus, we actually have to integrate over a certain area. It can be shown that doing this will reintroduce the well known Lorentzian absorption line [18]. In chapter 4, we will take a similar approach and transition from one atom to many atoms, what will also result in recovering the expected negative Lorentz profile.

3.3 Analysis with Phase Kick

Next, we will give the scattered field an additional phase kick $\phi_k \in [0, 2\pi)$, i.e. $\boldsymbol{E}^{(+)}_{scat} = \frac{k_0^2}{4\pi\epsilon_0 r}\hat{S}_- e^{i(k_0 r + \phi_k)}(\hat{\boldsymbol{r}} \times \boldsymbol{d}) \times \hat{\boldsymbol{r}}$. As we will see, with this phase kick we are able to control the line shape of the detected signal.

3.3.1 Energy Conservation

Introducing the phase kick doesn't change anything at $\boldsymbol{P}_{in}$ and $\boldsymbol{P}_{scat}$, as the phase information is lost in these expressions. But the interference part changes and we have to calculate the total flux anew.

Evaluating this numerically, we get:

$$W_{inter} = 2\omega\Omega\hbar\big(\cos\phi_k \mathrm{Im}(\hat{\rho}_{eg}) + \sin\phi_k \mathrm{Re}(\hat{\rho}_{eg})\big) \tag{94a}$$

$$\Rightarrow \quad W = \hbar\omega_0\hat{\rho}_{ee}\,(\gamma - \gamma\cos\phi_k + 2\Delta\sin\phi_k) \tag{94b}$$

For $\phi_k \to 0$, we have energy conservation but for $\phi_k \neq 0$, energy is not conserved. In the next chapter, we will show that introducing this phase kick allows us to change the detected line shape in forward direction. However, introducing a phase kick will lead to a breaking of energy conservation for the many atom scenario, too. A more thorough analysis concerning the energy conservation in this case will be done in chapter 6.4.

3.3.2 Detected Signal in Forward Direction

As already mentioned, introducing a phase kick enables us to change the line shape of the detected signal. Since only the interference part changes, we'll blend out the incident and scattered part in this analysis. For the detected signal in forward direction, we therefore get:

$$P_{scat}\Big|_{(\phi=0,\ \theta=\frac{\pi}{2})} = -\frac{\hbar\omega_0 k_0}{\pi r}\Omega\big(\cos\phi_k \mathrm{Re}(\hat{\rho}_{eg}) - \sin\phi_k \mathrm{Im}(\hat{\rho}_{eg})\big) \tag{95a}$$

$$= \frac{\hbar\omega_0 k_0}{2\pi r}\hat{\rho}_{ee}\big(\gamma\cos\phi_k + 2\Delta\sin\phi_k\big) \tag{95b}$$

This is similar to the result we obtained for the energy conservation. Note that for $\phi_k \to 0$, we get the old result eq. 93b. Accordingly, by giving the scattered light an additional phase kick, we get a mixing of the real and imaginary part of $\hat{\rho}_{eg}$. This gives us the possibility to control the line shape of the detected signal (in dependence of Δ):

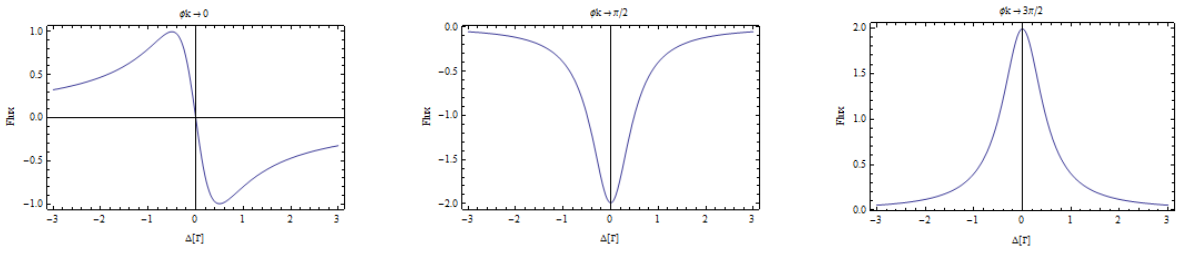

Figure 9: Detected signal of the interference part in forward direction with an additional phase kick ϕ_k. Depending on the value of ϕ_k, we can transform between Lorentz and Fano profiles.

We will analyse this further in the coming chapters. But first, the transition to many atoms will be done as this allows us to simplify our formalism considerably.

4 Generalization for Many Two-Level Atoms

We now generalize our formalism for a gas consisting of many identical two-level atoms. This will allow us to motivate an approximation which tremendously simplifies all the calculations concerning energy conservation. As a consequence, even more complex cases like excitation by laser pulses can be analysed. Furthermore, it's possible to show that the absorption line can be altered to a Fano profile by introducing a phase kick onto the atomic answer. Additionally, this formalism can be extended to three-level systems, in which the phase kick can be modelled with a second laser.

4.1 Transition to Many Two-Level Atoms

First, we take a look at the case of two atoms. An obvious main difference to the case of one atom is that, since both atoms don't occupy the same position in space, they have different path lengths to the detector. Thus, depending on the position of the detector, the two emitted waves will either add constructively or destructively (see fig. 10). We define the resulting phase-difference to be "negative".

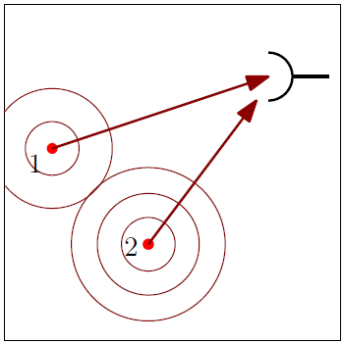

Figure 10: Two atoms (red) both emitting a spherical wave (dark red) which are detected at an detector (end of arrows). It is easy to see that both waves arrive with a phase-difference which depends on the detector position.

Another difference is that both atoms start emitting light at different times. As the incoming wave hits one of the atoms first, this atom will have already emitted light for some time before the second one gets excited (see fig. 11). This way, a "positive" phase-difference has to be factored in as well. Note that the terms "positive" and "negative" were chosen, since both contributions act in different directions.

As a starting point, let us still assume that we have only two atoms which are irradiated by a laser beam. First, we define the origin to be the center of mass of all atoms, e.g. in this case, the center of mass of the two atoms. The main idea now is to compare the two waves emitted by the atoms with an "imaginary" wave which comes from the origin. This way, we can introduce an effective field that replaces the ordinary superposition of the two scattered fields.

Let's begin with comparing the wave of an atom positioned outside the origin with a wave which originates from the origin. Since the atom and the origin have different distances to the detector, we get

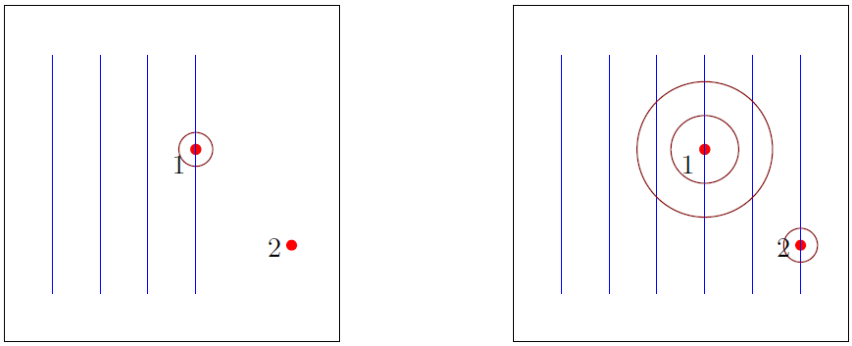

Figure 11: Two atoms (red) are being excited by a resonant laser beam (blue). Atom 1 starts radiating first (left), as the wave didn't reach atom 2 yet. Only a finite time later, the laser beam hits atom 2 and it starts radiating as well (right).

the following phase-difference (for the setup, see fig. 12):

$$\boldsymbol{R} = \boldsymbol{r} - \boldsymbol{r}_A \quad \text{(distance atom} \leftrightarrow \text{detector)} \tag{96a}$$

$$\Rightarrow \quad \Delta\phi_r \sim R - r \tag{96b}$$

$$= |\boldsymbol{r} - \boldsymbol{r}_A| - |\boldsymbol{r}| \tag{96c}$$

Using a Taylor-Expansion in $\frac{r_A}{r} \ll 1$, we get $|\boldsymbol{r} - \boldsymbol{r}_A| \simeq r - \hat{\boldsymbol{r}}\boldsymbol{r}_A$ and thus:

$$\Delta\phi_r \sim -\hat{\boldsymbol{r}}\boldsymbol{r}_A \tag{97}$$

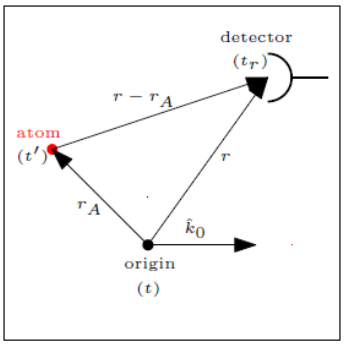

Figure 12: Configuration of our setup. $\boldsymbol{r}_A$ is the vector pointing from the origin to the atom, $\boldsymbol{r}$ is the vector connecting the origin with the detector and $\hat{\boldsymbol{k}}_0$ is the wave vector of the incident laser beam. Moreover, t' is the time of emission of the atom and t the time of emission of the origin. Further, we detect the signals at the fixed time t_r.

As already stated, since the ingoing wave doesn't hit the atoms simultaneously, a second phase-difference has to be considered. This one only depends on the distance in direction of the wave-vector of the incident

laser beam $\hat{\boldsymbol{k}}_0$. Therefore, the phase-difference is determined by the time-difference the laser beam needs to get from the atom to the origin (or vice versa).

$$\Delta\phi_t \sim \hat{\boldsymbol{k}}_0 \boldsymbol{r}_A \tag{98}$$

Consequently, the total phase difference between atom and origin is:

$$\Delta\phi \sim (\hat{\boldsymbol{k}}_0 - \hat{\boldsymbol{r}})\boldsymbol{r}_A \tag{99}$$

We will now implement this into our theory. To do so, we have to go back to eq. 33 and push the atom out of the origin. Thus, we have to replace $\boldsymbol{r} \to \boldsymbol{r} - \boldsymbol{r}_A$ with $\boldsymbol{r}_A$ the atom's position. Therefore, a factor $e^{-i\boldsymbol{k}\boldsymbol{r}_A}$ enters our formula, which represents the previously discussed phase-difference due to the distance between atom and detector. Furthermore, the Rabi-Frequency is evaluated at the atom's position and thus gets an extra phase factor $e^{i\boldsymbol{k}_0\boldsymbol{r}_A}$ [11]. This corresponds to the already discussed phase-factor resulting from the differences in excitation time. Note that since the atom sat in the origin in chapter 2.2.2, these new phase-factors just equalled 1 ($\boldsymbol{r}_A = 0$). This results in:

$$\boldsymbol{E}^{(+)}_{scat}(\boldsymbol{r}, t_r) = \eta\ \hat{S}_{ge}(t_r) J_-(t_r) \int_0^{\infty}\int_0^{2\pi}\int_0^{\pi} \omega^3 \sin\theta \left(\boldsymbol{d} - (\boldsymbol{d}\cdot\hat{\boldsymbol{k}})\hat{\boldsymbol{k}}\right) e^{i\boldsymbol{k}(\boldsymbol{r}-\boldsymbol{r}_A)}\ e^{i\boldsymbol{k}_0\boldsymbol{r}_A}\ \mathrm{d}\omega\mathrm{d}\phi\mathrm{d}\theta \tag{100a}$$

$$= 2\pi\eta\omega_0^3\ \hat{S}_{ge}(t_r) \int_0^{2\pi}\int_0^{\pi} \sin\theta \left(\boldsymbol{d} - (\boldsymbol{d}\cdot\hat{\boldsymbol{k}})\hat{\boldsymbol{k}}\right) e^{ik_0\hat{\boldsymbol{k}}\boldsymbol{r}}\ e^{ik_0(\hat{\boldsymbol{k}}_0-\hat{\boldsymbol{k}})\boldsymbol{r}_A}\ \mathrm{d}\phi\mathrm{d}\theta \tag{100b}$$

with $\eta = \frac{i}{(2\pi)^3 c^3 2\epsilon_0}$ and we already evaluated $J_-(t_r)$ as in chapter 2.2.2. Note that this expression resembles the scattered field of an atom sitting in the origin, modified by an additional phase factor $e^{ik_0(\hat{\boldsymbol{k}}_0-\hat{\boldsymbol{k}})\boldsymbol{r}_A}$ in the integral. Therefore, if we have N atoms with $\boldsymbol{r}_i$ the position of atom i, the total scattered field can be rewritten as follows:

$$\boldsymbol{E}^{(+)}_{scat} = \boldsymbol{E}^{(+)}_{scat,atom\ 1} + \boldsymbol{E}^{(+)}_{scat,atom\ 2} + ... + \boldsymbol{E}^{(+)}_{scat,atom\ N} \tag{101a}$$

$$= 2\pi\eta\omega_0^3\ \hat{S}_{ge}(t_r) \int_0^{2\pi}\int_0^{\pi} \sin\theta \left(\boldsymbol{d} - (\boldsymbol{d}\cdot\hat{\boldsymbol{k}})\hat{\boldsymbol{k}}\right) e^{ik_0\hat{\boldsymbol{k}}\boldsymbol{r}} \left(\sum_{i=1}^{N} e^{ik_0(\hat{\boldsymbol{k}}_0-\hat{\boldsymbol{k}})\boldsymbol{r}_i}\right) \mathrm{d}\phi\mathrm{d}\theta \tag{101b}$$

Accordingly, we are able to exchange the sum over all scattered fields with an effective field that resembles the scattered field of one atom sitting at the origin, corrected by a factor $\sum_{i=1}^{N} e^{ik_0(\hat{\boldsymbol{k}}_0-\hat{\boldsymbol{k}})\boldsymbol{r}_i}$ which accounts for the superposition of waves with different phases.

4.2 Evaluation of the Sum over all Atoms

Our next task is to evaluate the correction factor $\sum_{i=1}^{N} e^{ik_0(\hat{\boldsymbol{k}}_0-\hat{\boldsymbol{k}})\boldsymbol{r}_i}$. We will use two ways to do so: First, we evaluate the sum numerically with randomly determined atom positions. Thereafter, we'll give

a statistical argument for the found evaluation. At the end of this chapter, we'll eventually derive the effective scattered field.

4.2.1 Numerical Analysis

Our first step in evaluating $\sum_{i=1}^{N} e^{ik_0(\hat{\boldsymbol{k}}_0-\hat{\boldsymbol{k}})\boldsymbol{r}_i}$ is to do so numerically. Therefore, a program in Mathematica was written which:

- Creates an array of randomly placed atoms in a box with measures $(100 \times 100 \times 100)$ $[\frac{1}{k_0^3}]$.
- Plots the distribution in a 3D-Graph.
- Evaluates $\sum_{i=1}^{N} e^{ik_0(\hat{\boldsymbol{k}}_0-\hat{\boldsymbol{k}})\boldsymbol{r}_i}$ for a given θ, the randomly created atom positions and all possible discrete values of ϕ with a distance of $\frac{2\pi}{1000}$ between two succeeding angles.
- Creates a polar-plot of the real part, such that the result of the sum can be easily seen for every ϕ at once.

Here, we will only state the results. The code to this program can be found in Appendix C.1. For the wave vector k_0, the test value $k_0 = 10$ was chosen. Note that it's important that $\max(k_0 \cdot r_A)$ is at least $> 2\pi$, such that we have a sum of rapidly oscillating exponentials. The difference can be seen quite good for the case of $k_0 = 1$ and $k_0 = 10$, where we put 100 atoms into the box:

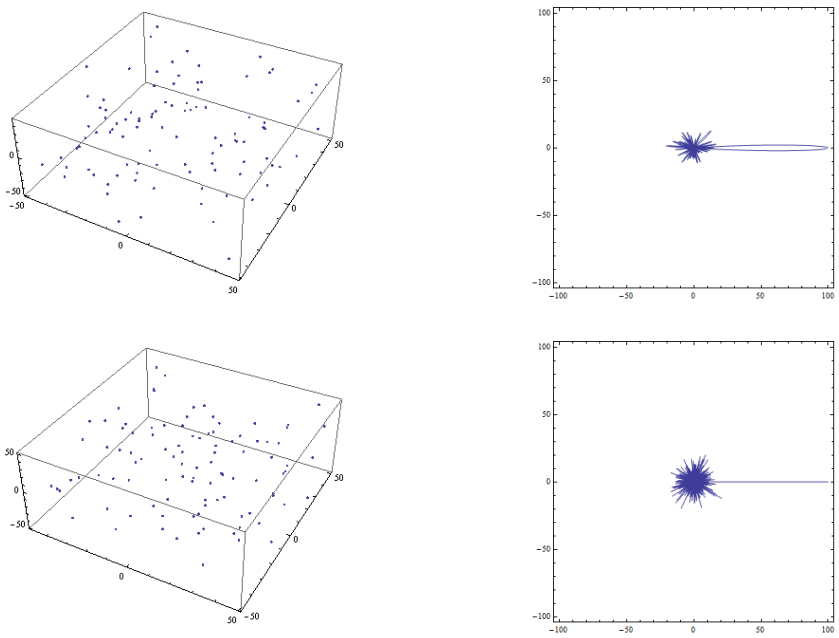

Figure 13: Evaluation of the sum for 100 atoms with (top) $k_0 = 1$ and (bottom) $k_0 = 10$. The left side is a plot of the corresponding atom distribution. The right side is a polar plot of the evaluated sum, where we see large values around the forward direction $\phi = 0$.

We will now take a look at the result for $N = 10, 100, 1000, 10000$ atoms:

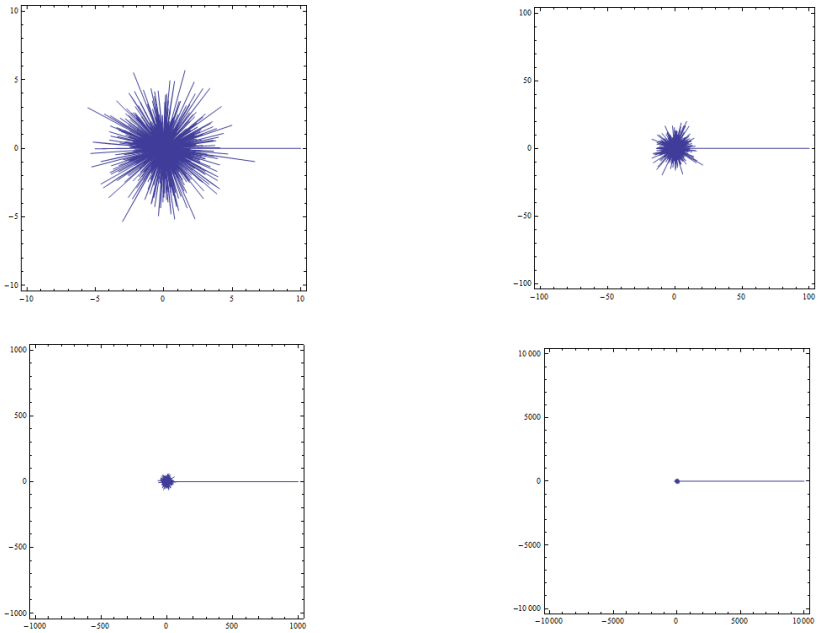

Figure 14: Polar plot in ϕ of the sum with (top left) $N = 10$ (top right) $N = 100$ (bottom left) $N = 1000$ and (bottom right) $N = 10000$ atoms.

It's easy to see that, even for low atom numbers, the forward direction dominates in the scattering characteristic. Thus, the factor $\sum_{i=1}^{N} e^{ik_0(\hat{\boldsymbol{k}}_0 - \hat{\boldsymbol{k}})\boldsymbol{r}_i}$ leads to enhanced forward scattering and the resulting, effective wave will be a plane wave parallel to the incident laser beam which excites the atoms. This is also very similar to the case of a very fine grating (Fraunhofer approximation):

Whenever we calculate the diffraction pattern of an object, we take its Fourier transform. In the case of a fine grating, most of the incident intensity will be scattered into the forward direction (0. maximum). Note also that the sum $\sum_{i=1}^{N} e^{ik_0(\hat{\boldsymbol{k}}_0 - \hat{\boldsymbol{k}})\boldsymbol{r}_i}$ looks quite similar to some definitions of the delta function. The only difference are the randomly distributed atom positions. But this randomness only enhances the convergence to a delta function as will be shown in the next chapter.

Another way to see this is to keep in mind that we have a sum of many rapid oscillating exponentials, which will annihilate each other but for the case of $\hat{\boldsymbol{k}}_0 - \hat{\boldsymbol{k}} = 0$ where the sum just equals to N. Of course, all these explanations are essentially different views of the same phenomena when summing over many exponentials with different phases.

The sum can also be evaluated for different values of θ. This has been done in the case of $N = 1000$ atoms for $\theta = \frac{\pi}{4}$ and $\theta = \frac{\pi}{6}$:

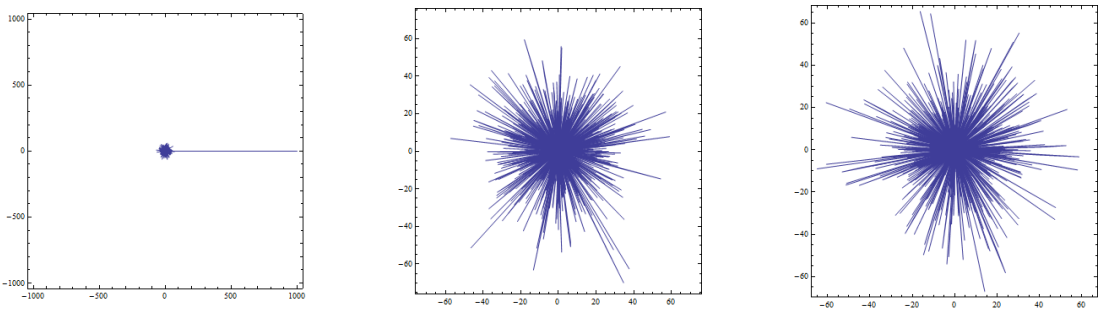

Figure 15: Polar plot in ϕ of the sum with (left) $\theta = \frac{\pi}{2}$ (middle) $\theta = \frac{\pi}{4}$ and (right) $\theta = \frac{\pi}{6}$.

As we see, compared to the forward scattering at $\theta = \frac{\pi}{2}$, for other values of θ we get only weak scattering.

4.2.2 Evaluation using the Central Limit Theorem

We will now choose another ansatz for evaluating the expression $\sum_{i=1}^{N} e^{ik_0(\hat{\boldsymbol{k}}_0 - \hat{\boldsymbol{k}})\boldsymbol{r}_i}$ to emphasize the results of the previous chapter. First, we note that fields are real quantities, therefore we are only interested in the real part of the sum, i.e. $\sum_{i=1}^{N} \cos\left(k_0(\hat{\boldsymbol{k}}_0 - \hat{\boldsymbol{k}})\boldsymbol{r}_i\right)$. This is similar to a sum of cosines with random phases which lie in the interval $[0, 2\pi)$. Accordingly, we model this sum by approximating

$$\sum_{i=1}^{N} \cos\left(k_0(\hat{\boldsymbol{k}}_0 - \hat{\boldsymbol{k}})\boldsymbol{r}_i\right) \simeq \sum_{i=1}^{N} \cos\left(a\varphi_i\right) \tag{102}$$

with a prefactor $a \in \mathbb{R}$ which determines the angular velocity and $\varphi \in [0, 2\pi]$ an evenly distributed random variable. For a high enough value of N, we have a lot of atoms with different phase shifts varying over several periods of the cosine. Since there is no real preferred position in a gas, all possible phase shifts will be distributed almost evenly. Of course, this won't be a perfect even distribution, but for our case approximating it as such suffices for the analysis.

To begin with, we evaluate $\sum_{i=1}^{N} \cos\left(k_0(\hat{\boldsymbol{k}}_0 - \hat{\boldsymbol{k}})\boldsymbol{r}_i\right)$ at its maximum $\hat{\boldsymbol{k}}_0 - \hat{\boldsymbol{k}} = 0$:

$$\max\left(\sum_{i=1}^{N} \cos\left(k_0(\hat{\boldsymbol{k}}_0 - \hat{\boldsymbol{k}})\boldsymbol{r}_i\right)\right) = \sum_{i=1}^{N} \cos\left(0\right) \tag{103a}$$

$$= \sum_{i=1}^{N} 1 \tag{103b}$$

$$= N \tag{103c}$$

This is the forward scattering peak we observed in the previous chapter. We will now assume that $\hat{\boldsymbol{k}}_0 - \hat{\boldsymbol{k}} \neq 0$ and use eq. 102. Since the phase φ is a random variable, the values of $\cos\left(a\varphi\right)$ will also be randomly distributed. The expectation value can be calculated by means of the "Law of the unconscious statistician" [19]

$$\langle \cos(a\varphi) \rangle = \int_0^{2\pi} p(\varphi) \cos(a\varphi)\ \mathrm{d}\varphi \tag{104}$$

$$= \frac{1}{2\pi} \int_0^{2\pi} \cos(a\varphi)\ \mathrm{d}\varphi \tag{105}$$

$$= \frac{\sin(2\pi a)}{2\pi a} \tag{106}$$

where $p(\varphi) = \frac{1}{2\pi}$ is the probabiliy distribution of φ. Consequently, the expectation value is a sinc-function which heavily depends on the prefactor a.

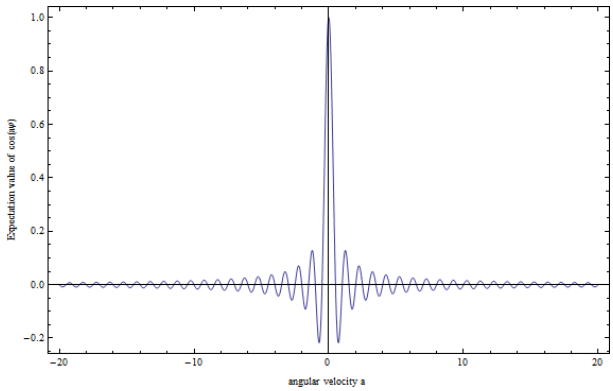

Figure 16: Expectation value of $\cos(a\varphi)$ *for different values of a.*

For $|a| < 1$, the expectation values of the cosine takes on quite large values. For $a \to 0$, it converges, as expected, to 1. We will see in the following that the expectation value of $\sum_{i=1}^{N} \cos(a\varphi_i)$ is just the sum of the individual expectation values $\langle \cos(a\varphi_i) \rangle$. Thus, for small values of a, the sum will evaluate to high values $\sim N$. We observed this effect already in the previous chapter by choosing k_0 too small. Furthermore, for high values of a, the sum will give a result near 0, at least compared to the maximum value N (for $\hat{\boldsymbol{k}}_0 - \hat{\boldsymbol{k}} = 0$).

Now, we will make use of one of the most important theorems in statistics: The central limit theorem. It roughly states the following:

> *"If a random variable is the sum of many independent random variables, then it has a Gaussian distribution."* [20]

The number of particles in a gas is roughly estimated of the order of Avogadro's number $6.022 \cdot 10^{23}$ and interactions between atoms are being neglected in our theory (ideal gas approximation). Therefore, we have a large sum of independent randomly distributed cosine functions and the central limit theorem can be applied. As a consequence, the result of $f(a) = \sum_{i=1}^{N} \cos(a\varphi_i)$ will be Gaussian distributed with

a mean and a standard deviation given by [20]

$$\langle f(a)\rangle = N\langle\cos(a\varphi)\rangle \tag{107a}$$
$$= N\frac{\sin(2\pi a)}{2\pi a} \tag{107b}$$
$$\sigma_f = \sqrt{N}\sigma_{\cos(a\varphi)} \tag{107c}$$
$$\leq \sqrt{N} \tag{107d}$$

with $\sigma_{\cos(a\varphi)}$ the standard deviation of a single cosine function. Since $\cos(a\varphi) \in [-1,1]$, the estimation $\sigma_{\cos(a\varphi)} \leq 1$ was made. For high enough a, we thus get $\frac{\langle f(a)\rangle}{N} \simeq 0$ since $\langle\cos(a\varphi)\rangle \ll 1$ and $\frac{\sigma_f}{N} \simeq \frac{1}{\sqrt{N}}$. Long story short, when we evaluate $\sum_{i=1}^{N} e^{ik_0(\hat{\boldsymbol{k}}_0-\hat{\boldsymbol{k}})\boldsymbol{r}_i}$ for $\hat{\boldsymbol{k}}_0 - \hat{\boldsymbol{k}} \neq 0$, our result will be Gaussian distributed with a mean value and standard deviation which are small compared to the result we get for $\hat{\boldsymbol{k}}_0 - \hat{\boldsymbol{k}} = 0$ (as long as N is large). So, as a final result, we can state

$$\sum_{i=1}^{\infty} e^{ik_0(\hat{\boldsymbol{k}}_0-\hat{\boldsymbol{k}})\boldsymbol{r}_i} = \begin{cases} \infty, & \text{if } \hat{\boldsymbol{k}}_0 - \hat{\boldsymbol{k}} = 0 \\ 0, & \text{otherwise} \end{cases} \tag{108}$$

where we formally set $N \to \infty$. As already seen in the previous chapter, the sum boosts scattering in forward direction. Because of this, we will neglect all other directions in the next chapter and derive the effective field under the condition that all emitted light is radiated along the direction of the incident laser beam. Of course, for this result, many approximations were needed, e.g. $r \to \infty$, $N \to \infty$ and that our atoms form an ideal gas. This should always be kept in mind since our result is only valid under these conditions.

As a demonstration of the central limit theorem, $\sum_{i=1}^{N}\cos(\varphi_i)$ was evaluated numerically with Mathematica for some example cases (see fig. 17, for the code, see Appendix C.2).

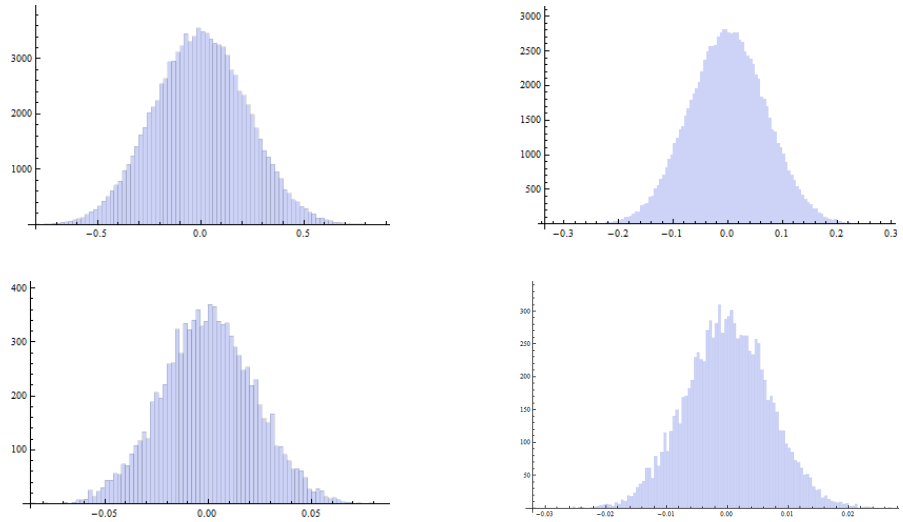

Figure 17: Histograms for the results of $\sum_{i=1}^{N} \cos(a\varphi_i)$ for different numbers of atoms N. The results have been normalized to N, i.e. the x-axis values have already been divided by N. (top left) N=10, 100000 sample values (top right) N=100, 100000 sample values (bottom left) N=1000, 10000 sample values (bottom right) N=10000, 10000 sample values. As expected, in all cases we get some kind of gaussian distribution with expectation value $\simeq 0$ and a standard deviation which becomes smaller with growing N.

4.2.3 Determining the Effective Field

We will now return to eq. 101b of the effective field:

$$\boldsymbol{E}_{eff}^{(+)}(t_r) = 2\pi\eta\omega_0^3 \, \hat{S}_{ge}(t_r) \int_0^{2\pi} \int_0^{\pi} \sin\theta \left(\boldsymbol{d} - (\boldsymbol{d}\cdot\hat{\boldsymbol{k}})\hat{\boldsymbol{k}}\right) e^{ik_0\hat{\boldsymbol{k}}\boldsymbol{r}} \left(\sum_{i=1}^{N} e^{ik_0(\hat{\boldsymbol{k}}_0-\hat{\boldsymbol{k}})\boldsymbol{r}_i}\right) \mathrm{d}\phi\mathrm{d}\theta \tag{109}$$

The integral just measures which waves with general wave-vectors $\boldsymbol{k}$ contribute to the scattered field at position $\boldsymbol{r}$. Here, $\hat{\boldsymbol{k}}$ is the direction of the general waves. Evaluating this in chapter 2.2.2 lead us to the result that a two-level atom scatters light spherical symmetrically in all directions. For the many atom case, we got exactly such a field with the exception that we additionally obtained a dirac delta-like prefactor which scatters all light in the forward direction. Therefore, we can approximate:

$$\int_0^{2\pi} \int_0^{\pi} \sin\theta \left(\boldsymbol{d} - (\boldsymbol{d}\cdot\hat{\boldsymbol{k}})\hat{\boldsymbol{k}}\right) e^{ik_0\hat{\boldsymbol{k}}\boldsymbol{r}} \left(\sum_{i=1}^{N} e^{ik_0(\hat{\boldsymbol{k}}_0-\hat{\boldsymbol{k}})\boldsymbol{r}_i}\right) \mathrm{d}\phi\mathrm{d}\theta \tag{110a}$$

$$\simeq \int_0^{2\pi} \int_0^{\pi} \sin^3\theta \; \mathrm{d}\phi\mathrm{d}\theta \; e^{i\boldsymbol{k}_0\boldsymbol{r}} \left(\boldsymbol{d} - (\boldsymbol{d}\cdot\hat{\boldsymbol{k}}_0)\hat{\boldsymbol{k}}_0\right) \tag{110b}$$

where we still perform the surface-integral over the dipole charateristic, such that all initially spherically scattered waves are summed up in forward direction. This can also be done formally by approximating $\sum_{i=1}^{N} e^{ik_0(\hat{\boldsymbol{k}}_0-\hat{\boldsymbol{k}})\boldsymbol{r}_i} \simeq \frac{8\pi}{3}\delta(\hat{\boldsymbol{k}}_0 - \hat{\boldsymbol{k}})$. Evaluating this expression further as in chapter 2.2.2 and using

$\boldsymbol{d} - (\boldsymbol{d} \cdot \hat{\boldsymbol{k}}_0)\hat{\boldsymbol{k}}_0 = d \cdot \boldsymbol{\epsilon}$, we finally get:

$$\boldsymbol{E}^{(+)}_{eff}(t_r) = \underbrace{\hat{S}_{ge}(t_r)\frac{k_0^2}{4\pi\epsilon_0}}_{\text{prefactors of single scatterer}} \cdot \quad i\frac{4}{3}k_0 d e^{i\boldsymbol{k}_0\boldsymbol{r}}\boldsymbol{\epsilon} \tag{111a}$$

$$= i\frac{k_0^3 d}{3\pi\epsilon_0}\hat{S}_-(t_r)e^{i(\boldsymbol{k}_0\boldsymbol{r}-\omega_0 t_r)}\boldsymbol{\epsilon} \tag{111b}$$

As we can see, the endresult is a plane wave with a correction factor compared to our initial result of a single scatterer. We'll see in the next chapter that this result gives us again energy conservation if the system is closed and no internal loss channels like excitation of kinetic energy are existent.

4.3 Detected Signal in Forward Direction

4.3.1 Without Phase Kick

First, we'll evaluate the detector signal. The Poynting vector without the unscattered field is given by:

$$\boldsymbol{P}_{scat} + \boldsymbol{P}_{inter} = 2\epsilon_0 c \,\mathrm{Re}\,\langle \boldsymbol{E}^{(-)}_{scat}\boldsymbol{E}^{(+)}_{scat}\rangle\,\hat{\boldsymbol{k}} + 2\epsilon_0 c\,\left(\mathrm{Re}\,\langle \boldsymbol{E}^{(-)}_{in}\boldsymbol{E}^{(+)}_{scat}\rangle + \mathrm{Re}\,\langle \boldsymbol{E}^{(-)}_{scat}\boldsymbol{E}^{(+)}_{in}\rangle\right)\,\hat{\boldsymbol{k}} \tag{112}$$

The scattered part evaluates to

$$\boldsymbol{P}_{scat} = \frac{2k_0^6 d^2 c}{(3\pi)^2\epsilon_0}\,\mathrm{Re}\,\langle \hat{S}_+\hat{S}_-\rangle\,\hat{\boldsymbol{k}} \tag{113a}$$

$$= \frac{2}{3\pi}k_0^2\hbar\omega_0\gamma\hat{\rho}_{ee}\,\hat{\boldsymbol{k}} \tag{113b}$$

$$= \frac{8\pi}{3}\frac{\hbar\omega_0}{\lambda_0^2}\gamma\hat{\rho}_{ee}\,\hat{\boldsymbol{k}} \tag{113c}$$

where we used eq. 41c. Equivalently, the interference part becomes:

$$\boldsymbol{P}_{inter} = \frac{2\epsilon_0 c E_{in} k_0^3 d}{3\pi\epsilon_0}\mathrm{Re}(i\,\langle \hat{S}_-\rangle - i\,\langle \hat{S}_+\rangle)\,\hat{\boldsymbol{k}} \tag{114a}$$

$$= \frac{2\epsilon_0 c E_{in} k_0^3 d}{3\pi\epsilon_0}\big(-2\mathrm{Im}(\hat{\rho}_{eg})\big)\,\hat{\boldsymbol{k}} \tag{114b}$$

$$= \frac{2\epsilon_0 c E_{in} k_0^3 d\gamma}{3\pi\epsilon_0\Omega}\hat{\rho}_{ee}\,\hat{\boldsymbol{k}} \tag{114c}$$

$$= -\frac{2}{3\pi}k_0^2\hbar\omega_0\gamma\hat{\rho}_{ee}\,\hat{\boldsymbol{k}} \tag{114d}$$

Here, we used eq. 41 and eq. 48. Note that the total energy rate per surface area of the scattered and interference part can just be calculated by taking the norm of the respective Poynting vectors. Before the plane wave approximation, we had to evaluate a quite complex surface integral.

The scattered energy density rate per surface area has the following dependence on the detuning Δ:

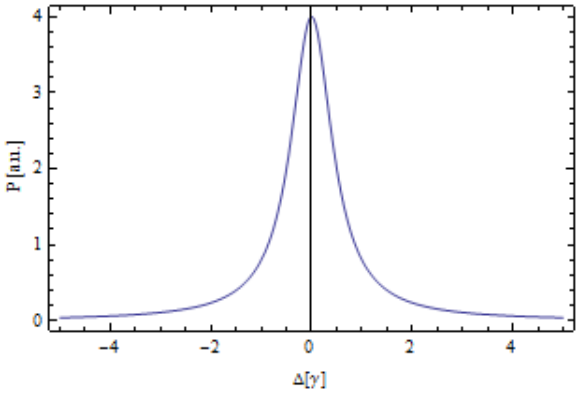

Figure 18: Detected energy density current of the scattered field in forward direction.

We get a Lorentzian profile for the scattered light. This is expected, since due to the finite emission time, the detected signal should be a Lorentzian (see chapter 2.4.2). Also, on resonance, the emission is highest and for greater detunings Δ, it slowly decays to 0 and the light won't excite the atom anymore.

Equivalently, the interference term has now the shape of a negative Lorentzian, what resembles the normal absorption profile we get when doing spectroscopy. In chapter 3.2.2, the interference part yielded a Fano profile for a pointlike detector in forward direction. Furthermore, we stated that when the signal is integrated over a certain area, the expected negative Lorentzian returns. Here, we have the same effect, but instead of integrating over a certain detector area, we chose to increase the number of atoms tremendously.

Of course, when we add the scattered and interference parts together, they add up to 0. Thus, the energy in the system is conserved. Since all light is scattered in forward direction, this would mean that on a time average, we would only detect seemingly unscattered light. However, in a real experiment, there is also light getting scattered in different directions than the forward direction, and an absorption profile emerges in forward direction.

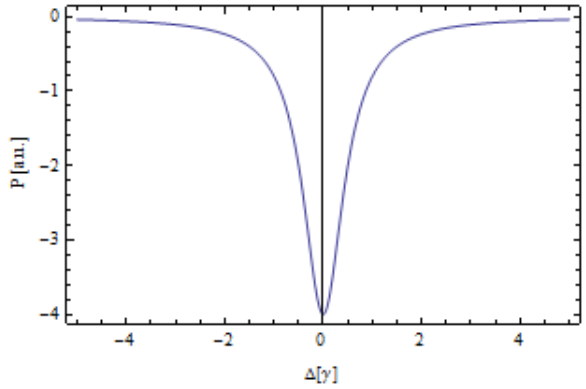

Figure 19: Detected energy density current of the interference between incident and scattererd field in forward direction.

4.3.2 With Phase Kick

We now add a phase kick $\phi_k \in [0, 2\pi)$ to the scattered field:

$$\boldsymbol{E}^{(+)}_{scat}(t_r) = i\frac{k_0^3 d}{3\pi\epsilon_0}\hat{S}_-(t_r)e^{i(\boldsymbol{k}_0\boldsymbol{r}-\omega_0 t_r+\phi_k)}\boldsymbol{\epsilon} \tag{115}$$

This changes nothing at $\boldsymbol{P}_{scat}$, since the phase information is lost due to the scalar product $\langle \boldsymbol{E}^{(-)}_{scat}\boldsymbol{E}^{(+)}_{scat}\rangle$. However, $\boldsymbol{P}_{inter}$ has to be calculated anew.

$$\begin{aligned}
\boldsymbol{P}_{inter} &= \frac{2\epsilon_0 c E_{in} k_0^3 d}{3\pi\epsilon_0}\mathrm{Re}(i\langle\hat{S}_-\rangle e^{i\phi_k} - i\langle\hat{S}_+\rangle e^{-i\phi_k})\ \hat{\boldsymbol{k}} && \text{(116a)}\\
&= -\frac{4cE_{in}k_0^3 d}{3\pi}\left(\mathrm{Im}(\hat{\rho}_{eg})\cos\phi_k + \mathrm{Re}(\hat{\rho}_{eg})\sin\phi_k\right)\ \hat{\boldsymbol{k}} && \text{(116b)}\\
&= -\frac{2cE_{in}k_0^3 d}{3\pi}\left(-\frac{\gamma}{\Omega}\hat{\rho}_{ee}\cos\phi_k + \frac{2\Delta}{\Omega}\hat{\rho}_{ee}\sin\phi_k\right)\ \hat{\boldsymbol{k}} && \text{(116c)}\\
&= \frac{2c\hbar k_0^3}{3\pi}\left(-\gamma\hat{\rho}_{ee}\cos\phi_k + 2\Delta\hat{\rho}_{ee}\sin\phi_k\right)\ \hat{\boldsymbol{k}} && \text{(116d)}\\
&= \frac{2}{3\pi}k_0^2\hbar\omega_0\hat{\rho}_{ee}\left(-\gamma\cos\phi_k + 2\Delta\sin\phi_k\right)\ \hat{\boldsymbol{k}} && \text{(116e)}
\end{aligned}$$

Note that we see here very nicely that giving the scattered field a phase kick $e^{i\phi_k}$ is the same as giving the coherences a phase kick $\hat{\rho}_{eg} \to \hat{\rho}_{eg}e^{i\phi_k}$. We then get for the total Poynting vector:

$$\begin{aligned}
\boldsymbol{P} &= \boldsymbol{P}_{scat} + \boldsymbol{P}_{inter} && \text{(117a)}\\
&= \frac{2}{3\pi}k_0^2\hbar\omega_0\hat{\rho}_{ee}\left(\gamma - \gamma\cos\phi_k + 2\Delta\sin\phi_k\right)\ \hat{\boldsymbol{k}} && \text{(117b)}
\end{aligned}$$

For $\phi_k \to 0$, we obtain the results from the previous chapter: Lorentzian profiles and energy conservation.

But for $\phi_k \neq 0$, energy conservation is broken and the detected signal changes depending on ϕ_k. We will analyse the detected signal by investigating the dependence of P_{inter} on Δ for several values of ϕ_k, since the scattered part only gives a constant offset. Remember that the interference part of the Poynting vector reflects the amount of power the atom adds to the incident field. For instance, for $\phi_k = 0$, we have a negative Lorentzian and thus, energy is taken out of the incident field and reemitted by scattering.

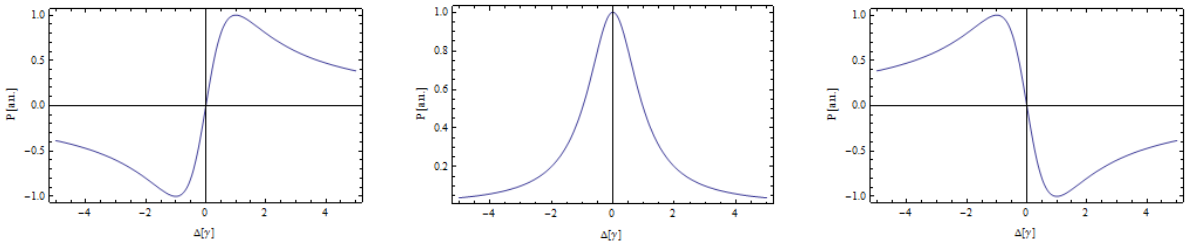

Figure 20: Norm of $\boldsymbol{P}_{inter}$ in dependancy of Δ for several values of ϕ_k. (left) $\phi_k = \frac{\pi}{2}$ (middle) $\phi_k = \pi$ (right) $\phi_k = \frac{3\pi}{2}$. Changing the phase kick obviously changes the interaction between the incident light and the atom, since we can switch between positive/negative Fano and Lorentz-lines by adjusting ϕ_k accordingly.

This is the same result we obtained in chapter 3.3.2: Introducing a phase kick ϕ_k leads to the possibility of changing the detected signal. In this specific case, we can adjust the ordinary negative Lorentzian profile to Fano-lines or even a positive Lorentzian. However, for $\phi_k \neq 0$, energy conservation doesn't hold anymore, since $P_{scat} + P_{inter} \neq 0$ (as was also observed in chapter 3.3.1).

5 Transition from c.w. to Pulsed Laser

We will now transition from a continuous laser wave to laser pulses. In the previous chapters, we used continuous waves to excite the atom, i.e. it absorbed and emitted light constantly. Now, however, the atom will get "kicked" into the excited state by the laser pulse and subsequently decay via spontaneous emission back to the ground state. The goal of this chapter is to analyse once more the energy distribution of the laser-atom system during their interaction. But before we can start, we will first have to look whether the previously used Poynting vector is still valid or not. Finally, it will be demonstrated that by giving the scattered field an additional phase kick, the same detector signals as in chapter 4.3.2 can be reproduced.

5.1 Revisiting the Poynting Vector

As a pulse shape, we will use a Gaussian envelope:

$$E_{in}(t) = E_{in}\ e^{-\frac{(\boldsymbol{k}_{in}\boldsymbol{r}-\omega_{in}t)^2}{2\sigma^2}} \tag{118a}$$

$$\Rightarrow \quad \boldsymbol{E}_{in}^{(+)} = E_{in}\ \hat{\boldsymbol{\epsilon}}\ e^{i(\boldsymbol{k}_{in}\boldsymbol{r}-\omega_{in}t)} e^{-\frac{(\boldsymbol{k}_{in}\boldsymbol{r}-\omega_{in}t)^2}{2\sigma^2}} \tag{118b}$$

This way, we have a carrier signal $e^{i(\boldsymbol{k}_{in}\boldsymbol{r}-\omega_{in}t)}$ and a Gaussian envelope $e^{-\frac{(\boldsymbol{k}_{in}\boldsymbol{r}-\omega_{in}t)^2}{2\sigma^2}}$ which are moving together with the same velocity. Our final signal therefore is a plane wave with frequency ω_{in} modified by a Gaussian envelope, propagating through space:

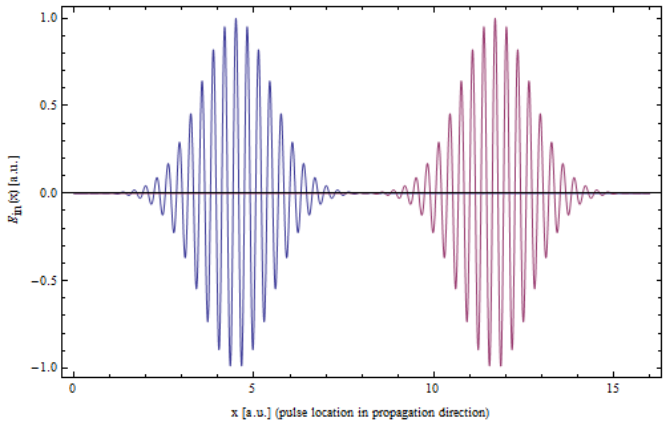

Figure 21: Laser pulse propagating along the x-direction at earlier times (blue) and later times (red). Since group - and phase velocity are equal, the shape of the resulting pulse stays constant.

Note that σ is a unitless parameter with which we can alter the width of the pulse. This will be discussed more precisely in the next chapter.

5.1.1 Verification of the Rotating Wave Approximation

When we first derived the Poynting vector in chapter 3, we were able to simplify our expression in the classical as well as in the quantum mechanical calculation due to the rotating wave approximation. This way, terms like $\mathrm{Re}\,\langle \boldsymbol{E}_{in}^{(-)} \boldsymbol{E}_{in}^{(-)} \rangle$ could be neglected as they were rapidly oscillating and thus didn't contribute to the Poynting vector. Furthermore, since the interaction between atom and laser field has no periodic time dependence anymore, we won't calculate the time-averaged Poynting vector of one characteristic period. Rather, we will integrate the Poynting vector over the whole interaction and decay time, i.e. from 0 to ∞, such that we gain a measure for the total energy of the atom-laser system.

We will perform this integral schematically to motivate that the rotating wave approximation still holds. To simplify the integral, we set w.l.o.g. $\boldsymbol{r} = 0$:

$$\mathrm{Re} \int_0^\infty \langle \boldsymbol{E}_{in}^{(-)} \boldsymbol{E}_{in}^{(-)} \rangle \, \mathrm{d}t \sim 2\ \mathrm{Re} \int_0^\infty e^{2i\omega_{in}t} e^{-\frac{(\omega_{in}t)^2}{\sigma^2}} \, \mathrm{d}t \tag{119a}$$

$$= \frac{E_{in}^2 \sqrt{\pi}\sigma}{\omega_{in}} e^{-\sigma^2} \tag{119b}$$

$$\mathrm{Re} \int_0^\infty \langle \boldsymbol{E}_{in}^{(-)} \boldsymbol{E}_{in}^{(+)} \rangle \, \mathrm{d}t \sim 2\ \mathrm{Re} \int_0^\infty e^{-\frac{(\omega_{in}t)^2}{\sigma^2}} \, \mathrm{d}t \tag{119c}$$

$$= \frac{E_{in}^2 \sqrt{\pi}\sigma}{\omega_{in}} \tag{119d}$$

It's easy to see that we get a damping factor $e^{-\sigma^2}$ from the oscillating term $e^{2i(\boldsymbol{k}_{in}\boldsymbol{r} - \omega_{in}t)}$. This means that the oscillations heavily damp the result of the integral depending on σ. Thus, if we choose σ large enough, we can still assume that the rotating wave approximation holds. Note that the peak width depends on σ, for instance the FWHM in time domain is given by:

$$t_{width} = \frac{\sigma}{\omega_{in}} \sqrt{8 \ln 2} \tag{120}$$

Therefore, if we place our detector at a certain location in space where the laser pulse will pass, the detected width of the pulse equals t_{width} as we only measure the variance in time of the pulse. Consequently, the width depends on σ as illustrated in fig. 22:

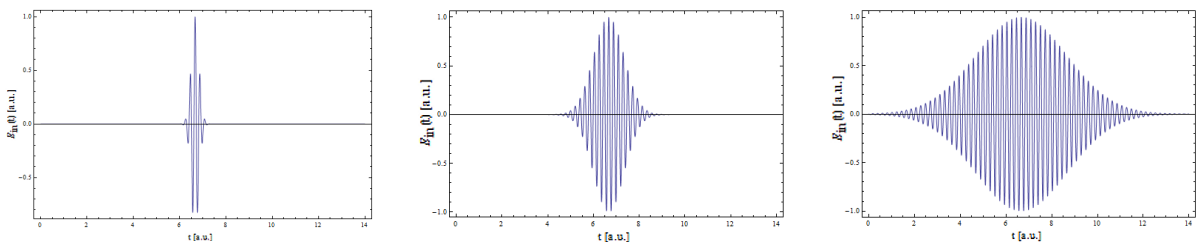

Figure 22: Pulse seen from a certain position in space dependent on time. The values for σ are (left) $\sigma = 5$, (middle) $\sigma = 20$ and (right) $\sigma = 60$.

5.1.2 Calculation of the Density Matrix Elements

The equations of motion for the density matrix elements are the same as in chapter 2.3.3. However, we have to take into account that the Rabi-Frequency now depends on time, i.e. $\Omega(t) \sim E_{in}(t) \sim e^{-\frac{(\boldsymbol{k}_{in}\boldsymbol{r}-\omega_{in}t)^2}{2\sigma^2}}$. Due to that, we have to solve the partial differential equations numerically, e.g. in Mathematica as in Appendix B.2 or D.2. Doing this with the example values $\gamma = \frac{1}{200}$ $[a.u.]$, $\Omega = 2$ $[\gamma]$, $\omega = 200$ $[\gamma]$, $\Delta = 0$ and $\sigma = 50$ $(\rightarrow t_{width} \simeq \frac{1}{2}$ $[\gamma^{-1}])$, we obtain the results illustrated in fig. 23. The units are given in multiples of the decay rate γ, as it is the most characteristic time-giving quantity in our experimental setup. Moreover, the Rabi frequency Ω can be decomposed into $E_{in} \cdot \frac{d}{\hbar}$, such that whenever we want to change the value of Ω, we do it by adjusting E_{in} accordingly (i.e. d remains constant). Sometimes, Δ will be given in units of Ω (see chapter 6). Furthermore, one can adjust at which time the pulse hits the atom by changing the value of $t_p = \frac{\boldsymbol{kr}}{\omega}$. Note that it should be chosen such that the pulse doesn't excite the atom before $t = 0$, as the boundary conditions at $t = 0$ for the density matrix elements would ruin the result.

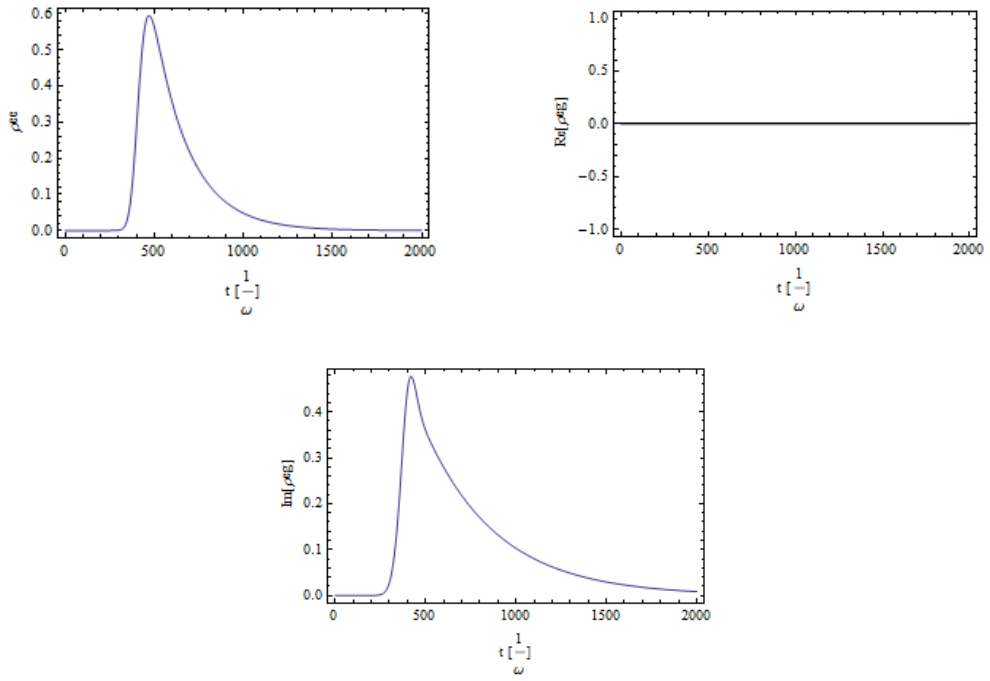

Figure 23: Solutions for the density matrix elements with a pulsed laser. (top left) $\hat{\rho}_{ee}$*, (top right)* $\mathrm{Re}(\hat{\rho}_{ee})$ *and (bottom)* $\mathrm{Im}(\hat{\rho}_{ee})$.

These results correspond very well to a laser pulse which "kicks" the atoms into the excited state, as $\hat{\rho}_{ee}$ grows very fast when the laser hits the atoms. Afterwards, as soon as the pulse has passed, we can observe spontaneous decay to come into action. Note that the real part of $\hat{\rho}_{eg}$ is zero. This is very similar to our stationary result of the continuous wave scenario in chapter 2.3.3, where we found that $\mathrm{Re}(\hat{\rho}_{eg}) \sim \Delta$.

5.2 Energy Conservation

We will now analyse if energy is conserved in a system where two-level atoms are being excited by a laser pulse with detuning Δ. To do this, we first calculate the expressions for the Poynting vectors $\boldsymbol{P}_{scat}$ and $\boldsymbol{P}_{inter}$. Although we are using the same formulas as before, the Poynting vectors are now time-dependent and we can therefore observe the energy distribution in our system as a function of time. Integrating over $\boldsymbol{P}_{scat}(t)$ and $\boldsymbol{P}_{inter}(t)$ will then give us the total energy density rate scattered and absorbed by the atoms. Similar as in the previous chapters, these two contributions have to cancel each other out when we integrate over the whole interaction and decay time for energy conservation to hold, i.e. the energy emitted by the atoms has to equal the energy that has been taken out of the laser pulse.

5.2.1 Without Phase Kick

We solve this again numerically in Mathematica and use as standard parameters $\gamma = \gamma_0 = \frac{1}{100}$ $[a.u.]$, $\Omega = 1[\gamma_0]$, $\omega = 100[\gamma_0]$, $\Delta = 0$ and $\sigma = 50$ ($\rightarrow t_{width} \simeq 1$ $[\gamma^{-1}]$). For these values, one gets quite beautiful results:

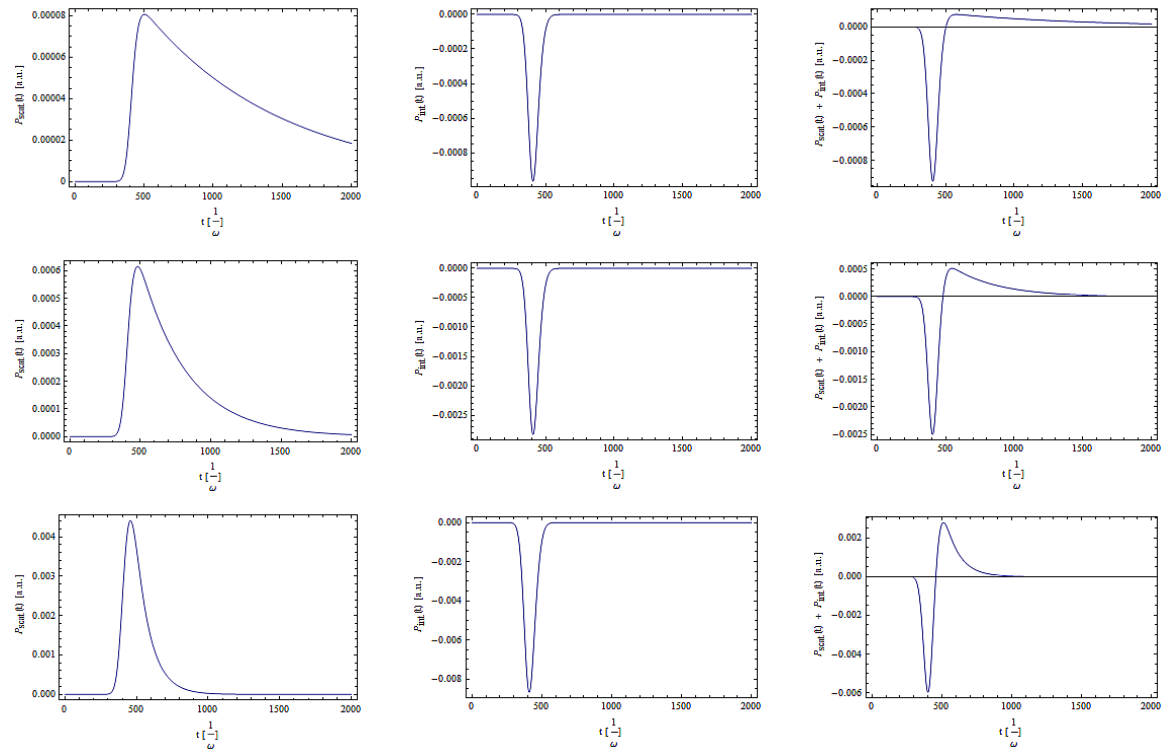

Figure 24: Columns: (left) $P_{scat}(t)$, (middle) $P_{int}(t)$ and (right) $P_{scat}(t) + P_{int}(t)$. Rows: (top) decay rate $\gamma = \frac{1}{10}\gamma_0$, (middle) $\gamma = \frac{3}{10}\gamma_0$ and (bottom) $\gamma = \gamma_0$. The signal of the scattered light falls of exponentially due to spontaneous emission and as expected, for lower decay rates the signal becomes less damped. Furthermore, during the time of interaction between atoms and laser pulse, energy is being transmitted from the laser into the atoms. This energy then gets emitted again in form of radiation (spontaneous emission) after the pulse has passed the atoms. Note that the spontaneous decay sets in directly after the interference part becomes 0.

As we see, during the time when pulse and atoms overlap or interact, energy is being transferred from the laser pulse into the atoms. This energy is afterwards reemitted in form of radiation via spontaneous emission. This is a quite plausible result, since it corresponds very well to the solutions of the density matrix elements we saw in the previous chapter. As a reminder: The laser pulse "kicked" the atoms into the excited state. This complies to the transfer of energy between atoms and pulse while they overlap. Afterwards, the excited state slowly decays due to spontaneous emission, which is only possible through the emission of radiation.

We will now check for energy conservation by integrating the total energy current density from $t = 0$ to ∞. This will be done for several values of γ, Ω and Δ:

Table 1: Energy of the system for several values of γ.

$\gamma[\gamma_0]$	W_{scat}	W_{int}	$W_{scat} + W_{int}$ [a.u.]
$\frac{3}{10}$	0.267	-0.267	$-8 \cdot 10^{-10}$
$\frac{7}{10}$	0.604	-0.604	$-5 \cdot 10^{-10}$
1	0.838	-0.838	$-5 \cdot 10^{-10}$
2	1.493	-1.493	$3 \cdot 10^{-10}$
7	2.910	-2.910	$-4 \cdot 10^{-10}$

Table 2: Energy of the system for several values of Ω.

$\Omega[\gamma_0]$	W_{scat}	W_{int}	$W_{scat} + W_{int}$ [a.u.]
$\frac{1}{100}$	$1.21 \cdot 10^{-4}$	$-1.21 \cdot 10^{-4}$	$-3 \cdot 10^{-13}$
$\frac{1}{10}$	0.012	-0.012	$-4 \cdot 10^{-12}$
$\frac{5}{10}$	0.276	-0.276	$-1 \cdot 10^{-10}$
1	0.838	-0.838	$-5 \cdot 10^{-10}$
3	1.027	-1.027	$3 \cdot 10^{-9}$

Table 3: Energy of the system for several values of Δ.

$\Delta[\gamma_0]$	W_{scat}	W_{int}	$W_{scat} + W_{int}$ [a.u.]
-5	0.045	-0.045	$-2 \cdot 10^{-11}$
-2	0.409	-0.409	$1 \cdot 10^{-10}$
0	0.838	-0.838	$-5 \cdot 10^{-10}$
2	0.409	-0.409	$1 \cdot 10^{-10}$
5	0.045	-0.045	$-2 \cdot 10^{-11}$

As we can see, to a very high precision the scattered and interference parts cancel each other. The relative error is always around the order of 10^{-9} $[a.u.]$, which is, at least from an experimental point of view, very low. However, we can most probably assume that these deviations come from numerical errors and the real result is much lower or even 0. As a motivation, we can first take a look at how well the solutions we obtained for the density matrix elements fulfill their equations of motion [21]. Concerning this, it has to be remarked that Mathematica's NDSolve returns a piecewise polynomial function of high enough order to approximate the real solution of the partial differential equation. Therefore, we can take these polynomials and insert them into the equations of motion to get an idea of how close they are to

the real solutions (see fig. 25).

The differences that occur are approximately of the same order as the deviations we got while calculating the total energy. Moreover, if we integrate over the plots in fig. 25, we also obtain a result of the order 10^{-9} $[a.u.]$.

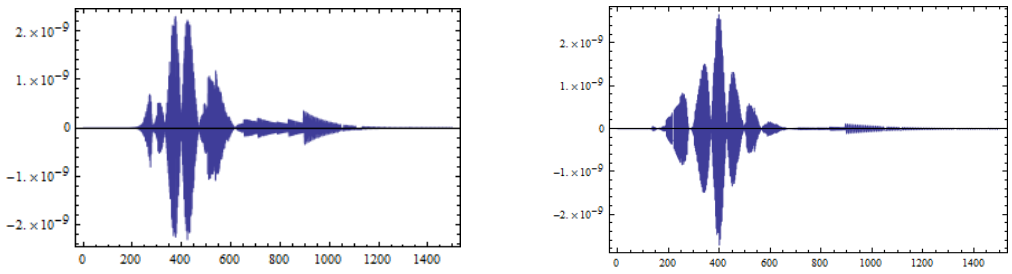

Figure 25: Deviations for (left) $\hat{\rho}_{ee}$ and (right) $\mathrm{Im}(\hat{\rho}_{eg})$. These calculations have been performed with the standard parameters for γ, Ω, etc. given in this chapter. Also, the units of the axis are the same as in fig. 24.

To further analyse this, we will now introduce an artificial loss channel by allowing spontaneous decay into some other level than our initial ground state (denoted as γ_{loss}):

$$\partial_t \hat{\rho}_{ee} = -(\gamma + \gamma_{loss})\hat{\rho}_{ee} + i\Omega(t)(\hat{\rho}_{eg} - \hat{\rho}_{ge}) \tag{121}$$

To get the same deviations as before in our energy calculation, γ_{loss} would have to be approximately of the order $\gamma_{loss} \simeq 10^{-10}[\gamma_0]$. As already stated, from an experimental standpoint this is small enough to be neglected and we can safely assume that energy conservation holds.

However, it is more likely that the source of this deviation comes from numerical uncertainties rather than a real physical loss channel we haven't taken into account yet. For instance, increasing the NDSolve-parameter "WorkingPrecision" or decreasing "MaxStepSize" improves our result, but not in a very efficient manner. Ultimately, one has to keep in mind that the achievable precision of the solution is limited by a) stability and convergence-behaviour of the numerical method b) memory capacity and c) calculation time. Therefore, an exact solution won't be possible and energy conservation can only be proven to a certain numerical precision.

For the results shown here and for most of the following calculations, the option "WorkingPrecision" of the Mathematica function "NDSolved" was set to "32" to avoid cutoff-errors. Furthermore, "MaxSteps" was set to infinity. For "NIntegrate", a "WorkingPrecision" of "16" was used together with a value of "20" for the option "MaxRecursion".

5.2.2 With Phase Kick

We will now again introduce a phase kick to the dipole answer, i.e. $\boldsymbol{E}^{(+)}_{scat}$ gains an additional factor $e^{i\phi_k}$. Thus, we obtain for the energy distribution of the system:

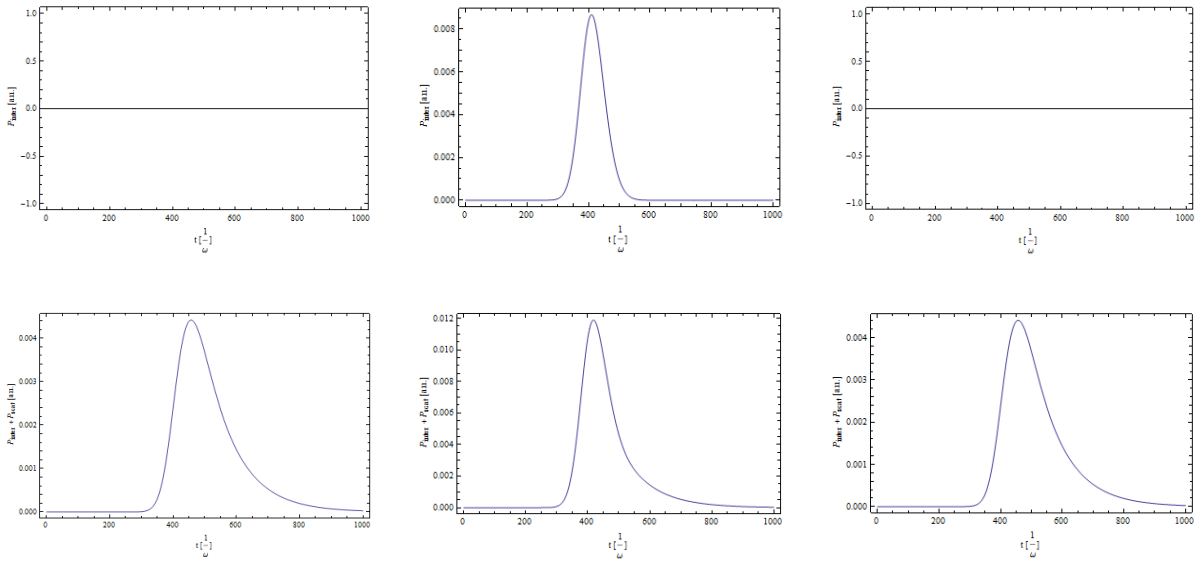

Figure 26: Columns: Phase kick ϕ_k of (left) $\frac{\pi}{2}$, (middle) π and (right) $\frac{3\pi}{2}$. Rows: (top) interference energy (bottom) total energy. Again, the standard parameters have been used to calculate these results. The interference part changes drastically with ϕ_k, but the scattered part remains unchanged as can also be seen from the formulas for the Poynting vector.

As we see, the energy distribution over time changes drastically. Furthermore, measured over the whole interaction and decay time, energy is not conserved anymore. We obtained this result already in all preceeding chapters. Therefore, either the kick performs work, or in a real physical system the realization of the kick does not break energy conservation and our artificial implementation of the kick up until now is slightly wrong. For instance, in all previous chapters the kick was already present during the excitation of the atom. However, in the experiment [4], excitation and phase kick are separated. This will be investigated further in the next chapter.

Table 4: Checking energy conservation for several values of ϕ_k. Note that these results have been obtained by choosing the standard parameters defined in the previous chapter for γ, Ω, etc.

ϕ_k	$\frac{\pi}{2}$	π	$\frac{3\pi}{2}$
W_{scat} [a.u.]	0.838	0.838	0.838
W_{int} [a.u.]	0	0.838	0
$W_{scat} + P_{int}$ [a.u.]	0.838	1.676	0.838

6 Lorentz Meets Fano Spectral Line Shapes

We will now describe the experiment [4] with our formalism by using a second laser for inducing the phase kick ϕ_k. This way, we can test for energy conservation in a real physically relevant system. Afterwards, the results will be compared with the simple two-level ansatz, which can be modified to give the same results. Moreover, as we work with pulses now, we can't just take the detected intensity and calculate it's frequency spectrum by analysing the dependence on the detuning Δ. Rather, the spectrum has to be calculated separately by Fourier transforming the electromagnetic fields. This will allow us to analyse the manipulation of the absorption profile more thoroughly.

6.1 Application: Three-Level System

In the previous chapters, we introduced the phase kick ϕ_k always by hand and not with a physical effect. We will change this now by coupling a third level to our initial two-level system, whereby a transition from $|1\rangle$ to $|2\rangle$ and vice versa is forbidden due to parity (see fig. 27). Accordingly, it is now possible to drive two transitions, i.e. $|1\rangle \leftrightarrow |e\rangle$ and $|e\rangle \leftrightarrow |2\rangle$.

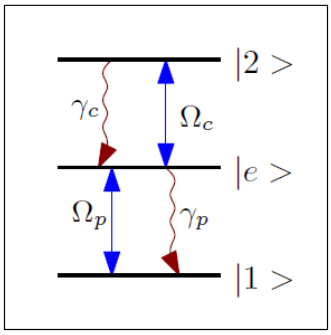

Figure 27: Three-level system in ladder form. Only the transitions $|1\rangle \leftrightarrow |e\rangle$ and $|e\rangle \leftrightarrow |2\rangle$ are possible, as the transition $|1\rangle \leftrightarrow |2\rangle$ is forbidden due to parity. Ω_p and Ω_c are the corresponding Rabi-Frequencies for driving the transitions. γ_p and γ_c are the decay rates due to spontaneous emission. Note that, other than depicted here, the states aren't separated equidistantly but such that a laser which drives one of the two transitions leaves the other one completely untouched. In the experiment, this is realized by using a XUV laser for the probe field and a NIR laser for the control field.

The field we analysed until now, the so called probe pulse, will drive the lower transition. To induce a phase kick onto the atomic response, a control pulse will be used which drives the upper transition $|e\rangle \leftrightarrow |2\rangle$. This control pulse has to be stronger than the probe pulse, such that it dresses the two states and consequently leads to a detuning for the $|1\rangle \leftrightarrow |e\rangle$ transition. In principle, this is analogue to a driven classical harmonic oscillator, where driving the system with a detuning $\Delta \neq 0$ leads to a phase shift of the driven oscillator. Furthermore, if the control laser is heavily detuned, i.e. $\Delta_c \gg \Omega_c$, the control laser just induces a phase kick and doesn't change the population of the state $|e\rangle$ [10].

6.1.1 Density Matrix Elements

To describe the dynamics of our three-level system, we need its Hamiltonian which can just be constructed by adding the Hamiltonians of the two possible transitions [10]:

$$V = \hbar\Delta_p \hat{S}_{11} - \hbar\Delta_c \hat{S}_{22} + \hbar\Omega_p \left(\hat{S}_{1e} + \hat{S}_{e1}\right) + \hbar\Omega_c \left(\hat{S}_{e2} + \hat{S}_{2e}\right) \tag{122}$$

Here, we again chose $\hat{S}_{xy} = |x\rangle \langle y|$. This leads to the following equations of motion for the density matrix elements:

$$\begin{pmatrix} \partial_t\hat{\rho}_{ee} \\ \partial_t\hat{\rho}_{11} \\ \partial_t\hat{\rho}_{22} \\ \partial_t\hat{\rho}_{12} \\ \partial_t\hat{\rho}_{21} \\ \partial_t\hat{\rho}_{1e} \\ \partial_t\hat{\rho}_{e1} \\ \partial_t\hat{\rho}_{2e} \\ \partial_t\hat{\rho}_{e2} \end{pmatrix} = \begin{pmatrix} -\gamma_p & 0 & \gamma_c & 0 & 0 & -i\Omega_p & i\Omega_p & -i\Omega_c & i\Omega_c \\ \gamma_p & 0 & 0 & 0 & 0 & i\Omega_p & -i\Omega_p & 0 & 0 \\ 0 & 0 & -\gamma_c & 0 & 0 & 0 & 0 & i\Omega_c & -i\Omega_c \\ 0 & 0 & 0 & A & 0 & i\Omega_c & 0 & 0 & -i\Omega_p \\ 0 & 0 & 0 & 0 & A^* & 0 & -i\Omega_c & i\Omega_p & 0 \\ -i\Omega_p & i\Omega_p & 0 & i\Omega_c & 0 & B & 0 & 0 & 0 \\ i\Omega_p & -i\Omega_p & 0 & 0 & -i\Omega_c & 0 & B^* & 0 & 0 \\ -i\Omega_c & 0 & i\Omega_c & 0 & i\Omega_p & 0 & 0 & C & 0 \\ i\Omega_c & 0 & -i\Omega_c & -i\Omega_p & 0 & 0 & 0 & 0 & C^* \end{pmatrix} \begin{pmatrix} \hat{\rho}_{ee} \\ \hat{\rho}_{11} \\ \hat{\rho}_{22} \\ \hat{\rho}_{12} \\ \hat{\rho}_{21} \\ \hat{\rho}_{1e} \\ \hat{\rho}_{e1} \\ \hat{\rho}_{2e} \\ \hat{\rho}_{e2} \end{pmatrix} \tag{123}$$

with $A = -\frac{\gamma_c}{2} - i(\Delta_c + \Delta_p)$, $B = -\frac{\gamma_p}{2} - i\Delta_p$ and $C = -\frac{1}{2}(\gamma_c + \gamma_p) + i\Delta_c$. This system of partial differential equations can easily be solved numerically with Mathematica 9.0 by using the implemented NDSolve-function (see Appendix D.2). Note that the Rabi-Frequencies are proportional to the field amplitude, i.e. they include the pulse-shape:

$$\Omega_p = \Omega_{p,0}\ e^{-\frac{(\boldsymbol{k}_{in}\boldsymbol{r}_p - \omega_{in}t)^2}{2\sigma^2}} \tag{124a}$$

$$\Omega_c = \Omega_{c,0}\ e^{-\frac{(\boldsymbol{k}_{in}\boldsymbol{r}_c - \omega_{in}t)^2}{2\sigma^2}} \tag{124b}$$

For simplicity, we assume w.l.o.g. that probe - and laser pulse have the same frequency and width. Furthermore, $\Omega_{x,0}$ is the Rabi-Frequency without any time-varying amplitude of the electric field, i.e. $\Omega_{x,0} = -\frac{E_{x,0}\hat{\boldsymbol{e}}\boldsymbol{d}}{\hbar}$. With $t_x = \frac{\boldsymbol{k}\boldsymbol{r}_x}{\omega_{in}}$, we can adjust at which time the individual pulses hit the atoms, as we have already done in the previous chapter. From now on, we will choose these parameters such that the control pulse hits the atoms separately and after the probe pulse.

6.1.2 Inducing a Phase Kick via a Control Laser

We are now able to solve the partial differential equations for different values of the probe - and control laser parameters. Our first goal is to check if it is really possible to modify $\hat{\rho}_{e1}$ with a phase factor by adjusting the control laser accordingly. Remember that giving $\hat{\rho}_{e1}$ a phase kick is similar to giving the

atomic dipole response an additional phase shift. To accomplish this, we start by investigating a special scenario: We assume the atoms to be in the state $\frac{1}{\sqrt{2}}(|1\rangle + |e\rangle)$ (e.g. after a $\frac{1}{4}$ Rabi - Oscillation). Furthermore, we neglect spontaneous decay for now and set the probe laser off, such that the atoms will remain in their current state. In theory, it should now be possible to introduce a phase kick with the control laser without changing the populations (see fig. 28).

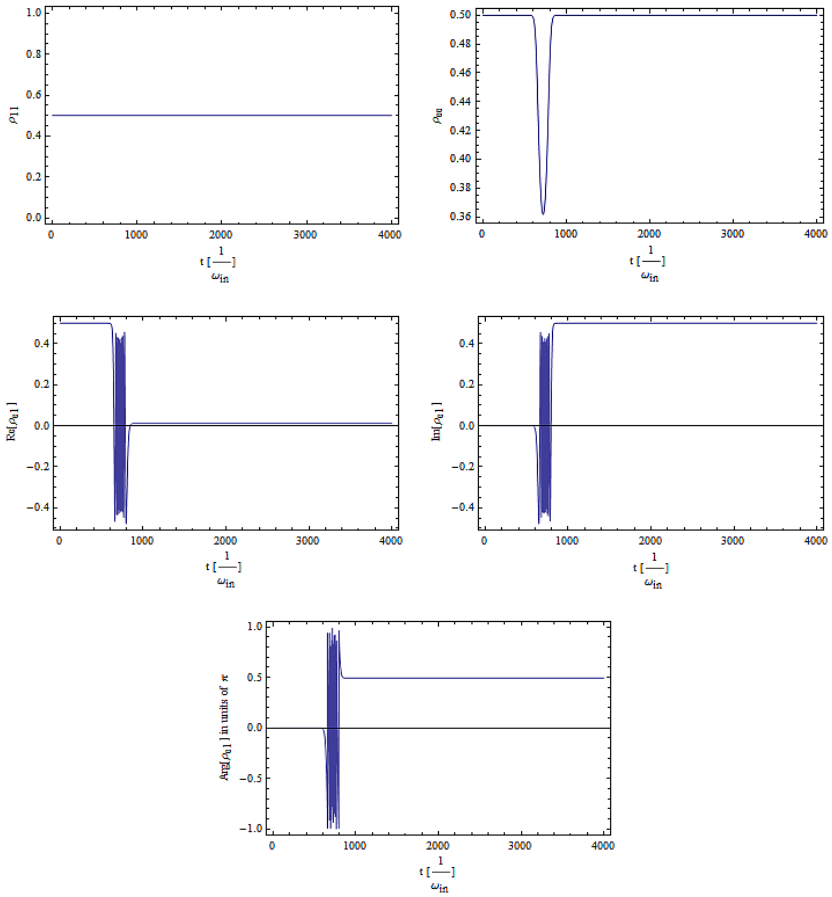

Figure 28: It is possible to give $\hat{\rho}_{e1}$ a phase kick with the control laser (here: $\phi_k = \frac{\pi}{2}$). For the calculation, following parameters were used: $\omega_{in} = 1$ [a.u.], $\Delta_c = 1$ [ω_{in}] , $\Omega_c = 1$ [ω_{in}], $t_c = 720$ [$\frac{1}{\omega_{in}}$], $\sigma = 50$, $\Omega_p = \gamma_p = \gamma_c = 0$. As the detuning Δ_c is quite small, there are still coherent evolutions induced by the control laser between $|e\rangle$ and $|2\rangle$.

The control laser hits the atoms at around $t = 720$ [$\frac{1}{\omega_{in}}$], what leads to oscillations in $\mathrm{Re}(\hat{\rho}_{e1})$, $\mathrm{Im}(\hat{\rho}_{e1})$ and the phase of $\hat{\rho}_{e1}$. This is exactly what one would expect, since the detuned control laser should indeed change the phase of $\hat{\rho}_{e1}$ dependent on time, leading to oscillations of the phase which stop when the pulse has passed [10]. Thus, we were able to induce a total phase kick of $\phi_k = \frac{\pi}{2}$ to $\hat{\rho}_{e1}$. Increasing the detuning will enable us to a) damp the coherent evolution out of $|e\rangle$ to $|2\rangle$ tremendously and b) alter the phase kick. Furthermore, this will reduce the oscillations, making it possible to perform a delta-like phase kick if the width of the control pulse is small enough. In the context of our later analysis, small enough means that the decay rate γ_p has to be much smaller compared to the kick-duration, making the

kick appear delta-like.

It is now possible to first excite the atoms with the probe pulse and then giving them a phase kick via the control pulse. In this case, the atoms are initially in the state $|1\rangle$. The dependence of the phase kick ϕ_k on the detuning Δ_c of the control laser is illustrated in fig. 29.

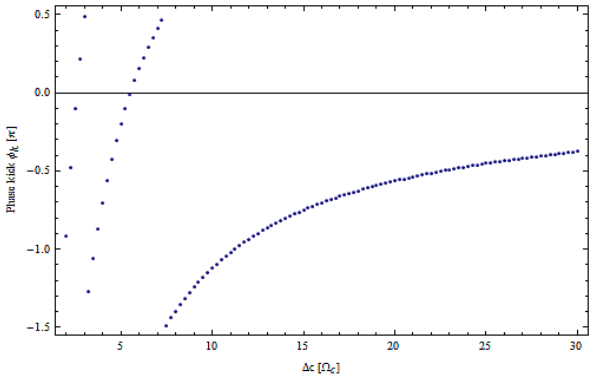

Figure 29: Phase kick ϕ_k induced by the control laser in dependence of its detuning Δ_c in units of π. The following parameters were used for the calculation: $\gamma_p = \frac{1}{200}$ $[a.u.]$, $\gamma_c = 1$ $[\gamma_p]$, $\Omega_p = 10$ $[\gamma_p]$, $\Omega_c = 400$ $[\gamma_p]$, $\omega_{in} = 200$ $[\gamma_p]$, $\Delta_p = 0$, $\sigma = 10$ $(\rightarrow t_{width} \simeq \frac{1}{10}$ $[\gamma^{-1}])$.

Note that the phase kick only depends on Δ_c, Ω_c and σ. The pulse position as well as the values for the probe pulse don't alter ϕ_k, as has to be expected.

6.1.3 Energy Conservation

We will now perform the same analysis as in chapter 5.2 concerning the total energy of the probe pulse - atoms system. However, the phase kick will now be implemented via the control laser instead, as previously, just by hand. Making sure that the pulses do not overlap, we obtain:

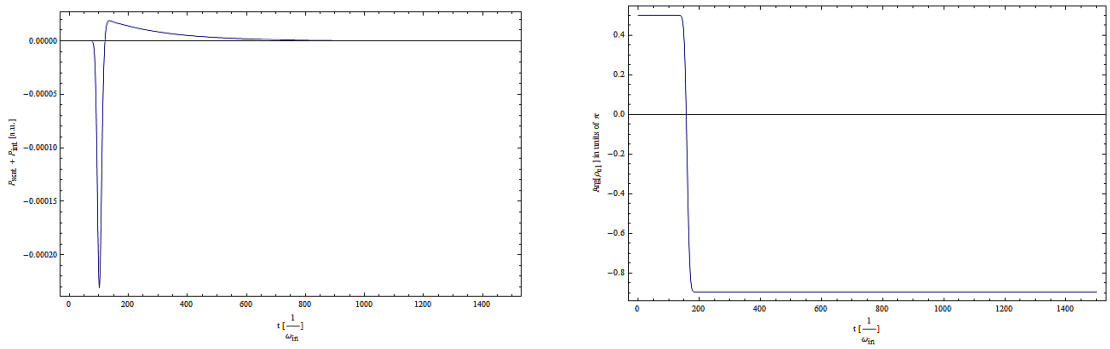

Figure 30: (left) Total energy distribution over time of the probe pulse - atoms system and (right) the phase of $\hat{\rho}_{e1}$. The energy distribution remains unchanged from the kickless case. Moreover, the control laser induces, as intended, a phase kick of $\phi_k = \frac{\pi}{2}$ onto the dipole response of the atoms. For the calculation, the same parameters as in fig. 29 were used, but with different pulse positions ($t_p = 100$ $[\frac{1}{\omega_{in}}]$, $t_c = 160$ $[\frac{1}{\omega_{in}}]$) and $\Delta_c = 8$ $[\Omega_c]$.

Integrating over the total energy distribution in time, we again obtain a result of the order of 10^{-9} $[a.u.]$, i.e. energy is still conserved in the limits of our numerical precision. Furthermore, the plot of the time dependent energy looks identical to the case without phase kick in chapter 5.2. Looking at the laser pulse setup in fig. 31, this can be explained quite vividly: First, the probe pulse hits the atoms and energy is transferred from the pulse into the atoms (absorption). When the pulse has passed the atoms, both are locally separated and energy cannot be exchanged between those two anymore. Therefore, as soon as the control pulse hits the atoms, the kick can't possibly change the energy distribution of the probe pulse - atoms system.

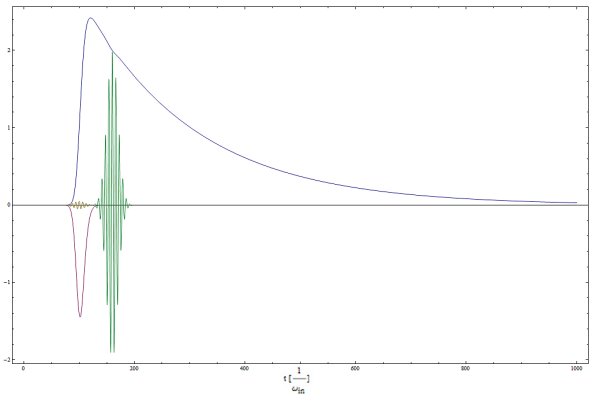

Figure 31: Setup of our experiment. First, the probe pulse hits the atoms (yellow), which leads to an transfer of energy out of the pulse into the atoms (red), resulting in an excitation of the atoms (blue). Later on, the control pulse (green) hits the atoms and induces a phase kick. Note that the red curve is proportional to $\mathrm{Im}(\hat{\rho}_{e1})$ *and the blue one to* $\hat{\rho}_{ee}$.

To sum it up, the pulse shape of the probe pulse limits the time during which the probe laser and the atoms can exchange energy. Therefore, if the control laser hits the atoms sufficiently later as the probe pulse, it leaves the total energy distribution of our probe laser untouched. Therefore, the phase kick can't be seen in the time dependent energy distribution, but only in the frequency spectrum.

In all previous chapters, the phase kick was already present during the excitation of the atoms. This lead to a breaking of energy conservation, as one can simply imagine that forcing a phase kick onto a driven harmonic oscillator costs definitely energy. We will later see that our simple two-level approach from chapter 5 leads to the same results presented here.

6.1.4 Frequency Spectrum

Since for separate pulses, energy conservation holds, we have to check now if the phase kick leads to the desired effect of altering the absorption line. If this is indeed the case, there has to be an additional modification in the frequency spectrum which ensures energy conservation.

To get the frequency spectrum of the detected intensity, we have to calculate the expression:

$$P(\omega) = 2\epsilon_0 c \ \mathrm{Re}\left\langle \boldsymbol{E}_{in}^{(-)}(\omega)\boldsymbol{E}_{scat}^{(+)}(\omega)\right\rangle \tag{125}$$

The frequency dependent fields can be obtained via a Fourier transform

$$\boldsymbol{E}^{(+)}_{scat}(\omega) = \int_{t_p}^{\infty} \boldsymbol{E}^{(+)}_{scat}(t)\ e^{2\pi i\omega t}\ \mathrm{d}t \tag{126a}$$

$$\boldsymbol{E}^{(-)}_{scat}(\omega) = \boldsymbol{E}^{(+)\dagger}_{scat}(\omega) = \int_{t_p}^{\infty} \boldsymbol{E}^{(-)}_{scat}(t)\ e^{-2\pi i\omega t}\ \mathrm{d}t \tag{126b}$$

where t_p is the time when the pulse hits the atoms. This gives us [8]:

$$P(\omega) = 2\epsilon_0 c\ \mathrm{Re}\int_{-\infty}^{\infty}\mathrm{d}t_1\int_{t_p}^{\infty}\mathrm{d}t_2\ \langle \boldsymbol{E}^{(-)}_{in}(t_1)\boldsymbol{E}^{(+)}_{scat}(t_2)\rangle\ e^{-2\pi i\omega(t_1-t_2)} \tag{127a}$$

$$\rightarrow 2\epsilon_0 c\left(\int_{-\infty}^{\infty}\mathrm{d}t_1\ \langle \boldsymbol{E}^{(-)}_{in}(t_1)\rangle\ e^{-2\pi i\omega t_1}\right)\left(\mathrm{Re}\int_{0}^{\infty}\mathrm{d}t_2\ \langle \boldsymbol{E}^{(+)}_{scat}(t_2)\rangle\ e^{2\pi i\omega t_2}\right) \tag{127b}$$

The simplifications used here can be motivated as follows: First, the incident field is classical and can therefore be separated from the expectation value. Furthermore, we can choose $t_p = 0$, such that the Gaussian envelope of the pulse can be integrated trivially, as the maximum of the pulse coincides in this case with $t = 0$. As the Fourier transform of a Gaussian is again just a Gaussian (and therefore a real function), it can be drawn out of the Re(...). Additionally, in all coming calculations we will neglect the oscillating terms $e^{\pm i\omega_{in}t}$, as these only shift the detected spectrum from $\omega = 0$ to $\omega = \omega_0$.

In addition, it's possible to show that $\int_{-\infty}^{\infty} P(\omega)\ \mathrm{d}\omega = \int_{-\infty}^{\infty} P(t)\ \mathrm{d}t$ by using $\int_{-\infty}^{\infty} e^{-2\pi i\omega(t_1-t_2)}\ \mathrm{d}\omega = \delta(t_1 - t_2)$, i.e. the total energy is the same in the time - and frequency domain. Thus, since energy is conserved in the time domain, it should also be conserved in the corresponding frequency spectrum.

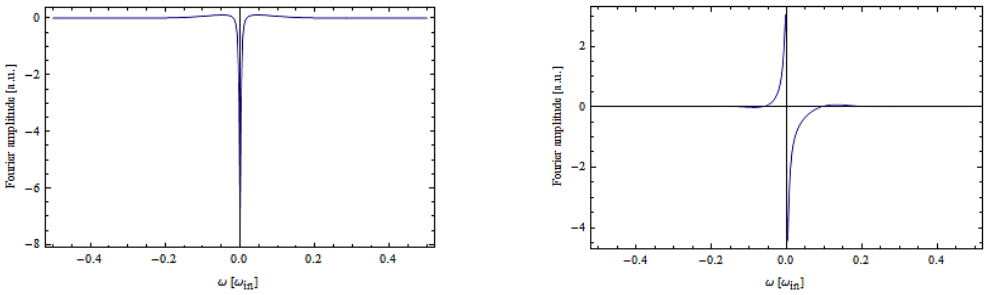

Figure 32: (left) Absorption line without control laser. The Lorentzian has small "ears", which originate from the finite width of the probe pulse. (right) Absorption line with control laser on. The induced phase kick is $\simeq \frac{\pi}{2}$. Small oscillations occur in the spectrum due to the control pulse. The following parameters were used for the calculation: $\gamma_p = \frac{1}{200}$ *[a.u.],* $\gamma_c = 1$ *[*γ_p*],* $\Omega_p = 2$ *[*γ_p*],* $\Omega_c = 200$ *[*γ_p*],* $\omega_{in} = 200$ *[*γ_p*],* $t_c = 20$ *[*$\frac{1}{\omega_{in}}$*],* $\Delta_c = 11.1$ *[*Ω_c*],* $\Delta_p = 0$*,* $\sigma = 10$*.*

As expected, the kick alters the detected line shape. However, additional oscillations occur in the spectrum. We will analyse this effect first by going back to the simpler two-level system and constructing a toy model. Afterwards, the obtained results will be compared to the results of the three-level system.

6.2 Returning to the Two-Level System

To analyse the important physics, we will first return to the simpler two-level case. As the phase kick should be separated from the excitation, we implement it the following way:

$$\boldsymbol{E}_{scat}^{(+)}(t) = i\frac{k_0^3 d}{3\pi\epsilon_0}\hat{S}_-(t)e^{i(\boldsymbol{k}_0\boldsymbol{r}-\omega_0 t_r+\theta(t-t_c)\phi_k)}\boldsymbol{\epsilon} \tag{128}$$

Here, we modified the phase kick with a Heaviside Theta Function, which switches the phase kick on at time t_c. Furthermore, we define $\theta(0) = 1$. This way, it is possible to give the atomic dipole response a delta-like phase kick at an arbitrary, adjustable time t_c.

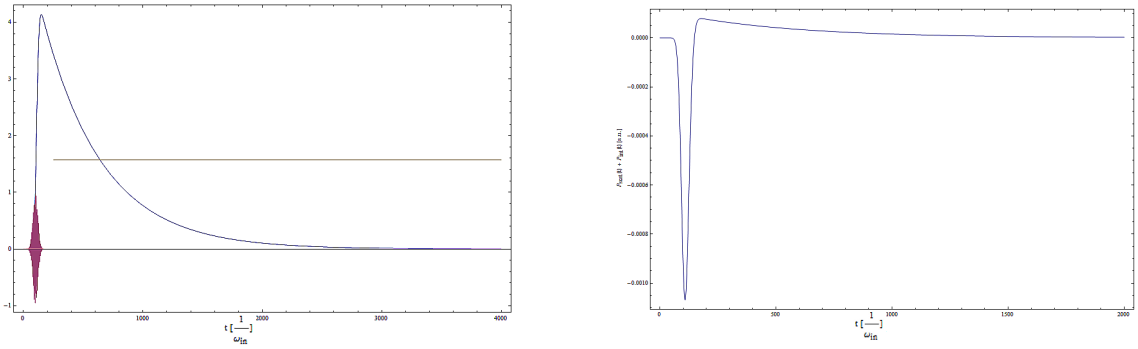

Figure 33: (left) Setup for probe pulse and phase kick. Red is the probe pulse that excites the atoms, yellow is the value of the phase kick and blue is $\hat{\rho}_{ee}$. The phase kick comes only after the excitation of the atoms. (right) Total energy distribution dependent on time. The system behaves similar as without the phase kick.

In this setup, when phase kick and probe pulse are separate, we have indeed again energy conservation. This is the same result we obtained in the previous chapter. Therefore, we will start now by analysing the frequency spectrum of the two-level scenario.

6.2.1 Approximation with Analytic Functions

As already said, it's easier to first introduce a toy model for investigating the energy conservation in the frequency spectrum, as we are then able to perform all calculations analytically. To derive an appropriate model, we first look at $\langle E_{scat}^{(+)}\rangle \simeq i\hat{\rho}_{eg} = -\mathrm{Im}(\hat{\rho}_{eg})$ (as $\mathrm{Re}(\hat{\rho}_{eg}) = 0$ for $\Delta = 0$) without a phase kick:

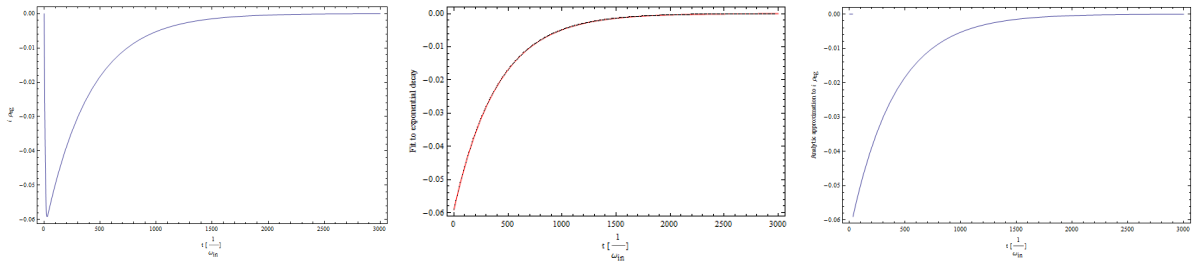

Figure 34: (left) $i\hat{\rho}_{eg}$ as a function of time. (middle) Fit to the free decay of $i\hat{\rho}_{eg}$ after the excitation with the fit function $c \cdot e^{-a(t-b)}$. Performing a Least-Square fit in Mathematica 9.0 gives for the parameters $a \simeq 0.0025$, $b \simeq -0.5859$ and $c \simeq -0.0592$. (right) Approximating $i\hat{\rho}_{eg}$ with the analytic function $-0.0591\ \theta(t-30)\ e^{-0.0025(t-30)}$, where t is in units of $\frac{1}{\omega_{in}}$. For the solution of the two-level density matrix elements, the following parameters were used: $\gamma = \frac{1}{200}$ [a.u.], $\Omega = 1$ [γ], $\omega = 200$ [γ], $\sigma = 10$ and $\Delta = 0$.

As we can see, the evolution after the excitation is indeed an exponential decay with decay rate $\frac{\gamma}{2}$, as already expected from the analytic solution of the free equation of motions for the density matrix elements. Furthermore, we simplify the probe pulse in our toy model by assuming a delta-like excitation, again represented by a Heaviside Theta Function $\theta(t - t_p)$. Note that in this case, $\langle E_{in}^{(-)}(\omega)\rangle$ is just a constant prefactor, as the Fourier transform of the delta-distribution is a constant. Therefore, the energy can be spread to all frequencies in the delta-kick case. For a real probe pulse with a certain width, this spread gets limited as the Fourier transform of a Gaussian with finite width is again a Gaussian with finite width.

We will now compare the frequency spectrum of our new toy model with the more realistic two-level model. For this, we will only plot $\langle E_{scat}^{(+)}(\omega)\rangle$ and neglect the additional envelope obtained from $\langle E_{in}^{(-)}(\omega)\rangle$, such that the two-level model and the toy model can be compared on equal terms. However, there is one major problem: Since the probe pulse is not delta-like, the excitation of the atoms needs a finite time, but in our toy model, the atoms become excited instantly. Thus, the frequency spectrum of the toy model will differ from the two-level case due to the position of the delta-kick. To illustrate this effect, the delta-kick will be performed at different times $t_p = \{\, 0, \frac{9}{200}, \frac{30}{200} \,\}$ $[\gamma^{-1}]$

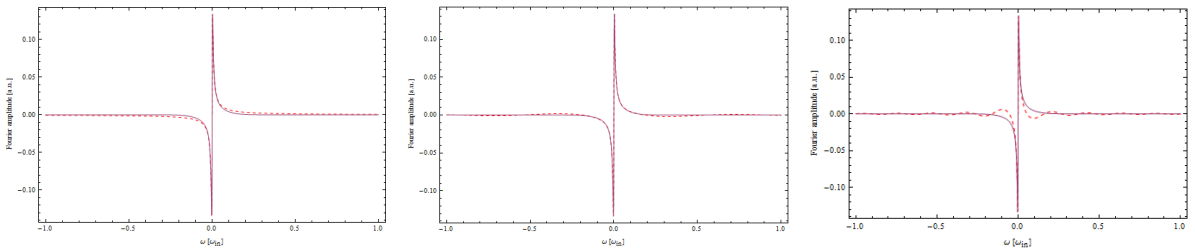

Figure 35: Frequency spectrum of the probe pulse for $\phi_k = \frac{\pi}{2}$. (left) $t_p = 0$, (middle) $t_p = \frac{9}{200}$ $[\gamma^{-1}]$ and (right) $t_p = \frac{30}{200}$ $[\gamma^{-1}]$. The red, dotted curves show the result of the toy model. The blue curves represent the original data of the two-level model. The phase kick is applied at $t_c = 0$.

Indeed, additional oscillations occur dependent on the kick-time. Furthermore, in the two-level case the

pulse width changes the detected spectrum slightly. These two observations originate, in principle, from the same effect that the atoms aren't instantly excited at $t = 0$.

More importantly, the results obtained by the toy model are very close to the two-level case. The only differences that occur come from the fact that in a real experiment, it's not possible to create a perfect delta-pulse to excite the atoms. However, the effects due to the finite pulse width can be reduced by increasing the lifetime γ^{-1} of the atomic transition.

Additionally, for $\phi_k = \frac{\pi}{2}$, the expected Fano profile was recovered. In fig. 36, we see that the well known line forms for $\phi_k = 0$, $\phi_k = \pi$ and $\phi_k = \frac{3\pi}{2}$ can be constructed as well.

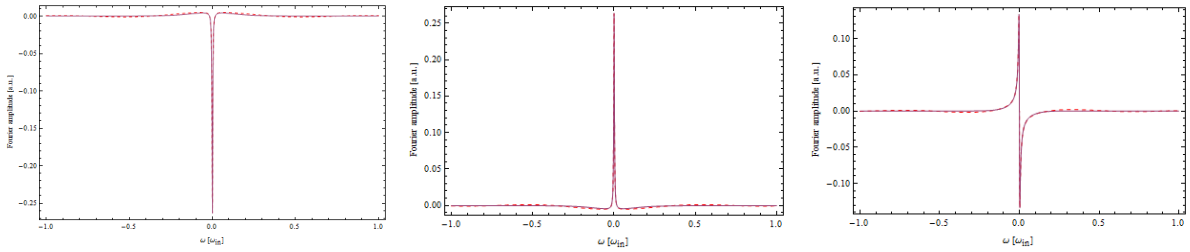

Figure 36: Manipulating the line form via ϕ_k. (left) $\phi_k = 0$, (middle) $\phi_k = \pi$ and (right) $\phi_k = \frac{3\pi}{2}$. The phase kick is still being applied at $t_c = 0$.

In the previous chapter, we found out that separating excitation pulse and phase kick leads to energy conservation. We will introduce this now into our toy model by applying the phase kick via the function $e^{i\theta(t-t_c)\phi_k}$ with $t_c > 0$:

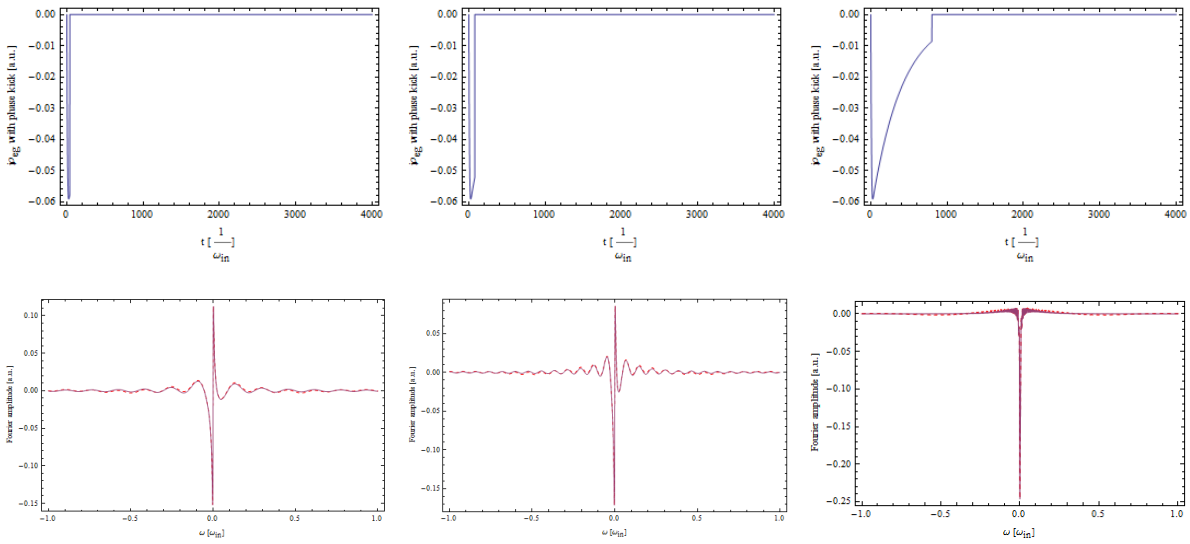

Figure 37: Spectrum with $\phi_k = \frac{\pi}{2}$ for different phase kick positions t_c. (top) $\mathrm{Re}(i\hat{\rho}_{eg}\, e^{i\theta(t-t_c)\frac{\pi}{2}})$ and (bottom) the corresponding frequency spectrum. (left) $t_c = 0.2\ [\gamma^{-1}]$, (middle) $t_c = 0.4\ [\gamma^{-1}]$ and (right) $t_c = 4\ [\gamma^{-1}]$.

Note that due to the delayed phase kick, additional oscillations appear in the spectrum. In the next

chapter, we shall see that these oscillations lead to a deformation of the spectrum without changing its energy content, therefore enabling us to switch between Lorentz and Fano profiles while total energy is conserved. Also, for large delays, the spectrum transforms to a negative Lorentzian again, as one would expect. The Fourier transform has been done numerically by modifying the already included Mathematica function "Fourier" (see Appendix D.1).

6.2.2 Analysis of the Frequency Spectrum

Putting everything together from the last chapter, our toy model now has the following form:

$$i\hat{\rho}_{eg}(t) \quad \xrightarrow{toy\ model} \quad P_{toy}(t) = -\theta(t)\ e^{i\theta(t-t_c)\phi_k}\ e^{-\gamma t} \tag{129}$$

The frequency spectrum of the detected signal can be obtained by calculating $\mathrm{Re}\big(\mathcal{F}\big(P_{toy}(t)\big)\big)$, where $\mathcal{F}$ denotes the Fourier transform as introduced in chapter 6.1.4. The Fourier transform can be done by simply using the "FourierTransform" - function of Mathematica 9.0.

First, we will take a look at the simple case of no phase kick, i.e. we set $\phi_k = 0$. This gives us, independent of t_c:

$$P_{toy}(\omega)\Big|_{\phi_k=0} = -\frac{\gamma}{\gamma^2+\omega^2} \tag{130}$$

This is, as expected, a negative Lorentzian. Further, let's assume that $t_c = 0$ and ϕ_k arbitrary, i.e. excitation and phase kick are coincident. Thus, we get:

$$P_{toy}(\omega)\Big|_{t_c=0} = \frac{-\gamma\cos(\phi_k) + \omega\sin(\phi_k)}{\gamma^2+\omega^2} \tag{131}$$

Note that if we include the oscillations of the electromagnetic fields $e^{-i\omega_{in}t}$ in $P_{toy}(t)$, this only shifts $\omega \to \omega - \omega_{in} = \Delta$. Thus, we obtain the exactly same results as in chapter 4.3, where the incident field was a continuous plane wave. This makes sense, as in both cases, the kick is being performed while the atoms interact with the probe laser.

Finally, we can assume $t_c > 0$ to get:

$$P_{toy}(\omega)\Big|_{t_c>0} = L_{toy}(\omega) + O_{toy}(\omega) \tag{132a}$$

$$\text{with} \qquad L_{toy}(\omega) = -\frac{\gamma}{\gamma^2+\omega^2} \tag{132b}$$

$$O_{toy}(\omega) = \frac{2\ e^{-\gamma t_c}\sin\left(\frac{\phi_k}{2}\right)\left(\omega\cos\left(\frac{\phi_k}{2}+t_c\omega\right)+\gamma\sin\left(\frac{\phi_k}{2}+t_c\omega\right)\right)}{\gamma^2+\omega^2} \tag{132c}$$

Thus, the spectrum can be split up into a negative Lorentzian $L_{toy}(\omega)$ and an oscillating term $O_{toy}(\omega)$. Calculating the total energy content of $P_{toy}(\omega)\big|_{t_c>0}$, one can easily determine that:

$$\int_{-\infty}^{\infty} O_{toy}(\omega)\ \mathrm{d}\omega = 0 \tag{133}$$

This means that the total energy is still the same as for the case without phase kick. Therefore, introducing a phase kick redistributes the energy in the spectrum without changing the energy content of the spectral line. This is realized with an oscillating term $O_{toy}(\omega)$, which vanishes when integrated over. Note that this redistribution also covers frequencies which lie outside the range of the normal negative Lorentzian. In the case of a delta-like probe pulse, these oscillations spead over all frequencies from $-\infty$ to ∞. However, in the case of a finite probe pulse, the spread will be limited to a certain range around the original Lorentzian's position.

To sum it up, the oscillations which appeared when setting $t_c > 0$ in the last chapter are actually necessary to ensure energy conservation. Consequently, the phase kick doesn't just alter the line shape from Lorentz to Fano and vice versa, it also introduces small oscillations. How the oscillating term $O_{toy}(\omega)$ changes dependent on t_c is being illustrated in fig 38.

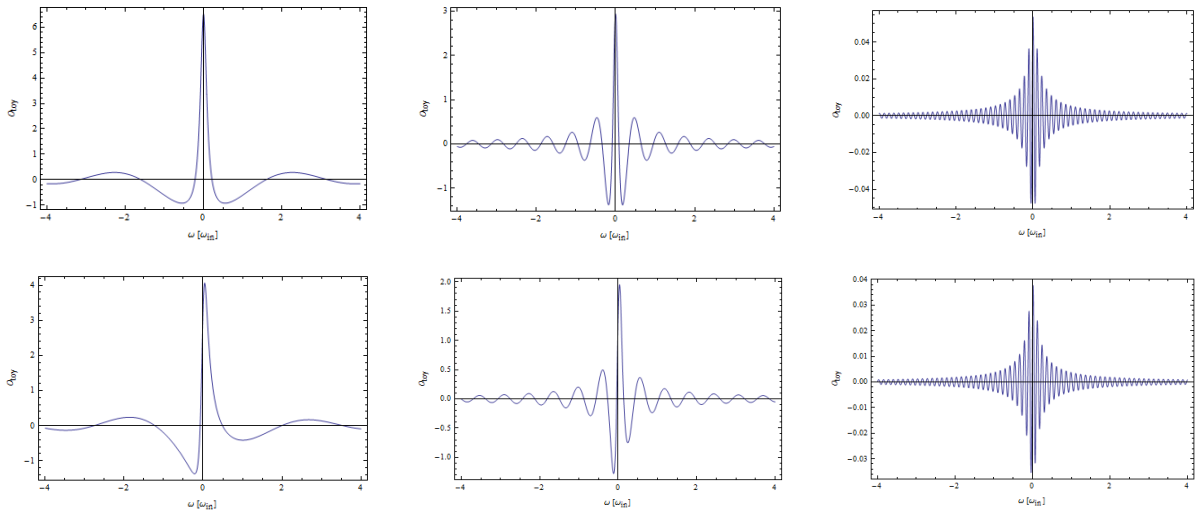

Figure 38: $O_{toy}(\omega)$ for different values of ϕ_k and t_c. (top) $\phi_k = \pi$ and (bottom) $\phi_k = \frac{\pi}{2}$. (left) $t_c = \frac{1}{5}$ $[\gamma^{-1}]$, (middle) $t_c = 1$ $[\gamma^{-1}]$, (right) $t_c = 3$ $[\gamma^{-1}]$. If the kick is applied at times $\leq \gamma^{-1}$, the line shape gets indeed altered. However, for greater values of t_c, strong oscillations occur which destroy this modification. Furthermore, the overall contribution of the oscillating term becomes smaller and for $t_c \to \infty$, it vanishes. For these plots, $\gamma = \frac{1}{10}$ $[a.u.]$ was used.

6.3 Verifying the Results of the Toy Model

6.3.1 Two-Level System

We will now check if our results are also true for the two-level model. To do so, we have to calculate the total energy of the frequency spectrum, i.e.

$$\int_{-\infty}^{\infty} \langle \boldsymbol{E}_{in}^{(-)}(\omega) \boldsymbol{E}_{scat}^{(+)}(\omega) \rangle \ \mathrm{d}\omega \tag{134}$$

This will be done for different phase kick values $\phi_k = 0,\ \frac{\pi}{2},\ \pi,\ \frac{3\pi}{2}$. The corresponding frequency spectra are illustrated in fig. 39.

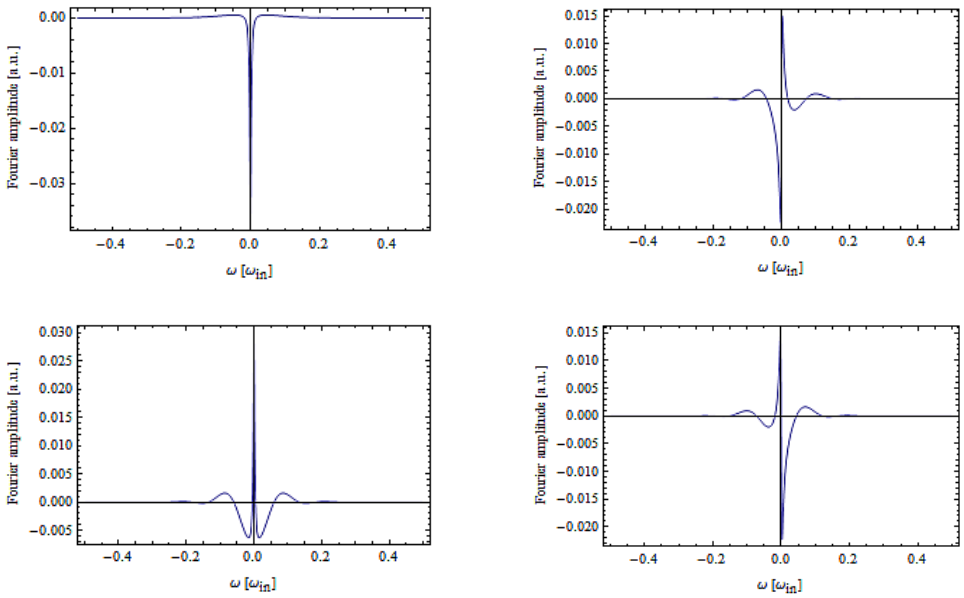

Figure 39: Frequency spectrum for (top left) $\phi_k = 0$, (top right) $\phi_k = \frac{\pi}{2}$, (bottom left) $\phi_k = \pi$ and (bottom right) $\phi_k = \frac{3\pi}{2}$. The parameters used here are: $\gamma = \frac{1}{200}$ [a.u.], $\Omega = 1$ [γ], $\omega_{in} = 200$ [γ], $\sigma = 10$ and $\Delta = 0$.

If we perform the integral to obtain the total energy, the differences of the results for the different values of ϕ_k are of the order of 10^{-6} [a.u.]. Since taking the Fourier transform of the density matrix elements certainly adds new uncertainties in the result, we can safely state that the energy content of the spectral line doesn't change with ϕ_k.

How the finite width of the probe pulse changes the spectral line can be seen very nicely in fig. 40 and 41. First, introducing a finite pulse width leads to "ears" around the spectral line, as can be seen in the case without phase kick. Furthermore, the oscillations that originate from the phase kick are being damped (fig. 41).

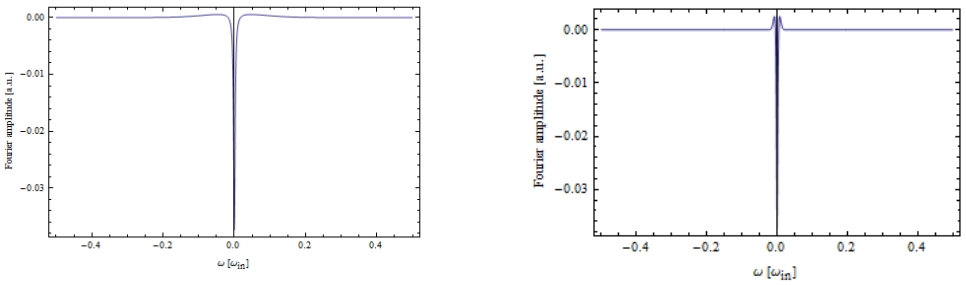

Figure 40: Negative Lorentzian for different pulse widths of the probe pulse. (left) Pulse width $t_{width} \simeq \frac{1}{10}\ [\gamma^{-1}]$ *and (right)* $t_{width} \simeq 1.3\ [\gamma^{-1}]$.

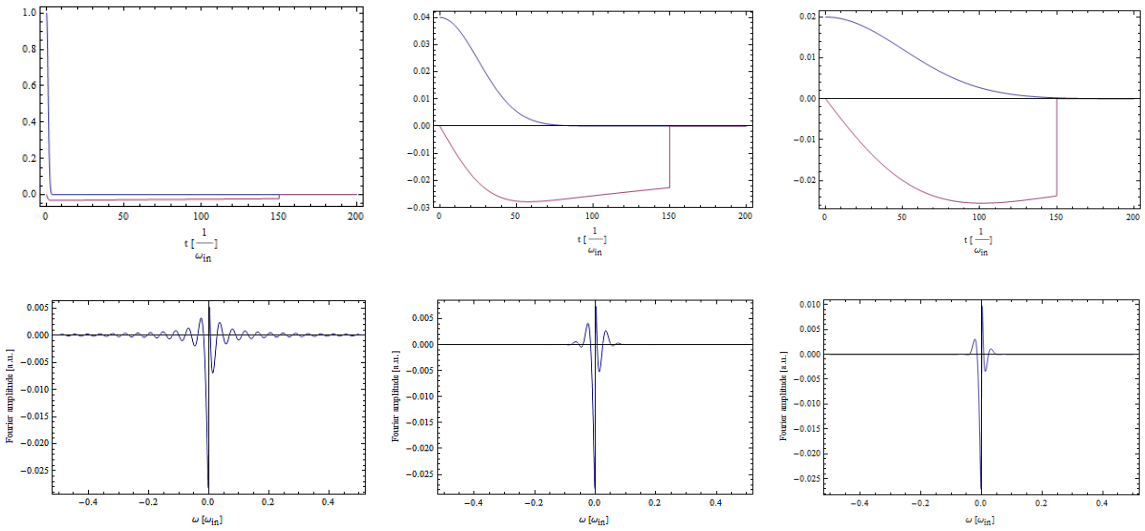

Figure 41: (top) The blue line represents the probe pulse, the red one $\mathrm{Re}(i\hat{\rho}_{eg})$. *(bottom) The corresponding frequency spectrum of the interference energy. (left) The pulse width is* $t_{width} \simeq \frac{1}{100}\ [\gamma^{-1}]$, *(middle)* $t_{width} \simeq \frac{1}{4}\ [\gamma^{-1}]$ *and (right)* $t_{width} \simeq \frac{1}{2}\ [\gamma^{-1}]$.

6.3.2 Three-Level System

Finally, we will take a look at the realistic three-level system again. In the previous chapters, the control laser introduced small oscillations which became stronger with increasing delay of the control pulse. This is also the case here:

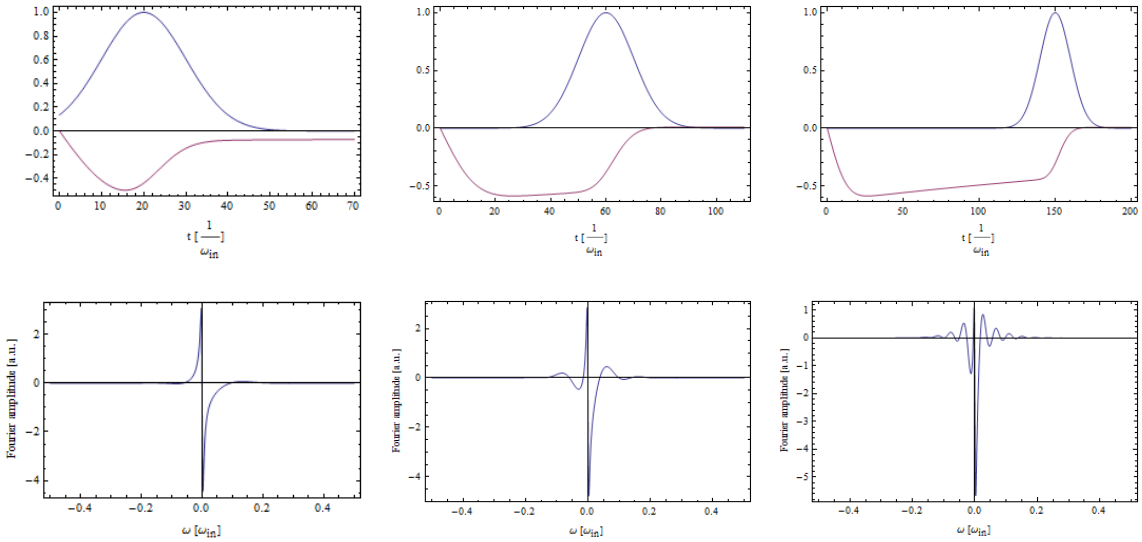

Figure 42: Additional oscillations occur if the delay of the control pulse is increased. (top) The red line represents again $-\mathrm{Im}(\hat{\rho}_{e1})$ and the blue one is the control pulse. Note that the pulse has in all cases the same width. (bottom) The corresponding frequency spectrum resulting from the above setup. The same parameters as in fig. 36 were used.

However, since the control pulse is not delta-like as in the previous examples, but has a finite width, an additional effect occurs which "distorts" the spectrum:

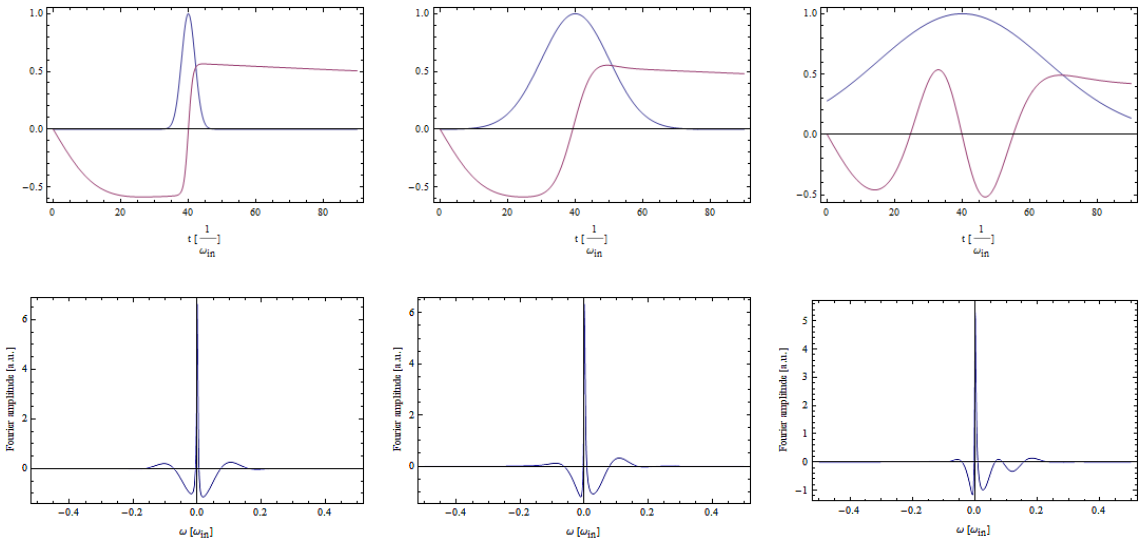

Figure 43: (top) Again, the setup with varying pulse widths. Additionally, the detuning has been adjusted for every pulse to ensure that the phase kick is in all three cases $\phi_k = \pi$. (left) $t_{width} \simeq \frac{2}{100}$ $[\gamma^{-1}]$, $\Delta_c = 2$ $[\Omega_c]$, (middle) $t_{width} \simeq \frac{1}{10}$ $[\gamma^{-1}]$, $\Delta_c = 5$ $[\Omega_c]$ and (right) $t_{width} \simeq \frac{3}{10}$ $[\gamma^{-1}]$, $\Delta_c = 8.5$ $[\Omega_c]$.

Since the total energy is conserved for the three-level system (see chapter 6.1.3), the results of the toy model can be applied here as well. As the toy model and the three-level case differ in the pulse widths

only, analysing the effect of changing these widths more thoroughly is certainly of high interest for further studies.

6.4 Overlapping Pulses in the Realistic System

One question that still remains is: What happens when probe - and laser pulse overlap? In the preceeding chapters, this lead to a breaking of energy conservation. However, analysing this in the more realistic three-level system, we obtain an intriguing result: The total energy is still conserved up to a relative, numeric error of 10^{-9} $[a.u.]$.

To illustrate this, the time dependent energy has been calculated for $\gamma_p = \frac{1}{200}$ $[a.u]$, $\gamma_c = 1$ $[\gamma_p]$, $\omega_{in} = 200$ $[\gamma_p]$, $\Omega_c = 2$ $[\gamma_p]$, $\Delta_c = 8$ $[\Omega_c]$, $\Delta_p = 0$ and $\sigma = 10$. In fig. 44, both pulses overlap completely.

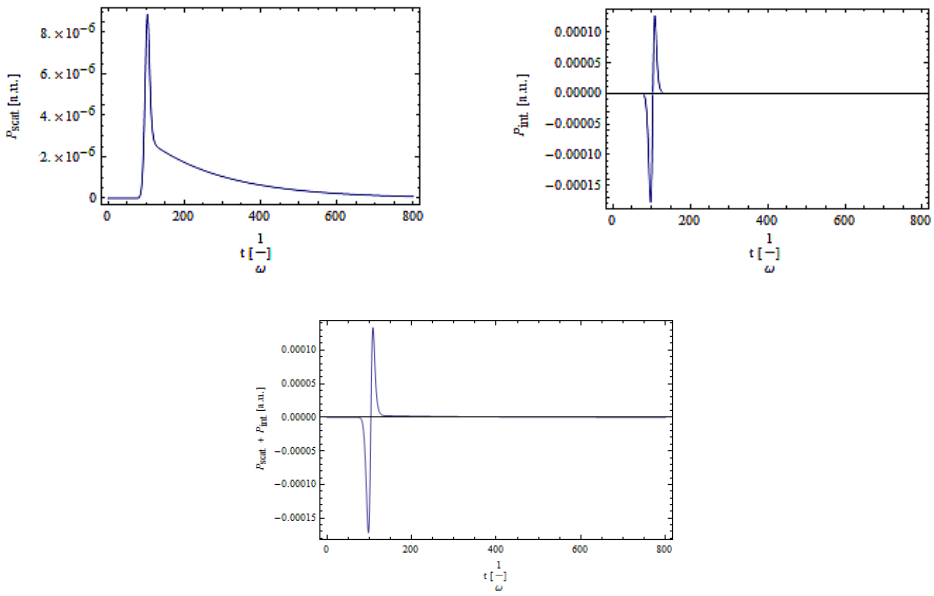

Figure 44: (top left) Scattered energy, (top right) interference energy and (bottom) total energy dependent on time. The influence of the control pulse can be easily seen in these plots. For instance, the phase kick changes the amount of energy the atoms scatter. Furthermore, the interference energy now also has a positive part instead of just being negative. This is the same effect that happens when detuning the probe laser.

Thus, on the one hand, due to the overlap of the pulses the amount of scattered energy gets reduced. On the other hand, the interference energy takes on the same form as if no control pulse was present, but the probe pulse detuned. This makes sense, since the control pulse changes how the atoms interact with the probe pulse. Furthermore, the control pulse leads indeed to a detuning for the probe pulse, matching these results.

The frequency spectrum for completely overlapping pulses looks the following way:

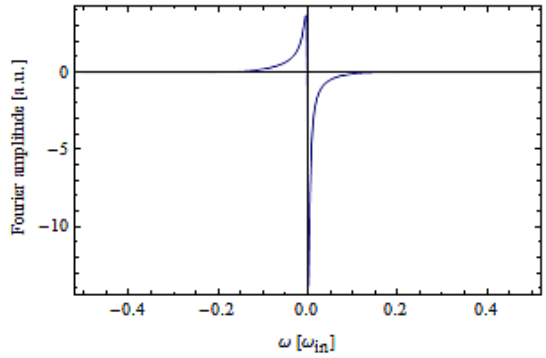

Figure 45: Detected frequency spectrum for completely overlapping pulses.

From fig. 46 (right), we see that for a complete overlap, the induced phase kick amounts to $\simeq \frac{3\pi}{2}$, matching the Fano profile illustrated here.

In fig. 46 (left), it's shown how the scattered and interference energy change with the distance between both pulses.

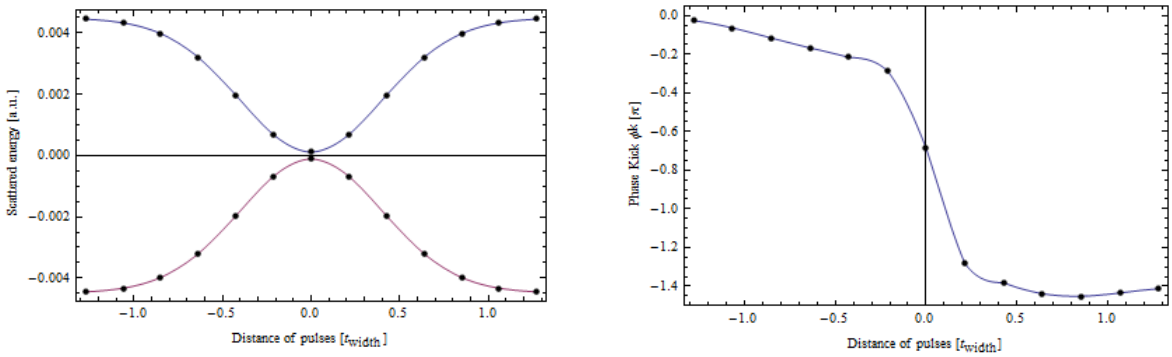

Figure 46: (left) Blue represents the scattered energy and red the interference energy/energy absorbed by the atoms. (right) Phase kick ϕ_k induced on $\hat{\rho}_{e1}$. In this example, probe - and control pulse have the same width.

As we see, both scattered and interference energy change in such a way that their sum remains constant, i.e. $= 0$. Therefore, energy is still conserved even when the pulses overlap. During the first few chapters of this thesis, an overlap between excitation and phase kick resulted in a breaking of energy conservation. However, this was only the case because the phase kick was introduced manually by multiplying $\hat{\rho}_{e1}$ with $e^{i\phi_k}$, leaving $\hat{\rho}_{ee}$ unaltered. Furthermore, when the pulses are separated, altering the position of the control pulse does not change the value of ϕ_k. But fig. 46 shows that, in the case of overlapping pulses, the position of the control laser plays indeed a role for the value of ϕ_k. These are very interesting results that should be studied further in the future.

7 Summary and Outlook for Further Studies

The main goal of this thesis is to better understand how energy is conserved in systems with time - dependent Fano control. The investigation is based on an experiment performed at the Max-Planck-Institut für Kernphysik in Heidelberg [4], where absorption lines of Helium are being transformed from Lorentz to Fano profiles and vice versa via a second laser. However, the framework and results derived here can also be applied to other physical systems, e.g. [5].

The natural starting point was to investigate energy conservation in simple optical systems, e.g. a single two-level atom which is being excited by a plane laser wave (chapter 3). To check for energy conservation, we used, analogue to Classical Electrodynamics, a semiclassical version of the Poynting vector for detectors far away from the atom (eq. 84):

$$\begin{aligned}\boldsymbol{P} =& 2\epsilon_0 c \ \mathrm{Re}\,\langle \boldsymbol{E}_{in}^{(-)} \boldsymbol{E}_{in}^{(+)} \rangle \ \hat{\boldsymbol{k}} + 2\epsilon_0 c \ \mathrm{Re}\,\langle \boldsymbol{E}_{scat}^{(-)} \boldsymbol{E}_{scat}^{(+)} \rangle \ \hat{\boldsymbol{r}} \\ &+ 2\epsilon_0 c \ \mathrm{Re}\,\langle \boldsymbol{E}_{in}^{(-)} \boldsymbol{E}_{scat}^{(+)} \rangle \ \hat{\boldsymbol{r}} + 2\epsilon_0 c \ \mathrm{Re}\,\langle \boldsymbol{E}_{scat}^{(-)} \boldsymbol{E}_{in}^{(+)} \rangle \ \hat{\boldsymbol{k}}\end{aligned}$$

Note that the electric field, after interacting with the atom, is composed of two contributions $\boldsymbol{E} = \boldsymbol{E}_{in} + \boldsymbol{E}_{scat}$. $\boldsymbol{E}_{in}$ represents the case as if no atom was present, i.e. the light just passes the atom undisturbed, and $\boldsymbol{E}_{scat}$ represents the case when atom and laser interact, i.e. it's the atom's response to the incident light. Since we have two possible ways of interaction, interference can occur. This is the very same principle we found when describing the origin of Fano lines. Therefore, it's not surprising that we can observe Fano lines with this framework.

To generalize this ansatz, a transition from one atom to many atoms was performed (chapter 4). In principle, an approach similar to the Fraunhofer approximation was used to simplify the expression for the resulting total scattered field of all atoms. Accordingly, it was shown that the sum over all scattered fields can be replaced by an effective, planar field, which originates from the center of mass of the atoms and travels in the same direction as the incident light.

With this approximation, it was then possible to extend the energy analysis to laser pulses (chapter 5 and 6). First, energy conservation has been tested in a simple two-level system that is being excited by a Gaussian laser pulse. Furthermore, the atomic response $\hat{\rho}_{eg}$ was modified by hand with a phase kick $e^{i\theta(t-t_c)\phi_k}$, since this should lead to a modification of the detected line shape [4]. And indeed, the line shape does transform as expected. However, we were able to observe additional oscillations which ensured that the energy content of the spectral line doesn't change during its transformation. This has also been verified analytically by using a toy-model, which approximated the behaviour of $\hat{\rho}_{eg}$ for delta-like excitation of the atom. With the help of this toy-model, it was possible to show that the spectrum can be decomposed into two parts: A negative Lorentz term and an oscillating term, which changes the resulting line shape depending on a) the phase kick ϕ_k and b) the time-span t_c between excitation and phase kick. It's very intriguing that the second term, which also gives rise to the additional oscillations, has no energy content, i.e. even though the line shape changes, the total energy of the spectral line remains constant. Furthermore, increasing t_c leads to stronger oscillations, which get damped to 0 for

$t_c \to \infty$, such that the original negative Lorentz is being recovered.

To sum it up, the phase kick leads to a redistribution of energy in the frequency spectrum, taking energy into or out of regions beside the original, negative Lorentz profile.

Inspired by the experiment [4], the phase kick was then implemented into our physical model via a second laser by extending the analysis to a three-level system. The results obtained for this realistic model are approximately the same as for the two-level system. The additional oscillations occur as well, but due to the finite width of the control pulse (which performs the phase kick), they appear to be asymmetric. This is an effect which should certainly be studied further. However, as the total energy is conserved in time-domain (and therefore also in the frequency spectrum), the original results should also apply here.

During the course of the thesis, the phase kick has also been induced by hand for e.g. the two-level atom which is being excited by a plane wave. This lead in all cases to a breaking of energy conservation, and one could assume that the phase kick performs work. However, in the realistic three-level model, an overlap between probe pulse and control pulse does not break energy conservation, as for overlapping pulses, the interaction between atom and probe pulse is altered. Therefore, the amount of light scattered by the atom due to an interaction with the probe pulse is modified as well. This is a very interesting result, since, unlike in the non-overlapping case, the scattering behaviour of the atom seems to be affected by the control pulse. Sadly, in the time frame set for this thesis, there was not enough time to investigate this effect more in-depth.

Thus, it was demonstrated that energy is conserved in systems with Fano control. Some of the investigations started in this thesis can certainly be taken one step further to improve the already obtained results and deepen the understanding of how energy conservation is realized. For instance, a more thorough study about the influence of the pulse widths on the detected spectrum would be one starting point. Examining the energy conservation of the three-level system driven by plane wave probe - and control lasers could also result in worthwhile results. Additionally, it would be of high interest if some of the stated effects, e.g. the change of the oscillations in the spectrum dependent on t_c or the pulse widths, can be observed in experimental setups.

Appendix A On the Derivation of the Scattered Field

A.1 Polarization Sums

Let's assume we have an electromagnetic wave that propagates in the $\hat{\boldsymbol{k}}$-direction. The possible polarizations $\hat{\boldsymbol{\epsilon}}_{\boldsymbol{k},1}$ and $\hat{\boldsymbol{\epsilon}}_{\boldsymbol{k},2}$ must obey the following orthogonal identities:

$$\hat{\boldsymbol{\epsilon}}_{\boldsymbol{k},1} \times \hat{\boldsymbol{\epsilon}}_{\boldsymbol{k},2} = \hat{\boldsymbol{k}} \tag{135a}$$

$$\hat{\boldsymbol{\epsilon}}_{\boldsymbol{k},1} \times \hat{\boldsymbol{k}} = -\hat{\boldsymbol{\epsilon}}_{\boldsymbol{k},2} \tag{135b}$$

$$\hat{\boldsymbol{\epsilon}}_{\boldsymbol{k},2} \times \hat{\boldsymbol{k}} = \hat{\boldsymbol{\epsilon}}_{\boldsymbol{k},1} \tag{135c}$$

$$\hat{\boldsymbol{k}} \cdot (\hat{\boldsymbol{\epsilon}}_{\boldsymbol{k},1} \times \hat{\boldsymbol{\epsilon}}_{\boldsymbol{k},2}) = 1 \tag{135d}$$

The sum over the polarizations can thus be evaluated as follows:

$$\sum_{i=1}^{2} (\boldsymbol{d} \cdot \hat{\boldsymbol{\epsilon}}_{\boldsymbol{k},i}) \hat{\boldsymbol{\epsilon}}_{\boldsymbol{k},i} = (\boldsymbol{d} \cdot \hat{\boldsymbol{\epsilon}}_{\boldsymbol{k},1}) \hat{\boldsymbol{\epsilon}}_{\boldsymbol{k},1} + (\boldsymbol{d} \cdot \hat{\boldsymbol{\epsilon}}_{\boldsymbol{k},2}) \hat{\boldsymbol{\epsilon}}_{\boldsymbol{k},2} \tag{136a}$$

$$= -\left(\boldsymbol{d} \cdot (\hat{\boldsymbol{k}} \times \hat{\boldsymbol{\epsilon}}_{\boldsymbol{k},2})\right) \hat{\boldsymbol{\epsilon}}_{\boldsymbol{k},1} - \left(\boldsymbol{d} \cdot (\hat{\boldsymbol{\epsilon}}_{\boldsymbol{k},1} \times \hat{\boldsymbol{k}})\right) \hat{\boldsymbol{\epsilon}}_{\boldsymbol{k},2} \tag{136b}$$

$$- \left(\hat{\boldsymbol{k}} \cdot (\hat{\boldsymbol{\epsilon}}_{\boldsymbol{k},1} \times \hat{\boldsymbol{\epsilon}}_{\boldsymbol{k},2})\right) \boldsymbol{d} + \left(\hat{\boldsymbol{k}} \cdot (\hat{\boldsymbol{\epsilon}}_{\boldsymbol{k},1} \times \hat{\boldsymbol{\epsilon}}_{\boldsymbol{k},2})\right) \boldsymbol{d} \tag{136c}$$

$$= -\left(\boldsymbol{d} \cdot (\hat{\boldsymbol{\epsilon}}_{\boldsymbol{k},1} \times \hat{\boldsymbol{\epsilon}}_{\boldsymbol{k},2})\right) \hat{\boldsymbol{k}} + \left(\hat{\boldsymbol{k}} \cdot (\hat{\boldsymbol{\epsilon}}_{\boldsymbol{k},1} \times \hat{\boldsymbol{\epsilon}}_{\boldsymbol{k},2})\right) \boldsymbol{d} \tag{136d}$$

$$= \boldsymbol{d} - (\boldsymbol{d} \cdot \hat{\boldsymbol{k}}) \hat{\boldsymbol{k}} \tag{136e}$$

for what we used the identity $[\boldsymbol{a}, \boldsymbol{b}, \boldsymbol{c}]\boldsymbol{d} = [\boldsymbol{d}, \boldsymbol{b}, \boldsymbol{c}]\boldsymbol{a} + [\boldsymbol{a}, \boldsymbol{d}, \boldsymbol{c}]\boldsymbol{b} + [\boldsymbol{a}, \boldsymbol{b}, \boldsymbol{d}]\boldsymbol{c}$ with $[\boldsymbol{a}, \boldsymbol{b}, \boldsymbol{c}] = \boldsymbol{a} \cdot (\boldsymbol{b} \times \boldsymbol{c})$ (see [22]).

A.2 Stationary Phase Argument

We will demonstrate the stationary phase argument with an example. Consider the following surface integral in spherical coordinates:

$$\int g(\theta) e^{ik(\theta)r} \mathrm{d}\Omega \tag{137}$$

With $g(\theta)$ some well behaved integrable function. Assuming $k(\theta)$ has a minimum (or saddle-point / maximum) at ω_0 and is infinitely often differentiable, we can Taylor expand $k(\theta)$ around this point:

$$e^{ik(\theta)r} \simeq e^{ik(\theta_0)r} e^{ik''(\theta_0)\ (\theta-\theta_0)^2 r} \tag{138}$$

The second term is for $r \to \infty$ and $\theta \neq \theta_0$ highly oscillating and won't contribute to the integral. Thus, most contribution will come from $\theta = \theta_0$ such that we can approximate:

$$\int g(\theta) e^{ik(\theta)r} \mathrm{d}\Omega \simeq g(\theta_0) \int e^{ik(\theta)r} \mathrm{d}\Omega \tag{139}$$

A more thorough analysis of the stationary phase argument can be found at [23]. Taking the case $\boldsymbol{kr} = kr\cos\theta \Rightarrow k(\theta) = k\cos\theta$ with $k \in \mathbb{R}_0^+$, the stationary points are $n \cdot \pi$ with $n \in \mathbb{R}_0$. This means that the phase of $e^{i\boldsymbol{kr}}$ is stationary only if $\boldsymbol{k}$ and $\boldsymbol{r}$ are antiparallel or parallel. This approximation has been used in chapter 2.2.2.

Appendix B Solving Density Matrix Elements in Mathematica

B.1 Analytically Solvable Cases

For the stationary case, the following Mathematica code was used:

```
ClearAll[ree, rgg, reg, rge, Ω, X, A];
A = {{-γ, i Ω, -i Ω}, {2 i Ω, -(γ/2 - i Δ), 0}, {-2 i Ω, 0, -(γ/2 + i Δ)}};
B = {0, -i Ω, i Ω};
X = {ree, reg, rge};
A.X // MatrixForm
sol = LinearSolve[A, -B]
```

This program is very straight forward, since it only uses the Mathematica-function LinearSolve to solve the linear equations.

The non-stationary case needs a bit more effort. For instance, to solve the equations of motion for the case without spontaneous emission, the differential equations have been split up into real - and imaginary parts ($y = \mathrm{Re}(\hat{\rho}_{eg})$ and $z = \mathrm{Im}(\hat{\rho}_{eg})$. Furthermore, the quantity $x = \hat{\rho}_{ee} - \hat{\rho}_{gg}$ was defined to simplify the calculations. Hence, we get:

$$\dot{x} = -4\Omega \cdot z - \gamma \cdot x \tag{140a}$$

$$\dot{y} = -\Delta \cdot z - \frac{\gamma}{2} \cdot y \tag{140b}$$

$$\dot{z} = \Delta \cdot y + \Omega \cdot x - \frac{\gamma}{2} \cdot z \tag{140c}$$

These differential equations (with $\gamma = 0$) have been solved using the DSolve-function of Mathematica, which looks for an analytical solution of our problem:

```
ClearAll[x, y, z, Ω, sol, X, A];
A = {{0, 0, -4 Ω}, {0, 0, -Δ}, {Ω, Δ, 0}};
A // MatrixForm
Eigenvalues[A] // FullSimplify
X[t_] = {x[t], y[t], z[t]};
system = X'[t] == A.X[t];
A.X[t] // MatrixForm
DSolve[{system, x[0] == -1, y[0] == 0, z[0] == 0}, {x, y, z}, t];
sol = % /. Sqrt[-Δ^2 - 4 Ω^2] → i Sqrt[(Δ^2 + 4 Ω^2)] // FullSimplify // Flatten
```

The case shown in chapter 2.3.3 has been calculated with the following code:

```
Evaluate[x[t] /. sol] // FullSimplify
Limit[%, Δ → 0] // FullSimplify
% /. Ω → 1;
Plot[%, {t, 0, 10}, PlotRange → All, Frame → True, FrameLabel → {"t [s]", "ρee - ρgg", "", ""}]
```

Eqs. 140 can also be analytically solved for the case $\Delta = 0,\ \gamma \neq 0$. This can be done with the same Mathematica-code by adjusting the differential equations appropriately.

B.2 Numerical Solution of a General Case

The general case ($\Delta \neq 0,\ \gamma \neq 0$) can only be solved numerically. This has been done in Mathematica by using the NDSolve-function, which solves partial differential equations with the "Numerical Method of Lines" [24].

The following code has been used to get the solution for the case $\gamma = 2\ \frac{1}{s}$ and $\Delta = \frac{3}{2}\gamma,\ \Omega = \frac{5}{2}\gamma$.

```
ClearAll[ree, rgg, reg, rge, Ω, A, B]
B = {{-γ, 0, i Ω, -i Ω}, {γ, 0, -i Ω, i Ω}, {i Ω, -i Ω, -(γ/2 - i Δ), 0}, {-i Ω, i Ω, 0, -(γ/2 + i Δ)}};
% /. γ → 2;
% /. Δ → 3;
A = % /. Ω → 5;
X[t_] = {ree[t], rgg[t], reg[t], rge[t]};
B // MatrixForm
B.X[t] // MatrixForm
"Solution for example values (γ = 2, Δ = 3)"
A // MatrixForm
system = X'[t] == A.X[t];
sol = NDSolve[{system, ree[0] == 0, rgg[0] == 1, reg[0] == 0, rge[0] == 0}, {ree, rgg, reg, rge}, {t, 0, 5}] // Flatten
Plot[Evaluate[ree[t] - rgg[t] /. sol], {t, 0, 5}, PlotRange → All, Frame → True, FrameLabel → {"t [s]", "ρee - ρgg", "", ""}]
```

Appendix C On the Plane-Wave Transition

C.1 Numerical Analysis

To evaluate $\sum_{i=1}^{N} e^{(k_0(\hat{\boldsymbol{k}}_0 - \hat{\boldsymbol{r}})\boldsymbol{r}_i)}$ in Mathematica, first an array of three-dimensional vectors with random entries in a certain range is created and (for visualisation) plotted. This is further used to perform the given sum, which will then be evaluated for different values of ϕ and saved in a table. Finally, the table-data is plotted in a polar-plot to illustrate the results of the sum for different values ϕ. The code can be executed by calling the function "$main[times, theta, n]$" in the same notebook. With "n", one can adjust the accuracy of the ϕ-evaluation ($\Delta\phi = \frac{2\pi}{n}$), "$theta$" is the polar angle and "$times$" is the

number of atoms.

```
ClearAll[rvec, rand, fillArr, expSum];
rvec[θ_] = {Cos[ϕ] Sin[θ], Sin[ϕ] Sin[θ], Cos[θ]};
rand[r1_, r2_] := RandomReal[{-50, 50}];
fillArr[times_] := Array[rand, {times, 3}];
expSum[times_, θ_] := Sum[Exp[10 i ((rvec[θ] - {1, 0, 0}).sol[[count]])], {count, 1, times}];

main[times_, theta_, n_] := DynamicModule[{c},
  ClearAll[sol, f, t, sumErg];
  sol = fillArr[times];
  Print["Spacial distribution of atoms:"];
  Print[ListPointPlot3D[sol]];
  sumErg = expSum[times, theta];
  Print["Evaluating sum " ProgressIndicator[Dynamic[c], {0, n - 1}] ];
  t = Table[Re[sumErg /. ϕ → (2 π) / n * c], {c, 0, n - 1}];
  ListPolarPlot[t, Joined → True, PlotRange → All, Frame → True, Axes → False]]
```

C.2 Illustration of the Central Limit Theorem

To produce the graphs in chapter 4.2.2, the following code was used:

```
ClearAll[CosSum, Histo, Distr];
CosSum[times_] := Sum[Cos[RandomReal[{0, 2 π}]] / times, {i, times}];
Histo[noofval_, noofsum_] := Module[{j},
  ClearAll[Distr];
  Distr = Array[0, noofval];
  Print["Evaluating sums " ProgressIndicator[Dynamic[j], {0, noofval}] ];
  Do[Distr[[j]] = CosSum[noofsum], {j, noofval}];
  Print[Histogram[Distr, 100]];]
```

This program creates a sum of cosine-functions with random phases, whereby the phases are distributed evenly between $[0, 2\pi]$. This is repeated for a given sample size (e.g. 100 times) and then saved in an array. Eventually, the results are plotted into a histogram with 100 bins. Again, the code can be executed by calling the function "$Histo[noofval, noofsum]$" in the same notebook. With "$noofval$", one can adjust the sample size and with "$noofsum$" the number of summands.

Appendix D On the Two - and Three Level Calculations

D.1 Numeric Fourier Transform in Mathematica

The following code has been used to calculate numeric Fourier transforms.

```
NFourier[f_, tmax_, tstep_, ωnum_] := Module[{fou, fouright, ω = IntegerPart[ωnum * tmax / (2 π)]},
  fou = Re[Fourier[Table[f, {t, 0, tmax, tstep}]]];
  fouright = Join[{Take[fou, - ω], Take[fou, ω + 1]}] // Flatten;
  Transpose[{Table[k * 2 π / tmax, {k, - ω, ω}], fouright}]
 ]
```

In principle, the Mathematica function "Fourier" is used, which calculates the Fourier spectrum of a discrete set of data. Therefore, one has to first discretize the given function before Fourier transforming

it. Furthermore, the resulting spectrum has to be transformed, such that the axes label is correct. Note that we already take the real part of the result, which is needed for calculating the energy.

D.2 Calculating Frequency Spectra

The following function has been used for creating the different plots of the Fourier transforms. In principle, it combines most code fragments used in all calculations concerning the two - and three level system.

```
ClearAll[ree, reg, rgg, rge, γ, Δϕ, Ω, Δ, X, matrix, system];
X[t_] = {ree[t], rgg[t], reg[t], rge[t]};
matrix = {{-(γ + Δϕ), 0, i Ω, -i Ω}, {γ, 0, -i Ω, i Ω}, {i Ω, -i Ω, -(γ/2 - i Δ), 0}, {-i Ω, i Ω, 0, -(γ/2 + i Δ)}};
system = X'[t] == matrix.X[t];
wplots[tcmin_, tcmax_, tcstep_, smin_, smax_, sstep_, ωmax_, ϕkmin_, ϕkmax_, ϕkstep_, toint_] :=
 Module[{counter = 0, fourfun, freq, val, fou, fou2, fou3, finallist},
  ClearAll[Δ, γ, E0, σ, ω0, Ω0, Δϕ, pos, tc, ϕk, Ω];
  regplot = Array[ph, 20];
  inte = Array[ph, 20];
  par1 = {Δ, 0/100, 0/100, 5/100};
  par2 = {γ, 5/1000, 5/1000};
  par3 = {E0, 1/20, 1/20};
  par4 = {σ, smin, smax, sstep};
  par5 = {ω0, 1, 1};
  par6 = {Ω0, 1/10, 1/10};
  par7 = {Δϕ, 0, 0, 5/1000}; (* additional loss channel to quantify energy conservation *)
  par8 = {pos, 0, 0};
  par9 = {tc, tcmin, tcmax, tcstep};
  par10 = {ϕk, ϕkmin, ϕkmax, ϕkstep};
  Ω = -E0 * Ω0 1/σ Exp[-(pos - ω0 t)^2/(2 σ^2)];
  Print["Current loop number: " Dynamic[counter]];
  spectrum = Table[counter++;
     sol = NDSolve[{system, ree[0] == 0, rgg[0] == 1, reg[0] == 0, rge[0] == 0}, {ree, rgg, reg, rge},
       {t, 0, 9000}, WorkingPrecision → 32, MaxSteps → Infinity];
     fourfun = NFourier[i Exp[i fc[t, tc, ϕk]] (reg[t] /. sol), 9000, 1/2, ωmax];
     freq = Take[fourfun, All, {1, 1}] // Flatten;
     val = Take[fourfun, All, {2, 2}] // Flatten;
     fou[ω_] := FourierTransform[1/σ Exp[-(ω0 t)^2/(2 σ^2)], t, ω];
     fou2 = Map[fou, freq];
     fou3 = fou2 * val;
     finallist = Transpose[{freq, fou3}];
     regplot[[counter]] = Plot[{1/σ Exp[-(ω0 t)^2/(2 σ^2)], ComplexExpand[Re[5 i Exp[i fc[t, tc, ϕk]] (reg[t] /. sol)]]},
       {t, 0, tcmax + 50}, PlotRange → All, Frame → True, FrameLabel → {"t [1/ω_in]", "", "", ""}];
     If[toint = 1, inte[[counter]] = NIntegrate[Interpolation[finallist][ω], {ω, -ωmax, ωmax},
        WorkingPrecision → 16, MaxRecursion → 15], 0];
     ListLinePlot[finallist, PlotRange → All, Frame → True,
      FrameLabel → {"ω [ω_in]", "Fourier amplitude [a.u.]", "", ""}],
     Evaluate[par1], Evaluate[par2], Evaluate[par3], Evaluate[par4], Evaluate[par5], Evaluate[par6],
     Evaluate[par7], Evaluate[par8], Evaluate[par9], Evaluate[par10]] // Flatten;
  Print[regplot[[1 ;; counter]]];
  If[toint = 1, Print[inte[[1 ;; counter]]], 0];
  spectrum]
```

This code can be used for the three-level case by changing the equations of motion accordingly.

References

[1] Augustin-Jean Fresnel, *Œuvres complètes d'Augustin Fresnel* (Imprimerie impériale, 1866, p. 248)

[2] Andrey E. Miroshnichenko, Sergej Flach and Yuri S. Kivshar, *Fano resonance in nanoscale structures*, Rev. Mod. Phys. 82, 2257-2298 (2010).

[3] Boris Luk'yanchuk, Nikolay I. Zheludev, Stefan A. Maier, Naomi J. Halas, Peter Nordlander, Harald Giessen and Chong Tow Chong *The Fano resonance in plasmonic nanostructures and metamaterials*, Nature Materials 9, 707-715 (2010).

[4] Christian Ott, Andreas Kaldun, Philipp Raith, Kristina Meyer, Martin Laux, Jörg Evers, Christoph H. Keitel, Chris H. Greene, Thomas Pfeifer, *Lorentz Meets Fano in Spectral Line Shapes: A Universal Phase and Its Laser Control* , Science Magazine, Vol 340 (2013).

[5] K. P. Heeg, C. Ott, D. Schumacher, H.-C. Wille, R. Röhlsberger, T. Pfeifer and J. Evers, *Fano control of spectral line shapes in cooperative emission from nuclei* (not published yet).

[6] Wolfgang Nolting, *Grundkurs Theoretische Physik 3* (Springer, Berlin, 7. Ed.).

[7] Matthias Bartelmann, *Notes to the lecture: "Theoretische Physik III: Elektrodynamik"* (University of Heidelberg, Winter term 2010).

[8] Marlan O. Scully and M. Suhail Zubairy, *Quantum Optics* (Cambridge University Press, 2001).

[9] Timo Weigand, *Notes to the lecture: "Quantum Field Theory I"* (University of Heidelberg, Winter term 2012).

[10] Jörg Evers, *Notes to the lecture: "Quantum Optics"* (University of Heidelberg, Summer term 2013).

[11] Zbigniew Ficek and Stuart Swain, *Quantum Interference and Coherence* (Springer, 2005).

[12] Miguel Orszag, *Quantum Optics - Including Noise Reduction, Trapped Ions, Quantum Trajectories, and Decoherence* (Springer, 2. Ed., 2008).

[13] G. S. Agarwal, *Quantum Statistical Theories of Spontaneous Emission and their Relation to Other Approaches*, Springer Tracts in Modern Physics Vol. 70 (Springer, New York, 1974).

[14] D. F. Walls and Gerard J. Milburn, *Quantum Optics* (Springer, 2. Ed., 2008).

[15] http://www.mpi-hd.mpg.de/praktika/FP16/ (January 26, 2014).

[16] http://www.kip.uni-heidelberg.de/matterwaveoptics/teaching/practical/F65_EIT_Anleitung.pdf (January 26, 2014).

[17] Hermann Haken and Hans Christoph Wolf, *Atom - und Quantenphysik* (Springer, 5. Ed., 1993).

[18] Ilja Gerhardt, *Scattering & Absorption of Light by a Single Molecule under a Subwavelength Aperture*, DISS. ETH NO. 16812 (Swiss Federal Institute of Technology Zurich, 2006).

[19] Davar Khoshnevisan, *Notes to the lecture: "Introductory Probability: Course Syllabus"*, http://www.math.utah.edu/~davar/math5010/summer2010/L10.pdf (University of Utah, Summer term 2010).

[20] Ulrich Schwarz, *Notes to the lecture: "Theoretical Statistical Physics"* (University of Heidelberg, Winter term 2012).

[21] http://reference.wolfram.com/mathematica/howto/CheckTheResultsOfNDSolve.html (January 29, 2014).

[22] http://mathworld.wolfram.com/ScalarTripleProduct.html (December 27, 2013).

[23] Mark Tuckerman, http://www.nyu.edu/classes/tuckerman/stat.mech/lectures/lecture_16/node2.html (New York University, January 4, 2014).

[24] http://reference.wolfram.com/mathematica/tutorial/NDSolvePDE.html (January 1, 2014).

Erklärung

Ich versichere, dass ich diese Arbeit selbstständig verfasst und keine anderen als die angegebenen Quellen und Hilfsmittel benutzt habe.

Heidelberg, den 28.02.2014